ABSTRACT

Title of Document: NEW INSIGHTS INTO THE ROLE OF F-ACTIN IN REGULATION OF MITOCHONDRIAL FISSION.

Sunan Li, Doctor of Philosophy, 2015

Directed By: Mariusz Karbowski Ph.D.,
Associate Professor,
Center for Biomedical Engineering and Technology and Department of Biochemistry and Molecular Biology,
University of Maryland School of Medicine

Mitochondrial dynamics, including fusion and fission, are vital for supplying cellular energy as well as controlling other tasks including apoptosis, aging and cellular differentiation. Defects of mitochondrial fission pathway have been implicated in a wide spectrum of human diseases such as Parkinson's disease and Alzheimer's disease. Although recent findings point to a role of the actin cytoskeleton in regulating mitochondrial division, little is known about the mechanism. Here, I report that transient *de novo* polymerization of F-actin on the outer mitochondrial membrane contributes to Drp1-dependent mitochondrial division in mammalian cells. Transient *de novo* F-actin assembly on the mitochondria occurs upon induction of mitochondrial fission and F-actin accumulates on the mitochondria without forming detectable submitochondrial foci. Impairing mitochondrial division through Drp1

knockout or inhibition prolonged the time of mitochondrial accumulation of F-actin and also led to abnormal mitochondrial accumulation of the actin regulatory factors cortactin, cofilin, and Arp2/3 complex, suggesting that disassembly of mitochondrial F-actin depends on Drp1 activity. Furthermore, downregulation of actin regulatory proteins Arp2/3 complex, cortactin and cofilin led to abnormal elongation of mitochondria, associated with mitochondrial accumulation of Drp1. In addition, depletion of cortactin inhibited Mfn2 downregulation- or FCCP- induced mitochondrial fragmentation. These data indicate that the dynamic assembly and disassembly of F-actin on the mitochondria participates in Drp1-mediated mitochondrial fission. Moreover, I also discovered a novel F-actin involved mechanism of mitochondrial fission regulated by deubiquitinase Usp30. Overexpression of $Usp30^{CS}$ predicted to lack deubiquitinase activity induced abnormal elongation and thinning of mitochondrial tubules. Furthermore, expression of $Usp30^{CS}$ preferably binds to Drp1, inducing a dramatic redistribution of Drp1 from the cytosol to the mitochondria, and accumulation of high molecular weight Drp1 species. Importantly, FCCP induced a gradual tubulation of Drp1-containing structures, accompanied with mitochondrial associated F-actin in a similar timeframe in $Usp30^{CS}$-expressing cells, suggesting that inhibition of Usp30 deubiquitnase activity stalls progression of Drp1-dependent mitochondrial division. In sum, here I report that mitochondrial F-actin polymerization is a required step of mitochondrial fission, regulated by actin-modifying proteins and deubiquitinase Usp30, providing in-depth vision and a novel mechanism of actin cytoskeleton participated mitochondrial fission.

NEW INSIGHTS INTO THE ROLE OF F-ACTIN IN REGULATION OF MITOCHONDRIAL FISSION.

By

Sunan Li

Dissertation submitted to the Faculty of the Graduate School of the
University of Maryland, College Park, in partial fulfillment
of the requirements for the degree of
[Doctor of Philosophy]
[2015]

Advisory Committee:
Dr. Mariusz Karbowski, Chair
Dr. Bret A. Hassel
Dr. Mervyn J. Monteiro
Dr. Brian Mark Polster
Dr. Shengyun Fang
Dean's Representative:
Dr. Edward A. Eisenstein

Dedication

This thesis work is dedicated to my husband, Yang, who has been a constant source of support and encouragement during the challenges of graduate school and life. I am truly thankful for having you in my life. This work is also dedicated to my parents, Bing and Weijun, who have always loved me unconditionally and whose good examples have taught me to work hard for the things that I aspire to achieve.

Acknowledgements

This thesis becomes a reality with the kind support and help of many individuals. I would like to extend my sincere thanks to all of them.

Foremost, I would like to express my sincere gratitude to my advisor Dr. Mariusz Karbowski for the continuous support of my Ph.D. study and research, for his excellent guidance, motivation, enthusiasm, immense knowledge, and for his patience correcting my writings and financially support of my research. I would also like to thank my committee members: Dr. Fang, Dr. Monteiro, Dr. Hassel, and Dr. Polster for guiding my research for the past several years and helping me to develop my project. Special thanks goes to Dr. Eisenstein, who was willing to participate in my defense committee as Dean's Representative at the last moment.

I would like to thank my fellow labmates in Dr. Karbowski's lab: Dr. Shan Xu, Edward Cherok and Shweta Das, for their kind help and co-operation through my study. I also thank all the staff in BioMET and my graduate program in University of Maryland for all their support and assistance helped me along the way.

Last of all, I would like to express my gratitude towards my beloved husband, parents and parents-in-law for their unconditional love and support during the past five years. I would not have been able to complete this thesis without their continuous love and encouragement.

Table of Contents

List of Tables

List of Figures

Abbreviations

Abp140	Actin binding protein 140
AD	Alzheimer's Disease
ADOA	Autosomal dominant optic atrophy
AIF	Apoptosis inducing factor
AMP	Adenosine monophosphate
AntA	Antimycin A
Arp2/3	Actin related protein 2/3
ATP	Adenosine triphosphate
BARD1	Breast cancer 1-associated RING domain 1
Bcl2	B-cell lymphoma 2
BH	Bcl-2 homology domain
BMH	bismaleimidohexane
BN-PAGE	Blue-native Polyacrylamide gel electrophoresis
BSA	Bovine serum albumin
Caf4	CCR4 Associated Factor
CAG	Cytosine-adenine-guanine
CCCP	Carbonylcyanide-e-chlorophenylhydrazone
CDK1	Cyclin-dependent kinase 1
CMT2A	Charcot-Marie-Tooth Neuropathy Type 2A
CN	Calcineurin
CRISPR	Clustered regularly interspaced short palindromic repeats
DAPI	4',6-Diamidino-2-Phenylindole
DMEM	Dulbecco's Modified Eagle Medium
DNA	Deoxyribonucleic acid
Drp1	Dynamin-related protein 1
DSB	Double strand break
DSP	Dithiobis(succinimidyl propionate)
DUB	deubiquitinase
ER	Endoplasmic reticulum
ERAD	Endoplasmic-reticulum-associated protein degradation
ERK	Extracellular signal-regulated kinases
F-actin	Filamentous actin
FACS	Fluorescent-associated cell sorting
FBNP17	Formin-binding protein 17
FCCP	Carbonylcyanide-4-trifluoromethoxyphenylhydrazone
FH domain	Formin homology domains
FKBP8	FK506 binding protein 8
FRAP	Fluorescence recovery after photobleaching
FRET	Fluorescence resonance energy transfer
G-actin	Global actin
GED	GTPase effector domain
GFP	Green fluorescent protein
GSK3	Glycogen synthase kinase 3

HCT116	Human colon carcinoma cell line 116
HD	Huntington's Disease
HDR	Homology directed repair
HECT	Homologous to the E6-AP Carboxyl Terminus
HM	Heavy membrane
HR	Homology Region 1
HTT	Huntingtin
IBRDC2	In Between Ring fingers-type E3 ubiquitin ligase
IMM	Inner mitochondrial membrane
IMS	Inter membrane space
INDEL	Insertion/deletion
INF2	Inverted formin 2
IP	Immunoprecipitation
JMY	Junction-mediating and regulatory protein
LatB	Latrunculin B
LLO	Listeriolysin O
LM	Light membrane
Lmod-2	Leiomodin 2
MAP kinase	Mitogen-activated protein kinase
MAPL	Mitochondrial anchored protein ligase
MARCH5	Membrane-associated RING-CH
Mcl1	Myeloid cell leukemia 1
Mdv1	Mitochondrial division protein 1
MEF	Mouse embryonic flibroblasts
Mff	Mitochondrial fission factor
Mfn1/2	Mitofusin 1/2
MiD49/51	Mitochondrial dynamics proteins of 49 and 51 kDa
MIEF1/2	Mitochondrial elongation factor 1/2
MIRO1	Mitochondrial Rho1
MOMP	Mitochondrial outer membrane permeabilization
MPP	Mitochondrial processing peptide
MPTP	1-methyl-4-phenyl-1,2,3,6-tetrahydropyridine
MRLC	Myosin regulatory light chain
mtDNA	Mitochondrial DNA
NHEJ	Non-homologous end joining
NO	Nitric oxide
NPF	Nucleating promoting factor
OMM	Outer mitochondrial membrane
Opa1	Optic atrophy 1
OPTI-MEM	OPTI- Minimal Essential Medium
OXPHOS	Oxidative phosphorylation
PAGFP	Photoactivatable green fluorescent protein
PAM	Protospacer adjacent motif
PBS	Phosphate buffered saline
PD	Parkinson's Disease
PH	Pleckstrin homology domain

PHD-finger	Plant homeodomain finger
PI	Propidium iodide
PINK1	PTEN-induced putative kinase 1
PRD	Proline-rich domain
RING-finger	Really Interesting New Gene-finger
RNase	Ribonuclease
ROS	Reactive osygen species
SA-β-Gal	Senescence-associated beta-galactosidase
SCF^{FBW7}	SKP1–cullin-1–F-box complex that contains FBW7 as the F-box protein
SENP	SUMO specific protease
SDS-PAGE	Sodium dodecyl sulfate polyacrylamide gel electrophoresis
SH3	SRC homology 3
shRNA	Small hairpin RNA
siRNA	Small interfering RNA
SMCR7/7L	Smith-Magenis syndrome chromosome region, candidate 7
ssODN	Single stranded oligodeoxynucleotide
STORM	Stochastic optical reconstruction microscopy
SUMO	Small ubiquitin-related modifier
TALEN	Transcription activator-like effector nuclease
TOM	Transporter outer membrane
TIRF	Total internal reflection fluorescence microscope
TPR	N-terminal tetratricopeptide-repeat
U2OS	Human Osteosarcoma Cell Line
Ub	Ubiquitin
UPS	Ubiquitin-proteasome system
Usp	Ubiquitin specific protease
UtrCH	Utrophin
VDAC	Voltage-dependent anion channel
WH2	(WASP)-homology domain
YFP	Yellow fluorescent protein
ZFN	Zinc finger nuclease

Chapter 1: General Introduction

Section 1: Structural and functional complexity of the mitochondria

Mitochondria are essential organelles providing energy in a form of ATP to support cell metabolism and cellular homeostasis. Mitochondria are a unique among other cellular organelles due to their double membrane structure, consisting of an inner mitochondrial membrane (IMM) and outer mitochondrial membrane (OMM). The OMM separates mitochondria from the cytosol with a similar protein-to-phospholipid ratio to plasma membrane. The OMM is permeable to a wide range of small molecules including ions, adenosine triphosphate (ATP) and nutrient chemicals. Translocase of outer membrane (TOM) forms a complex on the OMM and acts as a transport channel to allow proteins synthesized in the cytosol to be imported into the mitochondria (Dietmeier et al. 1997). The IMM is extensively folded and compartmentalized to form mitochondrial cristae, which provides a large surface area that is mostly occupied by oxidative phosphorylation (OXPHOS) complexes. The IMM encircles mitochondrial matrix, a mitochondrial compartment, containing soluble enzymes, mitochondrial DNA (mtDNA) and mitochondrial ribosomes. Mitochondrial cristae are the major location for proteins mediating ATP synthesis and controlling cellular oxygen consumption, including five multisubunit OXPHOS complexes (Gilkerson et al. 2003). Electrons are transferred from electron donors to electron receptors through redox reactions in complex I-IV to generate chemical proton gradient between inter-membrane space and matrix. Complex V, also known

as F0/F1 ATP-synthase synthesizes ATP through oxidative phosphorylation using the chemiosmotic proton gradient generated by electron flow through complexes I-IV (van den Heuvel & Smeitink 2001).

Mitochondrial DNA (mtDNA) also locates in the mitochondrial matrix. Unlike nuclear DNA packaged as chromatin, mtDNA is circular. It contains 37 genes that encode critical subunits of the OXPHOS system. The process of mtDNA replication is mediated by DNA polymerase gamma complex encoded by the POLG gene, the twinkle DNA helicase and single-stranded DNA-binding protein via two competing mtDNA replication models (1) the strand-displacement mode (2) the strand-coupled mode (Park & Larsson 2011). mtDNA has a 10-17 higher mutation rate than nuclear DNA, which is possibly due to the mitochondrial levels of free dNTP and reactive oxygen species (ROS). ROS are produced during cell metabolism as a by-product of electron transfer through the electron transport chain. This leads to two major mutagenic changes in mtDNA through the formation of 8-oxo-2'-deosyguanosine and single/double strand breaks. Mutations of mtDNA, and resulting OXPHOS defects, are closely linked to aging, apoptosis and numerous other pathologies (Tuppen et al. 2010).

In addition to energy generation, mitochondria also serve as a signaling platform critical for intrinsic apoptotic pathway initiation by a wide range of intracellular perturbations such as DNA damage and oxidative stress. When pro-death signals prevail, translocation of pro-apoptotic multi-BH-domain proteins to OMM originates mitochondrial outer membrane permeabilization (MOMP) through Bax/Bak dependent pore-forming activity, leading to the release of potential toxic

proteins such as cytochrome c and apoptosis inducing factor (AIF) into cytosol. The release of cytochrome c drives the assembly of the apoptosome and subsequent activation of caspase cascade that executes apoptosis (Neutzner et al. 2012). Therefore, mitochondria provide an amplification loop for initial pro-apoptotic signals, which spurs the completion of apoptosis.

Moreover, mitochondrial calcium signaling contributes to the cytoplasmic response, mitochondrial metabolism and cell fate determination. Ca^{2+} enters mitochondria via the uniporter, allowing the Ca^{2+} accumulation down its electrochemical gradient and exits mitochondria via the Na^{+}/Ca^{2+} antiporter by exchanging Ca^{2+} with Na^{+} (Santo-Domingo & Demaurex 2010). Mitochondrial Ca^{2+} uptake shapes the cytosolic Ca^{2+} signals upon the release of Ca^{2+} from ER in response to multiple stresses (Rizzuto et al. 2012). Besides buffering cellular Ca^{2+} ions, up-regulated mitochondrial Ca^{2+} alters mitochondrial bioenergetics properties, production of ROS, as well as induction of autophagy and apoptosis. However, excessive Ca^{2+} accumulation in mitochondria favors the opening of the permeability transition pore (PTP), and initiates the release of caspase cofactors switching from physiological metabolic regulation to induction of apoptosis (Giorgi et al. 2012; Campanella et al. 2004).

Section 2: Mitochondrial fusion and fission

Apart from a complex two-membrane structure, in cells mitochondria form intricate and highly dynamic tubular structures often referred as the mitochondrial network. The mitochondrial network constantly fuse and divide to maintain mitochondrial inheritance and health by managing their copy numbers and

morphologies in response to ever-changing physiological conditions (Chen & Chan 2005; Westermann 2010). Mitochondrial fusion and fission dynamics cycle consists of four steps: biogenesis, fusion, fission and degradation (Archer 2013a). Mitochondrial biogenesis synthesizes new mitochondria to maintain mitochondrial copy numbers, through integration of proteins from both the nuclear and mitochondrial genomes (Jornayvaz & Shulman 2010). The dynamic behavior of mitochondrial fusion and fission forms an incorporated system to balance mitochondrial morphology and shape mitochondrial compartments. Increasing fusion activity leads to elongated mitochondrial tubules, whereas increasing fission activity antagonizes fusion and results in short and fragmented mitochondria. The combined mitochondrial fusion and fission dynamics and mitochondrial specific autophagy (mitophagy) are actively regulated in response to metabolic stress and mitochondrial damage as a quality control system (Chen & Chan 2009). Furthermore, mitochondrial fusion dilutes damaged materials, including mutated mtDNA and oxidized proteins, by improving the exchange of mitochondrial content. When mitochondrial damage exceeds a critical level, asymmetric mitochondrial fission divide and isolate aberrant mitochondria, allowing them to be packaged into autophagic vacuoles and then transported to lysosome for elimination by mitophagy (Archer 2013b; Twig et al. 2008).

Subsection 1: Control of mitochondrial fusion

A) Mitofusins: The first known mitochondrial fusion protein, Fuzzy onion 1 protein (Fzo1p), was identified in *Drosophila melamogaster* in 1998 (Rapaport et al. 1998). Fzo1p is a transmembrane GTPase with two homologues Mitofusin1 (Mfn1) and

Mitofusin2 (Mfn2) in mammalian cells. Both Mfn1 and Mfn2 are integral OMM proteins with the bulk of the polypeptide facing the cytoplasm mediating OMM fusion. They share similar domain organization with a N-terminal GTPase domain to mediate membrane remodeling, two transmembrane domains and coil-coil domain responsible for protein interaction. Mfn1 and Mfn2 interact with each other via heptad repeat region (HR2) to mediate mitofusin oligomerization by assembling a dimeric antiparallel coiled-coil structure. Mitofusin homodimer or heterodimer tethers adjacent mitochondria to promote mitochondrial fusion activity in a hook and loop mechanism (Koshiba et al. 2004). Although Mfn1 and Mfn2 coordinate with each other to support fusion events, they exhibit different GTPase activity and are diversely expressed in various tissues, fulfilling distinct roles in cellular physiology (Sebastian et al. 2012; Schneeberger et al. 2013; Mourier et al. 2015; de Brito & Scorrano 2008). While Mfn1 and Mfn2 knockouts are embryonically lethal (Chen et al. 2003), conditional knockout mice ubiquitously lacking Mfn1 survived through adulthood with no obvious defects, whereas mice lacking Mfn2 presented a degeneration of purkinje cells and exhibit severe movement defects and die in the early postnatal period (Chen et al. 2007).

Mitochondria convert from filamentous network into short round structures upon the addition of apoptotic stimuli, suggesting that mitochondrial steps in apoptosis are molecularly linked to inhibition of mitochondrial fusion. Mfn1 is phosphorylated by Mitogen-activated protein (MAP) kinase cascade member extracellular-signal-regulated kinase (ERK) at atypical targeting site in HR1 domain, which is essential for modulating mitochondrial fusion via affecting its oligomeric

status, as well as apoptosis by influencing oligomerization of the OMM-associated pro-apoptotic protein Bak (Pyakurel et al. 2015). On the other hand, in healthy cells, Mfn2 promotes mitochondrial fusion by regulating pro-apoptotic Bcl2 family member Bak and Bax. In addition, Mfn2 induces apoptosis in hepatocellular carcinoma cells by triggering mitochondrial Ca+ influx from the ER, which opens the mitochondrial membrane permeability transition pore (MPTP) and releases cytochrome c and AIF (Wang et al. 2015). In addition, Bax and Bak induce mitochondrial fusion by altering Mfn2 oligomerization, subcellular distribution and membrane mobility in healthy cells, suggesting that Bax and Bak are also required for normal mitochondrial morphogenesis (Karbowski et al. 2006).

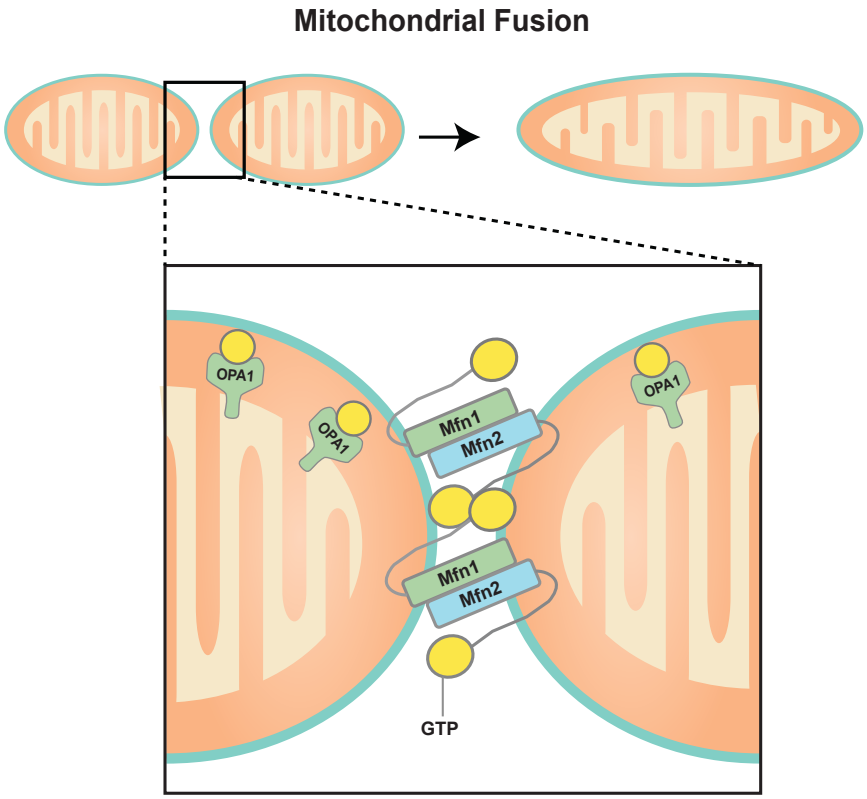

Figure 1.1 The mechanism of Mitochondrial Fusion.

B) Opa1: Inner mitochondrial membrane fusion is mediated by Optical Atrophy 1 (Opa1), which also belongs to the dynamin family of large GTPases. Opa1 has multiple isoforms, resulting from differential splicing of mRNA and proteolytic processing in the mitochondrial matrix and the intermembrane space. For example, Opa1 is encoded as a precursor that can be cleaved by mitochondrial processing peptidase (MPP) to produce the long isoform, and inner membrane peptidase zinc metallopeptidase OMA1 at S1 cleavage site (Ehses et al. 2009; Head et al. 2009) or the i-AAA protease Yme1L at C-terminal S2 cleavage site to produce the short isoform (Song et al. 2007). The long isoform, integrated in the IMM, and short isoform, residing in the intermembrane space, functionally complement each other for mitochondrial fusion (Anand et al. 2014). Opa1 processing mediated by mitochondrial proteases is important for regulation of mitochondrial morphology and metabolism. It has been reported that stimulation of Opa1 processing strongly correlated with induction of mitochondrial fragmentation (Ishihara et al. 2006). OMA1 is required in stress-induced cleavage of Opa1 and subsequent mitochondrial fragmentation, while loss of YME1L directly causes mitochondrial network fragmentation (Anand et al. 2014). In addition, Opa1 processing is also associated with mitochondrial integrity, including membrane potential, cristae remodeling and apoptosis. Disruption of mitochondrial membrane potential by mitochondrial uncoupler CCCP enhances accumulation of Opa1 short isoforms and is associated with mitochondrial fragmentation (Zhang et al. 2014). In addition, Opa1 protects cells from apoptosis independently of mitochondrial fusion (Frezza et al. 2006). OMA1 mediated Opa1 processing is activated by Bak and Bax oligomerization, and

subsequently the long isoform of Opa1 is eliminated by intrinsic pro-apoptotic stimuli (Jiang et al. 2014). Activation of OMA1 and Opa1 processing lead to disassembly of Opa1 oligomers and remodeling of cristae junctions, which results in delayed release of cytochrome c mobilization from mitochondrial cristae and, thus, inhibition of apoptosis (Yamaguchi et al. 2008).

Subsection 2: Control of mitochondrial fission

A) Drp1: Mitochondrial fission is mediated by Dynamin-related protein 1 (Drp1) in mammalian cells and its homolog Dnm1p in yeast (Labrousse et al. 1999; Smirnova et al. 2001). Similar to mitochondrial fusion proteins, Drp1 belongs to the dynamin superfamily. It has been shown that Drp1 shares similar structural features with dynamin including a N-terminal GTPase domain which binds to GTP and stimulates hydrolysis, a middle domain, an insert B and a C-terminal assembly domain (also named GTPase effector domain, GED) (Van Der Bliek 1999). Drp1 resides in the cytosol as homodimer or tetramer and is recruited to the OMM at the prospective mitochondrial fission sites. Upon recruitment, Drp1 self-assembles as spiral-like oligomers through intramolecular and intermolecular interaction with the GED domain, GTPase domain and middle domain (Griffin et al. 2005; Cerveny et al. 2007). Drp1 oligomerization enhances its GTP hydrolysis activity, which mediates membrane constriction and scission of mitochondrial tubules (Ingerman et al. 2005). Distinct posttranslational modifications and cellular signaling pathways regulate Drp1 activation. Drp1 has several conserved phosphorylation sites, including serine 656, serine 637 and serine 616, which are critical for its activation and inactivation. Serine 656 is phosphorylated by cyclic AMP-dependent protein kinase to inactivate Drp1

translocation, and is dephosphorylated by Calcinerurin (CN) to activate Drp1 recruitment and promote mitochondrial fission (Cribbs & Strack 2007). CN also dephosphorylates Drp1 at serine 637 in response to mitochondrial depolarization and cytosolic calcium accumulation, promoting Drp1 translocation to the OMM (Cereghetti et al. 2008). Drp1 also mediates mitotic mitochondrial division, which ensures mitochondria to be equally and uniformly distributed to daughter cells. Phosphorylation of Drp1 by cyclin B-CDK1 at serine 616 activates Drp1 and inducing mitochondrial fission in mitosis (Taguchi et al. 2007). The activation of Drp1 is reflected by the elevated ratio of serine 616 to serine 637 phosphorylation (Rehman et al. 2012). Recent studies also implicate a close link between Bcl2 family proteins and Drp1 activity. Bax colocalizes with Drp1 at subsequent mitochondrial fission sites during apoptosis (Karbowski et al. 2002). The presence of Bax/Bak oligomerization upon apoptosis stimulation activates and stabilizes mitochondrial-associated Drp1 via SUMOylation, which increases GTPase activity of Drp1 and stimulates mitochondrial fission in Bax/Bak-dependent apoptosis (Wasiak et al. 2007).

B) Mitochondrial receptors of Drp1: The recruitment of Drp1 to the mitochondria is mediated by an array of OMM-associated receptor proteins, including Mff (Mitochondrial fission factor), Fis1 (Mitochondrial fission protein 1) and MiD49/51 (Mitochondrial dynamics protein of 49 kDa and 51 kDa) complex.

The sequence of Mff features a short N-terminal repeat, a middle segment with strong coiled-coil forming propensity and a membrane anchor C-terminal hydrophobic segment. Depletion or downregulation of Mff produces interconnected mitochondria and partially inhibits CCCP-induced mitochondrial fragmentation

(Gandre-Babbe & van der Bliek 2008). Mff localizes in puncta on the OMM and is able to multimerize on OMM independent of Fis1 complex. It interacts with Drp1 both *in vivo* and *in vitro*, and regulates mitochondrial recruitment of Drp1, through the N-terminal cytosolic region (Otera et al. 2010). In addition to mitochondrial division, Mff, together with Drp1, also contributes to peroxisomal fission. Peroxisome-specific division factor Pex11p interacts with Drp1 via Mff, and mediates peroxisome division under a similar scenario of mitochondrial fission (Itoyama et al. 2013).

Fis1, another mitochondrial outer membrane protein, was proposed to function as a Drp1 receptor on the outer mitochondrial membrane. The domain organization of Fis1 features a N-terminal tetratricopeptide-repeat (TPR)-like domain exposed to the cytoplasm, and a C-terminal transmembrane domain to serve as a membrane anchor (James et al. 2003). In yeast, Fis1 is the sole factor mediating Drp1 recruitment to mitochondria by binding to Dnm1p through adaptor proteins Mdv1 and Caf4 via TPR motif (Zhang & Chan 2007). The role of Fis1 in mitochondrial recruitment in mammalian cells is controversial. While exogenous Fis1 expression induced mitochondrial fragmentation (Yoon et al. 2003), it has been reported that ablation of Fis1 has no effect on mitochondrial morphology and subcellular localization of Drp1 (Otera et al. 2010). However, reduction of Fis1 expression inhibited mitochondrial translocation and conformational change of pro-apoptotic protein Bax, as well as promoted ROS generation and loss of mitochondrial membrane potential. Overexpression of Fis1 induced cell death and cytochrome c release, further pointing to a role of Fis1 in cell death (Lee et al. 2004). In addition,

ectopic expression of Fis1 promotes peroxisomal fission, while silencing of Fis1 causes tubulation of peroxisomes, providing further evidence supporting the role for Fis1 in mammalian cells, in peroxisome morphogenesis, rather than mitochondrial fission (Shen et al. 2014).

MiD49 and MiD51 are two OMM proteins encoded by gene Smith-Magenis syndrome 7/7L (SMCR7/7L). MiD49/51 are N-terminally anchored in the mitochondrial outer membrane with C-terminal cytosolic domains. Unlike Fis1 and Mff, MiD49/51 do not localize on the peroxisomes (Palmer et al. 2013), which point to a more specific role in regulating mitochondrial dynamics. High expression of MiD49/51 results in elongated mitochondrial tubules, whereas low expression of MiD49/51 does not alter mitochondrial morphology (Palmer et al. 2011a). While $Fis1^{-/-}/Mff^{-/-}$ cells display defects in Drp1 recruitment and are highly resistant to CCCP-induced mitochondrial fragmentation, overexpression of MiD49 or MiD51 in $Fis1^{-/-}/Mff^{-/-}$ MEFs rescues recruitment of Drp1 to mitochondria and undergoes rapid shortening upon CCCP treatment, suggesting that MiD49/51 can mediate mitochondrial fission in the absence of Fis1 and Mff. Immunofluorescence analysis display that MiD49/51 form foci and constriction rings around mitochondria independent of Drp1, while co-immunoprecipitation shows that they directly interact with Drp1 (Losón et al. 2013). Collectively, the evidence suggests that they act as scaffolds for Drp1. The structure of MiD51 has been further studied. X-ray Crystallography demonstrates that MiD51 contains a nucleotidyltransferase domain that binds ADP and GDP with high affinity, however, mitochondrial fission still occurs at foci formed by a MiD51 nucleotide binding mutant, suggesting that the

nucleotidyltransferase is not directly relevant to the fission process (Losón et al. 2014). In addition, MiD51 is able to recruit Drp1, promote its assembly with MiD51 and GTP hydrolysis at constriction sites via a surface loop (residues 238-242), which is also well conserved in MiD49, implying for the role of MiD49/51 in promoting Drp1-dependent mitochondrial fission independently of ADP binding (Richter et al. 2014). Apart from mitochondrial fission, another group proposed a role of MiD49/51 (also called mitochondrial elongation factor 1/2; MIEF1/2) in mitochondrial fusion. In their hands ectopic expression of MiD49/51 resulted in extensive mitochondrial elongation and promotes mitochondrial fusion, whereas depletion of endogenous MiD49/51 by RNAi leads to mitochondrial fragmentation (Liu et al. 2013; Zhao et al. 2011).

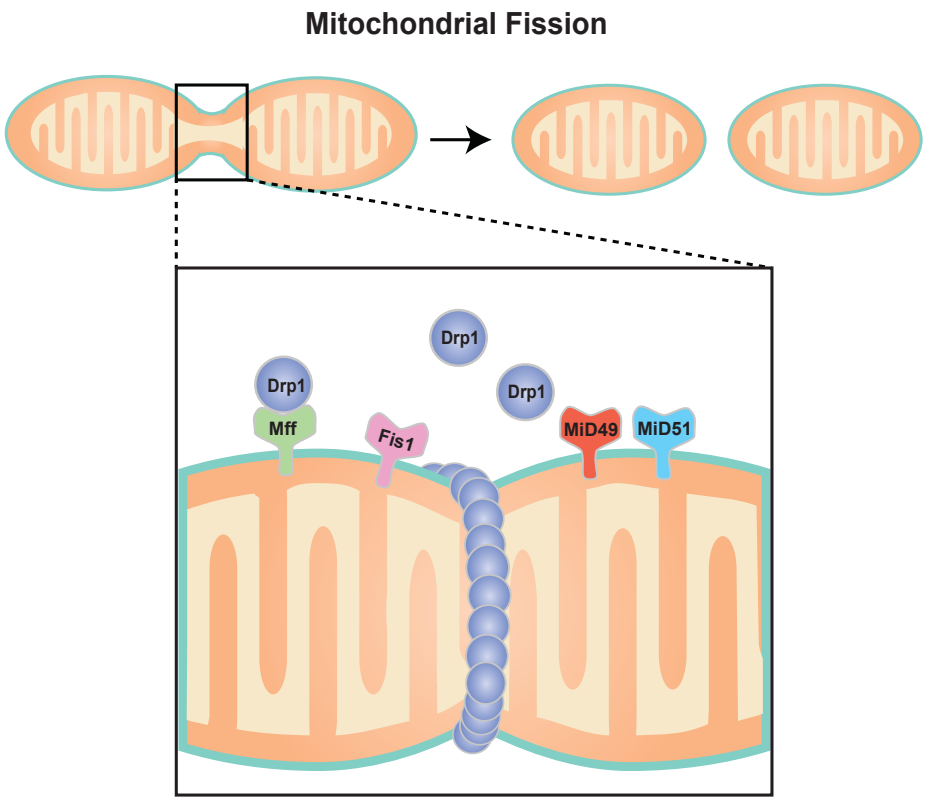

Figure 1.2 The mechanism of mitochondrial fission.

Subsection 3: Mitochondrial fusion and fission in disease

Imbalance of mitochondrial fusion and fission are implicated in various diseases and disorders including cancer, neurodegenerative, endocrine and cardiovascular diseases.

A) Cancer: Generally, cancer cells exhibit excessive proliferation and resistance to apoptosis, which hallmarks the importance of mitosis in tumor formation. Mitochondrial fission in mitosis, called mitochondrial mitotic division, coordinates mitochondria distribution in mitotic cells, ensuring equitable distribution of mitochondria to daughter cells. At G_1/S phase, inhibition of Drp1 leads to mitochondrial hyperfusion, which triggers DNA replication and cyclin E accumulation (Qian et al. 2012). Mitochondrial mitotic division is substantially coordinated by cyclin B1-CDK, a regulatory protein that contributes to cell cycle progression and Drp1 activation (Taguchi et al. 2007). Increased mitochondrial fission, resulting from an unbalanced Drp1 phosphorylation ratio of serine 616 to serine 637, has been shown in lung cancer cells. Drp1 inhibition by Drp1 inhibitor mdivi1, Drp1 siRNA or adenoviral Mfn2 have been used as therapies that inhibit cell proliferation and induces apoptosis, resulting in regression of tumor in a xenotrasplantation model (Rehman et al. 2012).

B) Alzheimer's Disease: Alzheimer's Disease (AD) is a chronic neurodegenerative disorder, characterized by memory loss, language problems, mood swings and behavior issues. The pathology of AD is distinguished by formation of amyloid plaques, neurofibrillary tangles and loss of connections between neurons. Abnormal

nitric oxide production in AD neurons has been shown to trigger Drp1 dimerization and mitochondrial fission via S-nitrosylation of Drp1 at cysteine 644. Consistent with this, levels of S-nitrosylated Drp1 are elevated in brains of AD patients (Cho et al. 2009). However, this molecular link between S-nitrosylation of Drp1 and AD remains controversial. Another report showed no significant difference of S-nitrosylated Drp levels in brains of age-matched normal and AD patients. Rather than S-nitrosylation, NO was found to trigger Drp1 phosphorylation at serine 616 resulting in activation of Drp1-dependent mitochondrial fission (Bossy et al. 2010).

C) Huntington's Disease: Huntington's Disease (HD) is an autosomal dominant disease characterized by symptoms such as choreoathetosis, dementia and premature death. The most common genetic cause of HD is the mutation of a protein called huntingtin (Htt) encoded by HTT gene with expansion of a CAG (cytosine-adenine-guanine) nucleotide triplet repeats, producing a chain of glutamine known as a polyglutamine tract (polyQ tract). A sequence of 36 or more CAG yields a misfolded form of Htt, called mHtt (mutant Htt), which forms protein aggregates that are believed to interfere with neuronal function in the brain (Beal & Ferrante 2004). It has been shown that mHtt triggers mitochondrial fragmentation in HD patient's fibroblasts and in a mouse model of HD prior to neurological deficits, via interacting with Drp1 and stimulating its GTPase activity (Song et al. 2011). Notably, increased levels of Drp1 S-nitrosylation were found in transgenic mouse model of HD and HD patients, and was proposed to induce early mitochondrial fragmentation followed by dendritic spines loss (Haun et al. 2013).

D) Charcot-Marie-Tooth Disease: Charcot-Marie-Tooth Disease is a group of genetically inherited disorders of the peripheral nervous system, which is characterized by progressive loss of muscle tissue and touch sensation. The subtype Charcot-Marie-Tooth disease type 2A (CMT2A) is due to autosomal dominant mutations of Mfn2 in neurons. More than 80 Mfn2 mutations have been reported in CMTA2 patients. The molecular pathogenic mechanisms is possibly due to mutated Mfn2 forming mitochondria clusters and clots, which impairs mitochondrial transport along axons towards the synapses damaging mitochondrial function in neurons (Klein et al. 2011; Züchner et al. 2004).

E) Autosomal dominant optic atrophy: Opa1 has been clinically reported as the most frequently mutated gene in autosomal dominant optic atrophy (ADOA), an optic neuropathy due to the loss of optic nerve fibers. ADOA is a mitochondriopathy that primarily affects retinal ganglion cells and their axons that transfer the visual signal from photoreceptors to the lateral geniculus in the brain. Dysfunctional Opa1 mutations found in patient fibroblasts revealed alterations of mitochondrial respiration activity, reduced energetic coupling and higher sensitivity to apoptosis (Kao et al. 2015). However, the mechanism of how Opa1 causes ADOA is still controversial.

Section 3: The role of F-actin in mitochondrial fission

Subsection 1: The role of F-actin in dynamin-mediated membrane remodeling

Dynamin superfamily proteins, including canonical Dynamins 1 and 2, Drp1, Mfns and Opa1, localize at membrane remodeling sites during many cellular

processes such as endocytosis, organelle morphogenesis, cell motility and phagocytosis. Dynamin1 featuring GTPase domain, pleckstrin homology (PH) that binds phosphatidylinositol lipids for membrane association, Proline-rich tail domain (PRD) that binds to Src homology 3 (SH3) domain of actin-binding proteins forms helical polymers as mechanochemical enzymes (Faelber et al. 2012). As a bridge, dynamin links actin cytoskeleton to membrane remodeling *via* various direct and indirect actin-binding proteins. Dynamin can bundle with actin filaments directly through the stalk region. Point mutation in the actin-binding domain of dynamin results in aberrant membrane ruffling and defective actin filaments assembly, whereas short actin filaments promote dynamin assembly into higher order structures, releasing actin-capping protein gelsolin (Gu et al. 2010a). The indirect connection of dynamin and actin filaments via actin regulatory proteins may also help position dynamin and generate membrane tension at endocytic sites (Ferguson & De Camilli 2012). Double knockout of Dynamin1 and Dynamin2 results in massive tubulation coated with actin meshwork nucleated by Arp2/3 complex and BAR binding protein endophilin 2, a group of proteins assisting dynamin-mediated membrane scission, at clarthin-dependent endocytic sites. The accumulation of endophilin 2 around the neck of arrested endocytic clathrin-coated pits depends on the activity of Arp2/3 complex (Ferguson et al. 2009). However, in the case of Shiga toxin-induced clathrin-independent endocytosis, actin was localized on membrane invaginations in endophilin A2-depleted cells, whereas endophilin 2 localized on the Shiga toxin-induced tubules in the absence of dynamin (Römer et al. 2010). Thus, actin, dynamin and endophilin 2 independently contribute to clathrin-independent tubulation.

Furthermore, another report indicates that membrane tension determines the actin dependence of clathrin-coated assembly (Boulant et al. 2011). Elevated membrane tension stalls clarthin assembly and sequesters local actin polymerization to endocytic sites. Actin meshwork is the driving force for membrane invagination and constriction in the latter stage when clathrin polymerization and assembly is hindered (Boulant et al. 2011). Even with the recent progress supporting the importance of actin cytoskeleton in clathrin-mediated endocytic processes, the mechanism of how dynamin interacts and connects actin cytoskeleton to membrane remodeling still remains unclear.

Subsection 2: The role of F-actin in mitochondrial fission

Recent studies reveal that actin cytoskeleton also take part in membrane constriction during mitochondrial fission, however the mechanism and degree to which F-actin contributes to mitochondrial fission remains ill-defined and controversial. Sheetz and colleagues first addressed the effects of F-actin polymerization on mitochondrial morphology (Kurt J De Vos et al. 2005). Disruption of F-actin by cytohalasin D and Latrunculin A/B did not affect mitochondrial tubules phenotype in CV1-4A and HeLa cells, indicating that F-actin was not required for maintenance of mitochondrial shape. Later however, other reports suggested that interfering with actin cytoskeleton altered mitochondrial morphology. Latrunculin application decreased mitochondrial size and shortened mitochondrial length in neurite and growth cone (Beck et al. 2012). Furthermore, overexpression of actin point mutants distinctively regulates mitochondrial morphology. While ectopic expression of actin R62D, which favors G-actin, decreased mitochondrial size and

occupancy, polymerization-competent actin G15S expression favoring F-actin assembly increased mitochondrial tubule size. These data suggest that elevated G-actin level results in mitochondrial fragmentation and decreased mitochondrial size and neurite mitochondrial occupancy in growth cones. In contrast to these findings, Higgs and colleagues reported that Latrunculin B treatment significantly increased mitochondrial length in U2OS cells (Korobova et al. 2013).

Nevertheless, pharmacological inhibition of actin polymerization altered Drp1-dependent and -independent mitochondrial fission and Drp1 recruitment in distinct ways. F-actin disruption by addition of Cytochalasin D or Latrunculin A reversed Drp1-dependent mitochondrial fission caused by ATP synthase inhibitor oligomycin or mitochondrial permeability transition pore inhibitor cyclosporine A (Kurt J De Vos et al. 2005). Moreover, immunofluorescence and Western blot analysis showed that inhibition of F-actin polymerization did not affect Drp1 patterns on mitochondria, however Drp1 recruitment initiated by mitochondrial fission was no longer increased (Kurt J De Vos et al. 2005), suggesting that F-actin polymerization is required during Drp1 recruitment from cytosol to mitochondria, but may not affect the existing mitochondrial Drp1 localization. A work by Cossart and colleagues revealed that cytochaslasin D reduced the number of cells displaying fragmented mitochondrial network induced by the pore-forming toxin listeriolysin O (LLO), indicating that action of actin filaments assembly is involved in LLO induced Drp1-independent mitochondrial fragmentation (Stavru et al. 2013). LLO induced Drp1-independent mitochondrial fission occurrs at ER-mitochondria contact sites,

supporting the possibility that in the absence of Drp1, actin filaments participate in mitochondrial fission via the ER-mitochondria contacts.

Inverted formin 2 (INF2), is a vertebrate protein that facilitates both actin assembly and disassembly. Higgs and colleagues reported that INF2 regulates mitochondrial fission in an actin-dependent step (Korobova et al. 2013). Downregulation of total INF2 and specific suppression of the prenylated (CAAX) isoform of INF2 that tightly bound to ER in U2OS cells resulted in mitochondrial elongation and decreased Drp1 puncta on the mitochondria. In contrast, constitutively active INF2-A149D causes a decrease in mitochondrial length and accumulation of Drp1 puncta on constricted mitochondria. Thus, these data suggest INF2 may facilitate Drp1 mediated mitochondrial fission by assisting Drp1 constriction around ER-mitochondria sites. Furthermore, INF2-A149D displayed a higher number of actin-enriched ER-mitochondrial contacts, and induced mitochondrial fragmentation, which was antagonized by LatB treatment, suggesting that INF2 involvement in mitochondrial fragmentation is actin dependent. Thus, it has been proposed that INF2 assists Drp1 mediated mitochondrial fission at ER-mitochondrial contact sites via activating actin polymerization, which may help position Drp1 at constriction sites and generate membrane force.

To further clarify the mechanism of how F-actin controls mitochondrial dynamics, the role of the actin motor protein myosins was also investigated. Myosins, a family of ATP-dependent motor proteins sharing properties of actin binding and force transduction, are responsible for actin-based motility. Myosins molecules feature a head domain that binds F-actin and generates force by ATP hydrolysis to

walk along the filaments, a neck domain acting as a connector and a tail domain carrying cargo molecules. Non-muscle Myosin II is a major type of motor protein providing contractile properties and is regulated by phosphorylation of heavy and light chains. Loss of function allelles of Drosophila homolog of myosin II heavy chain and light chain, zipper (zip) and spaghetti squash (sqh), in fly neurons lead to elongated neuronal mitochondria and less Drp1 association with mitochondria. In addition, F-actin immunoprecipitation by biotinylated phalloidin shows that the level of mitochondrial F-actin decreased when expressing loss of function alleles of zip or sqh (DuBoff et al. 2012). These data suggest that myosin II acts as a linker connecting F-actin and mitochondria, regulating mitochondrial fission in fly neurons. Furthermore, a recent study showed that myosin II also participate in the process of mitochondrial division in mammalian cells (Korobova et al. 2014a). In U2OS cells myosin II inhibitor Blebbistatin, but not Arp2/3 inhibitor CK666, significantly increased mitochondrial length and partially inhibited INF2 A149D induced mitochondrial fragmentation, suggesting that INF2 is acting in an Arp2/3 independent manner through myosin II. The subcellular localization of myosin II was further investigated to address the role of myosin II during F-actin dependent mitochondrial fission. Myosin II punctas, labeled by serine 19-phosphorylated myosin light chain (anti-P-MRLC) were found to be enriched at mitochondrial constriction sites. These punctas were significantly decreased when actin polymerization was inhibited by Latrunculin B and by INF2 downregulation. Live cell microcopy showed that low expression of GFP fused myosin IIA accumulated transiently at mitochondrial constriction sites. Thus, myosin II was proposed to mediate the membrane

constriction step during mitochondrial fission in an actin-dependent manner. Suppression of myosin II reduced the number of mitochondrial associated Drp1 puncta, suggesting that myosin II may serve as a docking molecule for Drp1.

Section 4: Ubiquitin-proteasome degradation in outer mitochondrial membrane associated pathway

Subsection 1: Ubiquitin proteasome system: an overview

Ubiquitin (Ub) is a ubiquitous 76 amino acid protein. Ub can be covalently linked to the lysines of target proteins, in the process known as ubiquitination. Ub binds to lysine residues on the protein substrate via an isopeptide bond or to the amino group of the N-terminus via a peptide bond. Ubiquitination acts as a signal for proteasome or lysosome degradation, as well as cellular signal transduction to regulate protein activity and interactions. Ubiquitination can be categorized as either monoubiquitination or polyubiquitination. Monoubiquitination occurs through an isopeptide bond generated between ubiquitin's glycine and substrate's lysine. Polyubiquitination is the formation of an Ub chain on a single lysine of the substrate protein, which is characterized by linking the C-terminal glycine of an Ub molecule to the specific lysine residue of already conjugated Ub molecules (e.g. K48, K63, K11). Primarily K48 and K11 polyubiquitination regulate proteasomal degradation of substrate proteins, whereas other types of Ub chains may be related to regulation of protein activities in various cellular processes, such as endocytic trafficking, DNA transcription and repair, and immune response and inflammation (Herrmann et al. 2007; Popovic et al. 2014). The ubiquitination cascade requires three steps: activation

by Ub-activating enzymes (E1s), conjugation by Ub-conjugating enzymes (E2s) and ligation by Ub ligase (E3s). Ub chains can be also removed from the substrate proteins by deubiquitinases (DUBs). Whereas the number of E1 and E2 are relatively limited, the diversity of E3 ligases allows the binding specificity of substrates during the process. The human genome encodes more than 600 putative E3 Ub ligases (Sévère et al. 2013). There are four major families of E3 Ub ligases: HECT (E6AP carboxyl terminus) domain, RING (Really Interesting New Gene) -finger, and RING related E3s such as U-box domain and PHD-finger. HECT domain accepts ubiquitin from E2 conjugating enzyme in the form of a thioester and directly transfers ubiquitin to targeted substrates. RING-finger domain is the largest family of E3 ligases containing a canonical Zn^{2+} coordinating domain that consists of conserved cysteine and histidine residues forming a cross-brace topology. RING finger domain simultaneously binds E2 enzymes and their substrates and serves as a scaffold to transfer ubiquitin to substrates (Metzger et al. 2012). U-box E3 ligases containing a 70 amino acid motif is a modified RING finger domain with zinc-binding sites replaced by hydrogen-bonding networks (Hatakeyama et al. 2001).

The significance of the Ub/proteasome degradation system (UPS) in regulating mitochondrial physiology through mediating mitochondrial protein degradation has been supported by the recently published evidence. E3 Ub ligases, which are responsible for mitochondrial protein degradation, localize either on the OMM or transiently interact with the mitochondria. The majority of evidence points to a role of the UPS in the control of OMM-associated protein degradation in a process similar to the ERAD (ER-associated protein degradation) pathway.

Subsection 2: Role of E3 Ub ligases in control of mitochondrial steps in apoptosis

Apoptosis is a type of programmed cell death process to remove dying cells from the organisms and is organized by cysteine-aspartic proteases called Caspases. Apoptotic signaled cytochrome c release is initiated from mitochondria to cytosol mediated by Bcl2 (B-cell lymphoma 2) family proteins and activates Caspases to execute programmed cell death. The balance between anti- and pro-apoptotic Bcl2 family serves as Caspases checkpoint by governing the OMM permeabilization. BH3-only proteins, which promote apoptosis, are generally present in different compartments of the cell and are localized to the OMM upon apoptosis stimuli, whereas multi-BH domain proteins including both anti- and pro-apoptotic proteins reside on the OMM (Neutzner et al. 2012). The recruitment of BH3-only proteins to the OMM shifts the ratio of pro- and anti-apoptotic proteins and triggers the permeabilization of OMM, thereby causing the release of a number of proteins, such as cytochrome c and AIF from intermembrane space (IMS) to cytosol, initiating the Caspase cascade (Suen et al. 2008). The UPS controls Bcl2 family proteins in distinct pathways, indicating a vital role of Ub-dependent protein degradation in regulating the mitochondrial steps of apoptosis.

Mcl1, a multi-BH domain anti-apoptotic Bcl2 family member, is rapidly degraded via the ubiquitin-proteasome system during apoptosis and upon cellular stress. Unlike other Bcl2 family proteins, Mcl1 has a short half-life of about 40-60 min. The unstable nature of Mcl1 is utilized by various stress stimuli as a rapid signal cascade for mitochondrial stress sensor. Mcl1 turnover is regulated by distinct E3 Ub ligases including ARF-BP1/Mule and SCF^{FBW7}. HECT domain E3 Ub ligase ARF-

BP1/Mule interacts with Mcl1 via its unique BH3 domain and mediates Mcl1 K48-linked polyubiquitination, thereby tagging Mcl1 for proteasomal degradation upon DNA damage-induced apoptosis (Inoue et al. 2013; Zhong et al. 2005). SCF^{FBW7} (Skp1-Culin1-F-box complex containing the F-box substrate recognition factor FBW7) interacts with and targets Mcl1 for ubiquitination depending on Mcl1 phosphorylation level (Inuzuka et al. 2011). Mutations of Mcl1 phosphorylation sites of glycogen synthase kinase 3 (GSK3) lead to both inhibition of Ub-dependent degradation and loss of interaction between Mcl1 and SCF^{FBW7} complex (Maurer et al. 2006). Depletion of SCF^{FBW7} complex hinders Mcl1 degradation causing accumulation of Mcl1 in DNA damage induced apoptosis (Inuzuka et al. 2011). Usp9x (Ubiquitin specific protease 9x) was reported to remove K48-linked Ub chain from Mcl1, thereby stabilizing Mcl1 in both untransformed cells and in tumors (Schwickart et al. 2010). The direct interaction between Usp9x and Mcl1 is inhibited by a GSK3 inhibitor, indicating that Mcl1 phosphorylation by GSK3 is critical for Usp9x deubiquitination. Increased Usp9x expression promotes cell survival in tumors, whereas knockdown of Usp9x enhances Mcl1 degradation and sensitizes cells to various apoptosis stimuli. In addition to above discussed factors, p97 (valosin-containing protein), a highly conserved AAA-ATPase, provides the driving force to extract Mcl1 from OMM, mediating the retrotranslocation of Mcl1 from the mitochondria to cytosol (Xu et al. 2011). Loss of membrane attachment allows p97 to deliver Mcl1 to proteasome and subsequent Mcl1 turnover by cytosolic UPS components.

In addition to Ub-dependent degradation of Mcl1, accumulating evidence reports that mitochondrial turnover of pro-apoptotic protein Bax (Bcl2 associated X protein) is also regulated by Ub-proteasome system. Normally, dormant Bax monomers are either cytosolic or loosely attached to the OMM as an inactive form. Upon apoptosis induction, Bax changes its conformation and accumulates on the OMM, and subsequently induces OMM permeabilization, resulting in release of cytochrome c and other pro-apoptotic protein to cytosol (Wolter et al. 1997; Hsu & Youle 1998). IBRDC2, an IBR (in-between RING)-type E3 ligase, specifically accelerate the removal of active Bax from the OMM (Benard et al. 2010). IBRDC2 translocates to mitochondria upon apoptosis induction, in synchrony with Bax activation. While overexpression of IBRDC2 increases Bax ubiquitination, knockdown of IBRDC2 leads to accumulation of active Bax on mitochondria and spontaneous apoptosis. Ub-proteasome system also regulates Bax activity through degradation of apoptosis related non-Bcl2 family proteins. RING domain E3 ligase BARD1 (BRCA1-associated RING domain 1) translocation to the mitochondria associates with stimulation of Bax oligomerization at OMM in response to the loss of mitochondrial membrane potential and apoptosis. Baxβ, an alternatively spliced variant of Bax, is constitutively active and closely regulated by proteasomal degradation (Tembe & Henderson 2007).

Subsection 3: Role of Ub-proteasome system in control of mitochondrial fusion and fission

The OMM-localized components of the UPS also regulate mitochondrial fusion and fission.

A) Ubiquitin-dependent control of mitochondrial fusion and fission proteins:

OMM integral fusion proteins Mfn1 and Mfn2 are stabilized by proteasome inhibitor MG132 in mammalian cells, pointing to a role of Ub-proteasome system in Mfns turnover. MARCH5, a mitochondrial anchored E3 ligase with four transmembrane segments (Karbowski et al. 2007), is well-studied. MARCH5$^{-/-}$ MEFs are sensitized to cell death upon electron transport chain complex III inhibitor Antimycin A treatment, possibly by regulating Mfn1 degradation (Park et al. 2014). MARCH5 binds to Mfn1, which has a shorter half-life about 4-6 hours, and subsequently ubiquitinates it depending on acetylation status of Mfn1. Under mitochondrial stress induced by Antimycin A, Mfn1 level is elevated and mitochondrial tubules are extensively elongated. At the same time, MARCH5-Mfn1 interaction and MARCH5-dependent Mfn1 ubiquitination and degradation are significantly enhanced, along with increased acetylated Mfn1, providing a novel E3-substrate coupling on OMM in regulating mitochondrial dynamics and cell viability. Furthermore, cells with reduced MARCH5 levels display cellular enlargement and flattening accompanied by increased senescence-associated β-galactosidase (SA-β-Gal) activity (Park et al. 2010). Ectopic expression of Mfn1 mutant in MARCH5 shRNA cells abolished the increase in SA-β-Gal activity, indicating that loss of MARCH5 promotes cellular senescence by Mfn1 accumulation on mitochondria. In addition, Mfn1 is ubiquitinated by MARCH5 at G_2/M phase and degraded in a proteasome-dependent manner, postulating a new Ub-proteasome dependent cell-cycle regulatory mechanism (Park & Cho 2012). Mfn2 appears to localize to both mitochondria and ER, and was proposed to tether mitochondria and ER in addition to its role in

mitochondrial fusion (de Brito & Scorrano 2008). It has been reported that, MARCH5 can bind to and ubiquitinate only the mitochondrial subset of Mfn2 (Sugiura et al. 2013). The resulting K63-linked ubiquitination promoted oligomerization of Mfn2 and the attachment of mitochondria to the ER in a proteasomal degradation-independent manner. Drp1 has been also identified as a physiological ubiquitination substrate of MARCH5 (Karbowski et al. 2007; Park et al. 2010).

In addition to the above discussed E3 Ub ligases, the OMM-associated deubiqutinase Usp30 has been also proposed to control mitochondrial membrane dynamics. Downregulation of Usp30 resulted in mitochondrial elongation(Nakamura & Hirose 2008; Yue et al. 2014). Mfn1, Mfn2 and other mitochondrial outer membrane proteins have been identified as the potential substrates of Usp30 in regulating mitochondrial dynamics (this will be discussed in chapter 4) (Yue et al. 2014).

B) SUMO-dependent control of mitochondrial fission: In addition to Ub, a 12 kDa small ubiquitin-like modifier (SUMO) also contributes to regulating mitochondrial dynamics. SUMOylation is a post-translational modification involving E1 heterdimer, E2 Ubc9 and E3-mediated multi-step cascade, by a mechanism similar to ubiquitination (Flotho & Melchior 2013). There are three SUMO (SUMO 1-3) paralogs in mammals. SUMO2 and SUMO3 differ by only a few N-terminal amino acids, whereas SUMO1 shares about 50% amino acid sequence with the other two. Unlike ubiquitination-targeted protein degradation, SUMOylation results in regulation of protein localization and activity, assembly or disassembly of protein complexes and modification of other posttranslational modification. Drp1 activity can

be modified by SUMOylation to regulate mitochondrial dynamics and response to various stresses. Pull-down results showed that Drp1 can be conjugated with SUMO1, and thereby protected from degradation (Harder et al. 2004). MAPL, an OMM anchored RING-finger E3 ligase, was reported to mediate Drp1 SUMOylation and reduce mitochondrial fusion rates promoting mitochondrial fission (Braschi et al. 2009), supporting the notion that MAPL modulates mitochondrial dynamics through regulating Drp1 SUMOylation.

deSUMOylation of conjugated proteins occurs through highly active SUMO cysteinyl proteases, which recognize tertiary structure of SUMO and cleave it from conjugated substrates. In mammalian cells, silencing of cytosolic SUMO protease SENP5 resulted in increasing Drp1 SUMO-1-ylation, as well as enhanced mitochondrial Drp1 translocation and mitochondrial fragmentation (Zunino et al. 2007). Another SUMO protease SENP3 is greatly reduced in response to oxygen/glucose deprivation, an *in vitro* model for ischaemia, increasing Drp1 SUMO-2/3-ylation resulting in decreased Drp1 association with mitochondria (Guo et al. 2013). Thus, loss of SENP3 decreased mitochondrial fragmentation and inhibited release of cytochrome c, establishing a crosstalk between unfolded protein response and mitochondrial dynamics.

Chapter 2: Transient F-actin assembly on outer mitochondrial membrane contributes to mitochondrial fission

Publication: Sunan Li, Shan Xu, Brian A. Roelofs, Liron Boyman, W. Jonathan Lederer, Hiromi Sesaki, and Mariusz Karbowski. Transient assembly of F-actin on the outer mitochondrial membrane contributes to mitochondrial fission. 2015. 208(1): 109-123.

Section 1: Introduction

As discussed in the previous section, mitochondrial fusion and fission balance is critical for cellular homeostasis maintenance and mitochondrial function in response to stress. A wide spectrum of diseases such as peripheral nervous system disorder Charcot-Marie-Tooth neuropathy type 2A and autosomal dominant optic atrophy (ADOA) concerning deficiencies in the oxidative phosphorylation system (OXPHOS) includes genetic and biochemical alterations of mitochondrial fusion and fission (Archer 2013b; Westermann 2010; Chaturvedi & Beal 2013).

Mitochondrial division is a multistep process relying on the action of several proteins. As discussed in detail in the previous section, mitochondrial recruitment of Drp1, the essential protein of mitochondrial fission, from the cytosol to the OMM is mediated by integral OMM-associated Drp1 receptors, Mff, MiD49/51, and Fis1 (Palmer et al. 2013; Otera et al. 2010; Onoue et al. 2012; Losón et al. 2013). Upon recruitment to mitochondria, Drp1 forms homo- and hetero- oligomers, composing of spirals around constricted sites on mitochondria in the final steps of mitochondrial fission that mediate membrane scission (Sesaki et al. 2014). This process appears to be facilitated by ER tubules that colocalize with mitochondrial fission sites.

Subsequently, disassembly and retrotranslocation of Drp1 from mitochondria to cytosol completes the mitochondrial fission pathway. Recent evidence supports a role for the F-actin cytoskeleton in the mitochondrial fission process (Kurt J. De Vos et al. 2005; Beck et al. 2012; Stavru et al. 2013; DuBoff et al. 2012; Palmer et al. 2011a; Korobova et al. 2014b; Korobova et al. 2013). Although many lines of evidence suggest the role of actin cytoskeleton in regulating mitochondrial morphology (overview in Chapter 1 Section 3), the exact mechanism remains unclear. Here in this chapter, I will discuss data supporting the notion that transient Drp1-independent *de novo* polymerization of F-actin on the OMM contributes to mitochondrial division in mammalian cells.

Section 2: Materials and Methods

Subsection 1: Cell culture

HeLa cells, wild type mouse embryonic fibroblasts (MEFs), $Drp1^{-/-}$ MEFs were provided by Dr. H. Sesaki from Johns Hopkins University. $Mff^{-/-}$ MEFs and $Mfn2^{-/-}$ MEFs were provided by Dr. D. Chan from California Institute of Technology. HeLa cells and MEFs were cultured in Dulbecco's Modified Eagle Medium (DMEM) supplemented with 10% heat-inactivated fetal bovine serum, 2 mM Glutamax, 1 mM sodium pyruvate, 1 mM nonessential amino acids, 100 U/ml penicillin in 5% CO_2 at 37°C. $Drp1^{-/-}$ MEFs were isolated from $Drp1^{-/-}$ E10.5 embryos and immortalized spontaneously by serial passage (over 30 times) (Wakabayashi et al. 2009). Mouse embryonic stem cell lines containing gene trap Mff disruption (line AZ0438) was injected into blastocysts to generate mouse cell lines, which $Mff^{-/-}$ MEFs were

isolated from (Losón et al. 2013). $Mfn2^{-/-}$ MEFs were derived from $Mfn2^{-/-}$ e10.5 embryos which were mechanically dispersed by repeated passage (Chen et al. 2003).

Subsection 2: Transfection

Cells were transfected with X-tremeGENE HP (Roche) or Lipofectamine 2000 (Invitrogen) transfection reagents, according to manufacturer's instructions. Cells were plated in 2-well chamber slides (model 1 German borosilicate; Labtec) or cell culture dish 18-24 hours before transfection (70%-90% confluency) and then incubated overnight. DNA were diluted with OPTI-MEM to a final concentration of 0.01 ug/ul and mixed gently. Transfection reagent was directly added in to DNA diluent in a ratio of 1:3 (DNA (ug): Transfection reagent (ul)) without contact with the walls of the plastic tubes and mixed gently. Transfection reagent-DNA complex were incubated in room temperature for 30 min and then added to cells in a dropwise manner. Cells were incubated for 16-20 hours before analysis.

Subsection 3: Cell cycle analysis

Cell cycle arrest at G_1/S phase is performed by double thymidine block. HeLa cells were treated with 2 mM thymidine for 18 hours to block DNA synthesis, followed by 3 washes with PBS and then releasing the cells into thymidine-free DMEM for 9 hours. After incubation in thymidine-free DMEM, cells were incubated with 2 mM thymidine for an additional 18 hours, followed by washing with PBS for 3 times. Afterwards, cells were reincubated in thymidine-free DMEM to restart the cell cycle and fixed by 4% formaldehyde 8-10 hours after releasing from the thymidine block. Cell cycle status of the synchronized cells was examined by flow cytometry

using propidum iodide (PI) staining. Cells were harvested, gently vortexed to avoid clumping and fixed with 70% ethanol overnight at 4°C. After fixation, cells were washed with cold PBS and incubated with 500ul RNase and 500ul PI for 45 min in the dark, and then transferred to FACS (Fluorescence-associated cell sorting) tubes for flow cytometry to verify synchronization of cell cycle status.

Subsection 4: DNA expression constructs

mRuby-Lifeact construct (Riedl et al. 2008) was provided by Dr. T. Blanpied (University of Maryland School of Medicine, Baltimore, MD). mCherry-UtrCH was (Burkel et al. 2007) purchased from Addgene (plasmid 26740; deposited by W. Bement). The mito-YFP construct was descibed earlier (Karbowski et al. 2007). $Drp1^{K38A}$ was provided by Dr. C. Blackstone (NIH, Bethesda, MD) and was described earlier (Karbowski et al. 2002).

Subsection 5: Immunofluorescence

Immunofluorescence was performed as previously described (Benard et al. 2010; Xu et al. 2011). For immunofluorescence, cells grown in 2-well chamber slides (model 1 German borosilicate; Labtec) were fixed with prewarmed 4% formaldehyde solution in PBS for 20 min at room temperature, and then permeabilized with 0.15% Triton X-100 solution in PBS for 20 min at room temperature. After blocking with 7.5% BSA blocking buffer (Bovine Serum Albumin fraction V in PBS) for 45 min, samples were incubated with primary antibodies diluted in 7.5% BSA blocking buffer for 90 min at room temperature, followed by 3 washes with 7.5% BSA blocking buffer and incubation with secondary antibodies diluted in 7.5% BSA blocking buffer

for 60 min at room temperature. Samples were washed with PBS at room temperature, and imaged directly in PBS within 2 d after immunofluorescence processing. The primary antibodies were: anti-Tom20 polyclonal antibody (dilution 1:2,000; clone FL-145; Santa Cruz Biotechnology, Inc.), anti-cytochrome c mAb (1:300; clone 6H2.B4; BD), and anti-Mff polyclonal antibody (1:1,000; ProteinTech). Secondary antibodies were anti–mouse or anti–rabbit Alexa Fluor 488 (1:500; Molecular Probes), or anti–mouse or anti–rabbit Alexa Fluor 546 (1:500; Molecular Probes). F-actin in fixed cells was detected using Alexa 546-Phalloidin, according to the manufacturer's protocol (Molecular Probes). In brief, after blocking with 7.5% BSA in PBS, cells were incubated with 6.7 U/ml Alexa 546-Phalloidin in blocking buffer for 60 min at room temperature, washed and then processed for immunofluorescence with respective primary antibodies.

Subsection 6: Image acquisition and analysis

Images were acquired using a fluorescent microscope (AxioObserver Z1; Zeiss MicroImaging), equipped with a 100/1.45 a-Plan-FLUAR objective lens (Zeiss MicroImaging), an ApoTome unit (enabling high-resolution structured illumination image acquisition), a Definitive Focus module, and a CCD camera (QuantEM 512SC; Photometrics) at room temperature. The ApoTome filters were set to maximum noise elimination. The software used for image acquisition was AxioVision 4.8 (Zeiss MicroImaging). Image cropping and global adjustments to brightness and contrast were performed using Photoshop CS6 software (Adobe). Live cell imaging was performed using the above-described system. Cells were grown in 2-well chamber slides (model 1 German borosilicate; Labtec) and imaged in Phenol Red–free

DMEM, supplemented with 10% heat-inactivated fetal bovine serum, 2 mM Glutamax, 1 mM sodium pyruvate, 1 mM nonessential amino acids, 100 U/ml penicillin, 100 mg/ml streptomycin, and 25 mM Hepes, pH 7.4, at room temperature.

Section 3: Results

Subsection 1: Abnormal accumulation of F-actin on the elongated mitochondria

F-actin has been implicated to participate in Drp1-dependent and Drp1-independent mitochondrial fission, as well as Drp1 recruitment from cytosol to mitochondria. However, the molecular mechanism and the degree to which crosstalk between Drp1 activity and F-actin contribute to mitochondrial division remain unclear. First, I analyzed the spatial relation between F-actin and mitochondria in wild type and $Drp1^{-/-}$ MEFs. Cells were fixed and stained with Alexa-Phalloidin for F-actin and cytochrome c to detect mitochondria, followed by structured illumination imaging. I found that there were no overlap between Alexa-Phalloidin and cytochrome c in wild type MEFs, indicating that F-actin was not colocalizing with the mitochondria (Fig2.1A). In contrast, about 20% of $Drp1^{-/-}$ MEFs with elongated mitochondrial phenotype revealed a mitochondria-colocalizing pattern of F-actin (Fig2.1B). This colocalization was primarily restricted to the perinuclear mitochondria. In addition, we inhibited mitochondrial fission by transfecting $Drp1^{K38A}$ in HeLa cells. $Drp1^{K38A}$ is a dominant negative protein defective in its GTPase activity, leading to mitochondrial elongation and swelling. Only $5.7 \pm 4.6\%$ HeLa cells displayed some F-actin colocalization with mitochondria (Fig.2.2A), while HeLa cells transfected with $Drp1^{K38A}$ exhibited F-actin colocalized with elongated

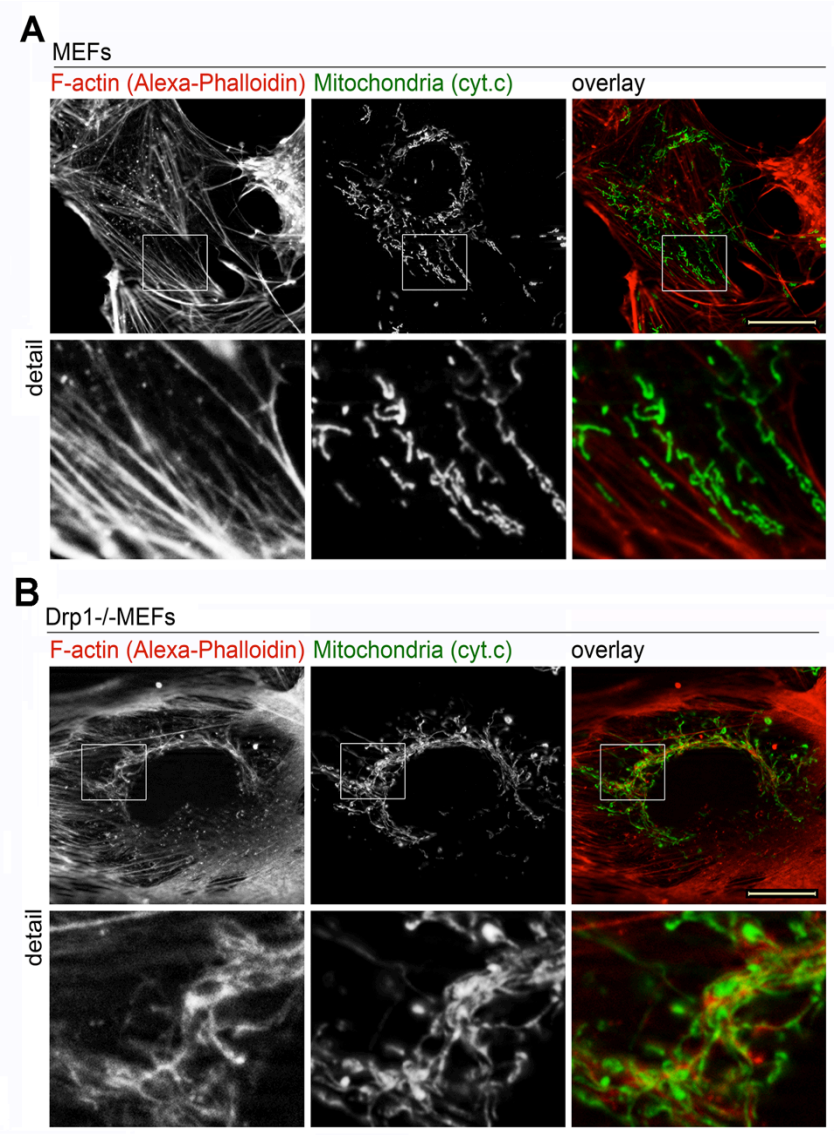

Figure 2.1 Mitochondrial F-actin localization in wild type and Drp1$^{-/-}$ MEFs. Wild type (A) and Drp1$^{-/-}$ (B) MEFs were fixed with 4% formaldehyde and then immunostained with Alexa-Phalloidin to detect F-actin (red on the overlay image) and anti-cytochrome c mAb for mitochondria (green on the overlay image), followed by structured illumination imaging. Higher magnifications of areas marked with white rectangles are shown in detail images. Bar: 20 μm; (detail) 5 μm.

tubular, but not swollen mitochondria (Fig.2.2B), suggesting that in the absence of functional Drp1 F-actin accumulated on abnormally elongated mitochondrial networks. The spatial relation between F-actin and mitochondria was also tested in mitochondrial Drp1 receptor Mff knockout (Mff$^{-/-}$) MEFs. Depletion of Mff resulted

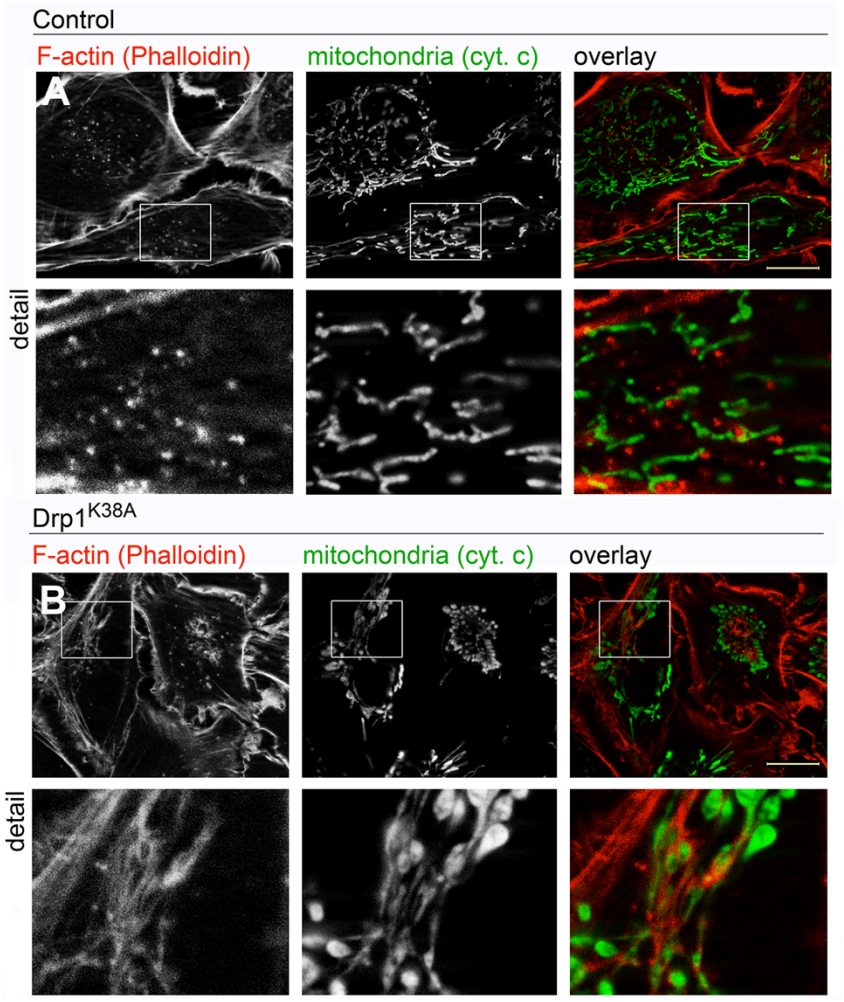

Figure 2.2 Mitochondrial F-actin localization in Drp1^{K38A}-expressing cells. Control HeLa cells (A) and HeLa cells transfected with Drp1^{K38A} (B) were fixed with 4% formaldehyde and then immunostained with Alexa-Phalloidin to detect F-actin (red on the overlay image) and anti-cytochrome c mAb for mitochondria (green on the overlay image), followed by structured illumination imaging. Higher magnifications of areas marked with white rectangles are shown in detail images. Bar: 20 µm; (detail) 5 µm.

in mitochondrial elongation because Drp1 cannot be recruited to the OMM in Mff$^{-/-}$ MEFs. F-actin was also found to colocalize with mitochondria in about 34% of Mff$^{-/-}$ MEFs (Fig. 2.3), indicating that inhibition of mitochondrial fission either by loss of Drp1 or reduction of Drp1 interaction with mitochondria resulted in abnormal mitochondrial accumulation of F-actin. Confirming the specificity of F-actin

colocalization with mitochondria in Drp1$^{-/-}$ and Mff$^{-/-}$ MEFs, no colocalization between F-actin and mitochondria was found in Mfn2$^{-/-}$ MEFs. Thus, these data suggests that accumulation of F-actin on elongated mitochondrial tubules was specifically induced under the scenario that mitochondrial fission is inhibited by depletion of Drp1 or Mff.

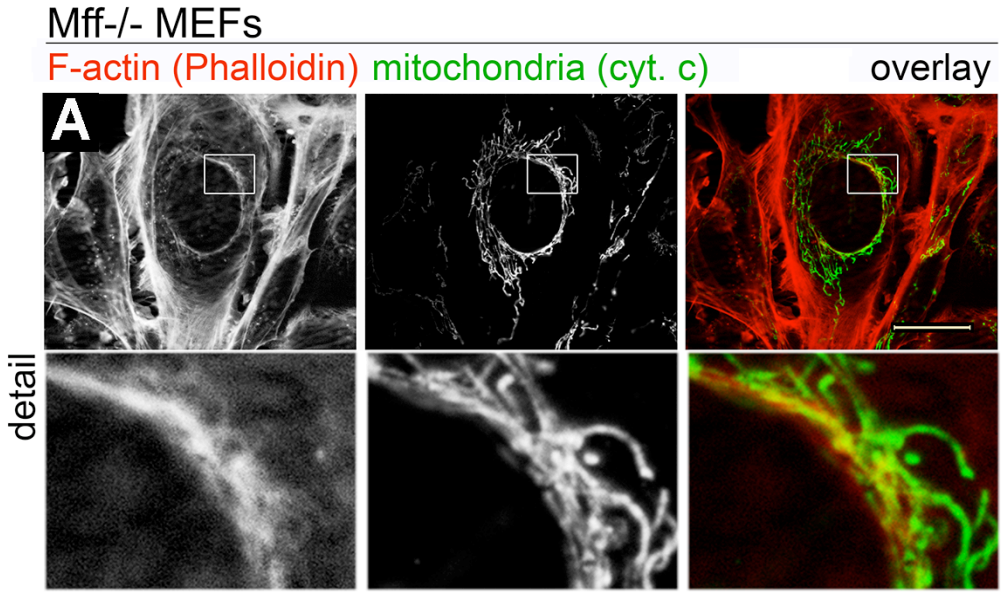

Figure 2.3 Mitochondrial F-actin localization in Mff$^{-/-}$ MEFs. Mff$^{-/-}$ MEFs were fixed with 4% formaldehyde and then immunostained with Alexa-Phalloidin to detect F-actin (red on the overlay image) and anti-cytochrome c mAb for mitochondria (green on the overlay image), followed by structured illumination imaging. Higher magnifications of areas marked with white rectangles are shown in detail images. Bar: 20 μm; (detail) 5 μm.

Subsection 2: Transient de novo F-actin polymerization on the mitochondrial upon stress-induced mitochondrial fission

Transient F-actin assembly has been implicated in various membrane remodeling events such as dynamin-dependent endocytosis (Mooren et al. 2012). Furthermore, knockout of dynamin, a large GTPase essential for endocytotic vesicle

scission, led to abnormal accumulation of F-actin at the defective vesicle scission sites (Ferguson et al. 2009). A similar scenario may also underlie mitochondrial accumulation of F-actin in mitochondrial fission deficient $Drp1^{-/-}$ and $Mff^{-/-}$ MEFs and HeLa cells transfected with $Drp1^{K38A}$.

To verify this possibility, we tested the degree to which F-actin assembles on mitochondria upon stress-induced mitochondrial fission. Drp1 mediated mitochondrial fission can be induced by mitochondrial toxins, including the uncoupling agents carbonyl cyanide 4-(trifluoromethoxy) phenylhydrazone (FCCP), and 2-[2-(3-Chlorophenyl) hydrazinylyidene] propanedinitrile (CCCP; Gandre-Babbe and van der Bliek, 2008; Palmer et al., 2011). Wild type MEFs and $Drp1^{-/-}$ MEFs were treated with 10 μM FCCP, followed by immunostaining with Alexa-Phallodin to detect F-actin and anti-cytochrome c antibody to detect mitochondria. At 2 min into FCCP treatment, about 100% of $Drp1^{-/-}$ MEFs displayed a clear mitochondrial accumulation of F-actin, in contrast to about 33% in the case of wild type MEFs (Fig. 2.4). Similar mitochondrial F-actin accumulation was also detected in HeLa cells transfected with dominant negative mutant $Drp1^{K38A}$ (Fig. 2.5). Another mitochondrial toxin cytochrome c reductase inhibitor Antimycin A (AntA), was utilized to induce Drp1 dependent mitochondrial fission. As with FCCP treatment, mitochondrial accumulation of F-actin was more pronounced in $Drp1^{-/-}$ MEFs after 5 min of 10 μM AntA treatment (Fig.2.6). In addition, mitochondrial accumulation of F-actin was also detected in about 100% of $Mff^{-/-}$ MEFs at 2 min of FCCP treatment (Fig.2.7A). I also tested mitochondrial colocalization of Drp1 in untreated and FCCP-treated wild type MEFs and $Mff^{-/-}$ MEFs. Mff ablation significantly reduced

mitochondrial localization of Drp1. Furthermore there was only a minor increase in mitochondrial Drp1 in FCCP-treated cells (Fig.2.7B). Thus, mitochondrial accumulation of F-actin appears to preferentially occur in cells in which Drp1 fission complex formation is inhibited, and in control cells may occur before Drp1 activation.

The mitochondria-enriched z-sections corresponding to the vertical middle part of the cells are shown in Fig.2.8. These images largely lack the cortical F-actin signal, which is detectable in the bottom of the cells, corresponding to z-sections below those enriched in the mitochondria. The typical z-stacks shown in Fig.2.8 reveal the relative intensity of mitochondria-associated F-actin versus cortical F-actin.

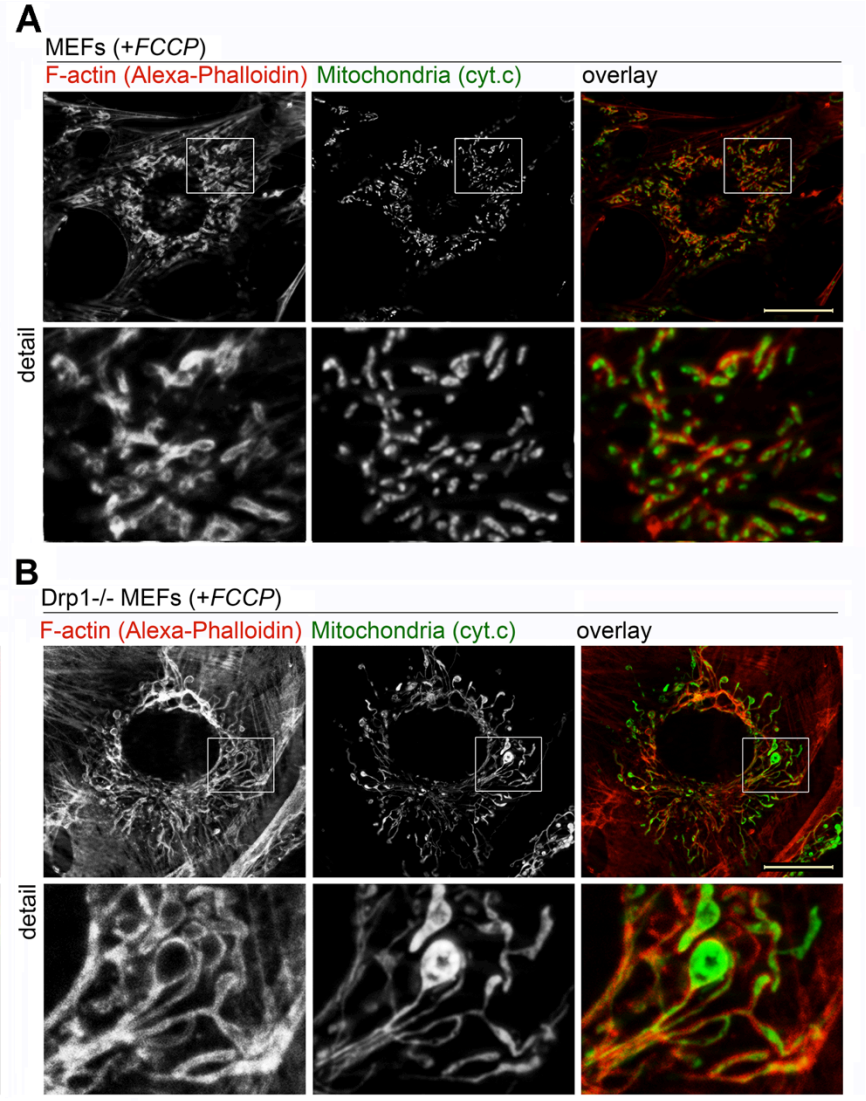

Figure 2.4 Mitochondrial F-actin localization in wild type and Drp1$^{-/-}$ MEFs upon 2 min FCCP treatment. Wild type (A) and Drp1$^{-/-}$ (B) MEFs were treated with 10 uM FCCP for 2 min, fixed with 4% formaldehyde and then immunostained with Alexa-Phalloidin to detect F-actin (red on overlay image) and anti-cytochrome c mAb for mitochondria (green on overlay image), followed by structured illumination imaging. Higher magnifications of areas marked with white rectangles are shown in detail images. Bar: 20 µm; (detail) 5 µm.

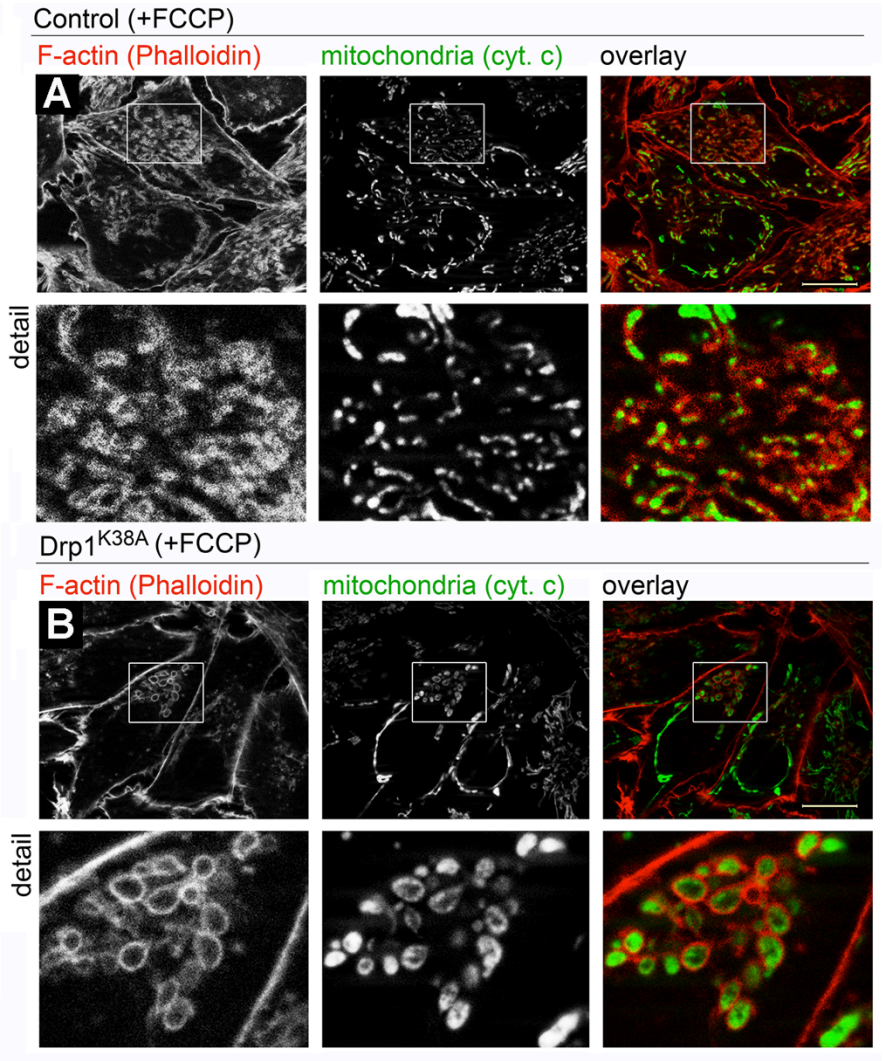

Figure 2.5 Mitochondrial F-actin localization in Drp1^{K38A}-expressing cells upon 2 min FCCP treatment. Control HeLa cells (A) and HeLa cells transfected with Drp1^{K38A} (B) were treated with 10 uM FCCP for 2 min, fixed with 4% formaldehyde and then immunostained with Alexa-Phalloidin to detect F-actin (red on overlay image) and anti-cytochrome c mAb for mitochondria (green on overlay image), followed by structured illumination imaging. Higher magnifications of areas marked with white rectangles are shown in detail images. Bar: 20 μm; (detail) 5 μm.

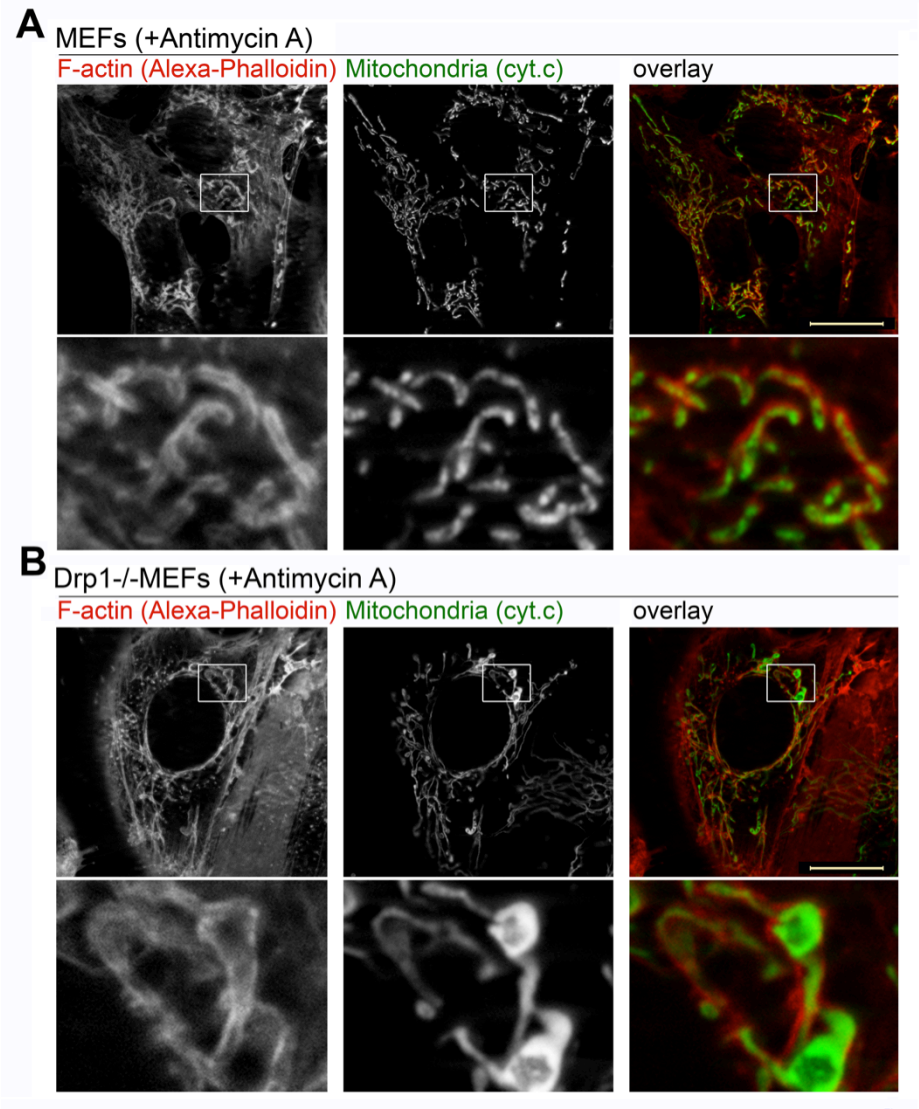

Figure 2.6 Mitochondrial F-actin localization in AntA-treated wild type and Drp1$^{-/-}$ MEFs. Wild type MEFs (A) and Drp1$^{-/-}$ MEFs (B) were treated with Antimycin A for 5 min and immunostained with anti-cytochrome c mAb (green on overlay image) and Alexa-Phalloidin (red on overlay image), followed by structured illumination imaging. Higher magnifications of areas marked with white rectangles are shown in detail images. Bar: 20 μm; (detail) 5 μm.

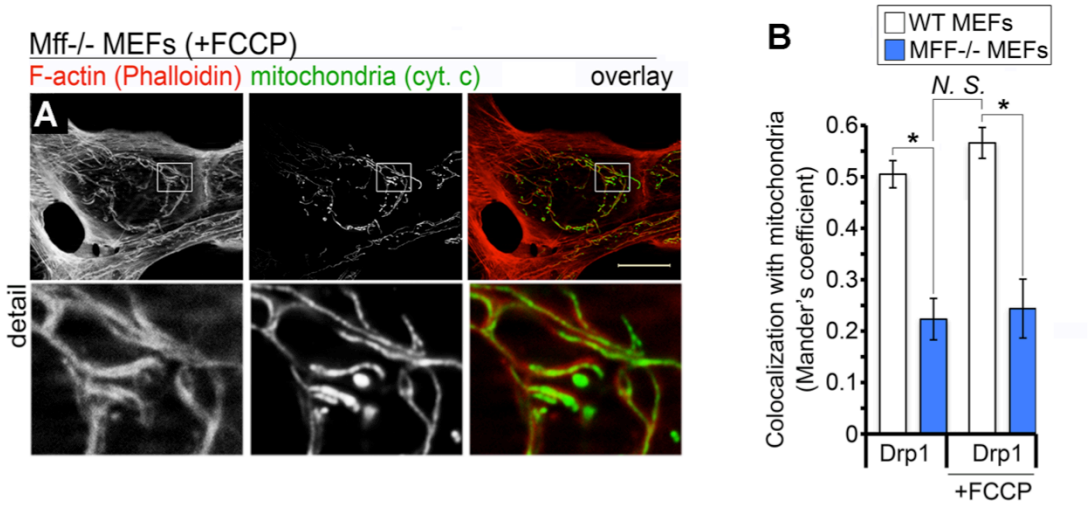

Figure 2.7 Mitochondrial F-actin localization and mitochondrial association of Drp1 in FCCP treated Mff$^{-/-}$ MEFs. (A) Mff$^{-/-}$ MEFs were treated with FCCP for 2 min, fixed with 4% formaldehyde, and then immunostained with Alexa-Phallodin to detect F-actin (red on overlay image) and anti-cytochrome c mAb to detect mitochondria (green on overlay image), followed by structured illumination imaging. Higher magnifications of areas marked with white rectangles are shown in detail images. Bar: 20 μm; (detail) 5 μm. (B) Colocalization of Drp1 with mitochondria was analyzed in wild type and Mff$^{-/-}$ MEFs. The values represent Mander's correlation coefficient (Rr) that reveal the degree of association of pixels in different channels of the image. Rr = 1 indicates complete colocalization, whereas Rr = 0 indicates random colocalization, and Mander's score roughly correlates with percentage of overlap. Data represent the mean ± SD of 15 images/condition. Each image used for the analysis contained at least two cells.

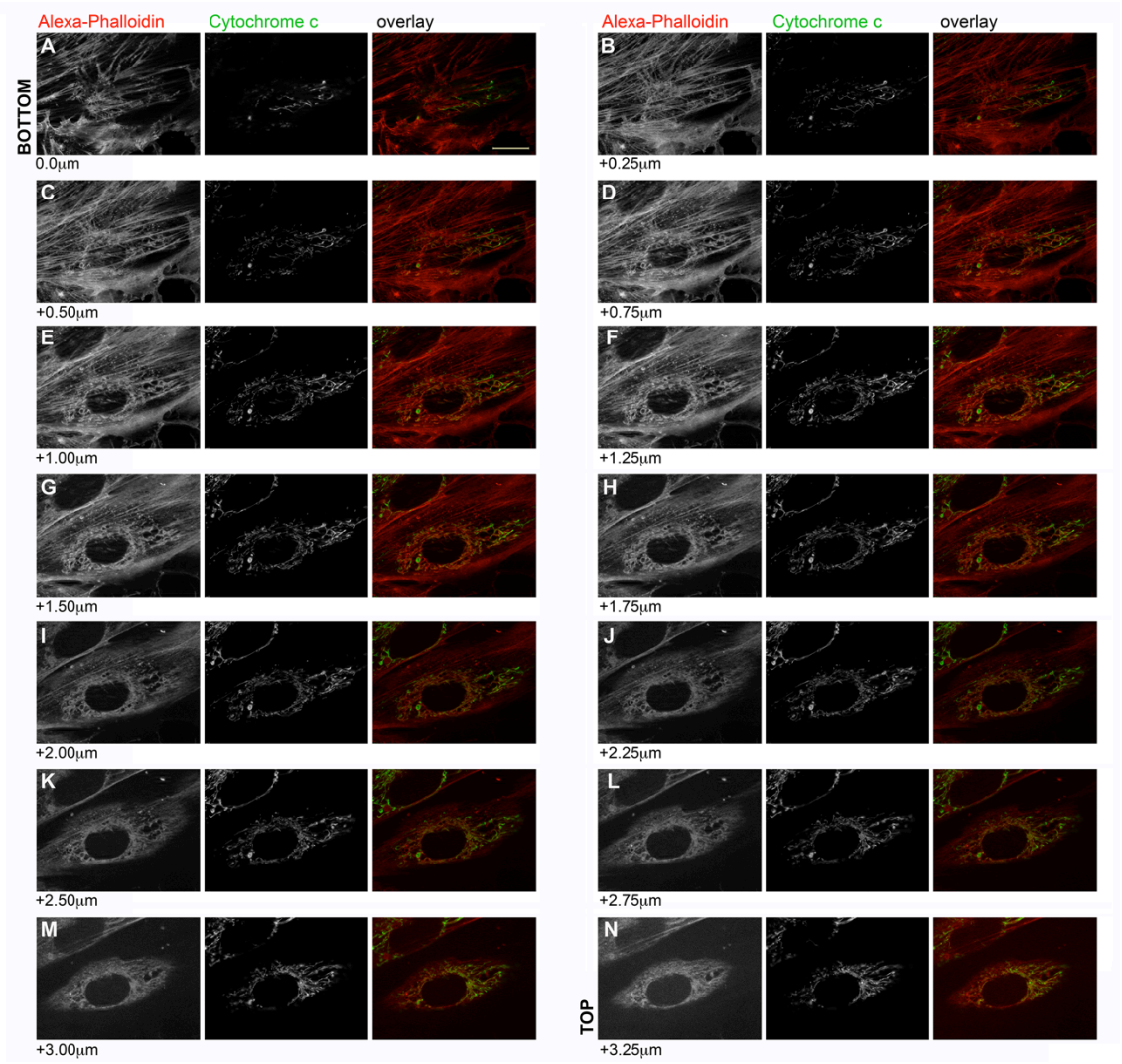

Figure 2.8 Spatial relations of F-actin and mitochondria in FCCP-treated Drp1$^{-/-}$ MEFs. Drp1$^{-/-}$ MEFs treated with FCCP for 2 min were immunostained with anti-cytochrome c mAb (green on overlay images) and Alexa-Phalloidin (red on overlay images), followed by structured illumination imaging. The sequence of single z-sections (0.25 um intervals), from the bottom (A) to the top (N) of the cells is shown. Bar: 20 μm.

To further clarify the temporal mechanism of how F-actin is recruited to mitochondria, various cell types including HeLa cells, wild type MEFs, Drp1$^{-/-}$ MEFs, Mff$^{-/-}$ MEFs and Mfn2$^{-/-}$ MEFs, were treated with FCCP for various time periods ranging from 2 to 30 min (Fig. 2.9). The data showed an increase in the number of cells with F-actin positive mitochondria in FCCP-treated wild type, Drp1$^{-/-}$ MEFs, Mff$^{-/-}$ MEFs and Mfn2$^{-/-}$ MEFs upon treatment, peaking at 2-5 min of treatment, followed by a gradual decline in the number of cells with F-actin positive mitochondria. Furthermore, parallel analysis of Mfn$^{-/-}$ MEFs and HeLa cells revealed transient increases in the number of cells with F-actin-positive mitochondria occurring at comparable rates as FCCP-treated wild type MEFs. Similar to FCCP treatment, AntA treatment also induces a transient increase of mitochondrial F-actin in both wild type and Drp1$^{-/-}$ MEFs. In sum, these data suggests that F-actin transiently accumulates on the mitochondria during stress-induced mitochondrial fission. The temporary increase in the number of cells with mitochondrial translocation of F-actin suggests F-actin transiently accumulates on mitochondria during mitochondrial toxin-mediated Drp1-dependent mitochondrial fission. Considering that the number of cells with F-actin positive mitochondria peaks at 2-5 min, the cycling of F-actin between cytosol and mitochondria occurs before membrane scission events. Furthermore, the number of cells with mitochondrial positive F-actin increased at 2-5 min followed by a gradual decline regardless of the presence of functional Drp1, indicating that mitochondrial F-actin assembly and disassembly upon stress-induced mitochondrial fission is independent of Drp1 function.

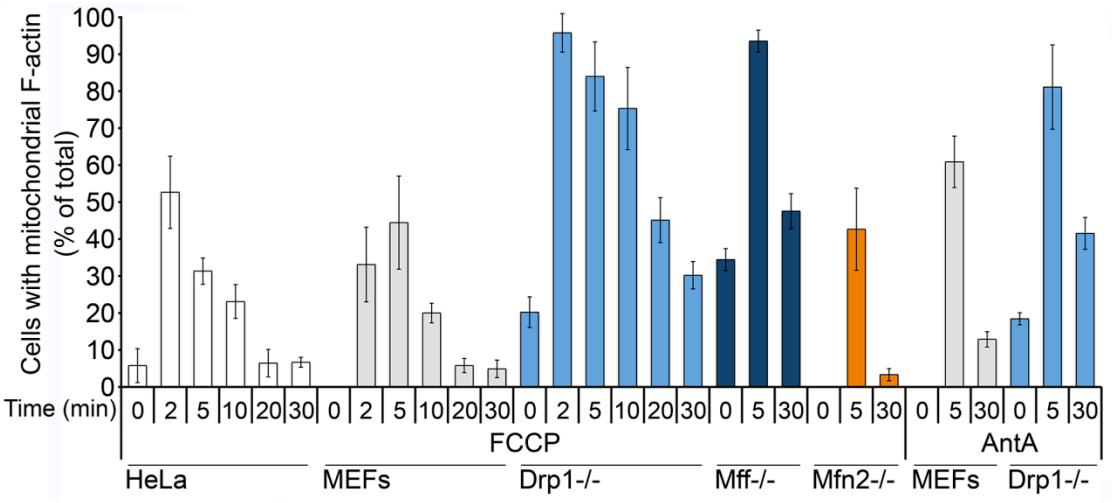

Figure 2.9 Quantitative analysis of the number of cells showing mitochondrial accumulation of F-actin. Wild type, Drp1$^{-/-}$, Mff$^{-/-}$ and Mfn2$^{-/-}$ MEFs, as well as HeLa cells, were treated with FCCP or AntA as indicated in the figure followed by immunofluorescence and structured illumination imaging. Cells with mitochondrial F-actin were counted. Means ± average deviation (AvDev) of triplicate counting of 150 cells/condition are shown.

Subsection 3: *de novo* actin polymerization is required for mitochondrial fission

We tested whether mitochondrial fission requires *de novo* actin polymerization. We utilized Latunculin B (LatB), an actin polymerization inhibitor, to prevent *de novo* F-actin assembly. Considering the toxicity of LatB, we treated the wild type MEFs with LatB for 32 min, then immunostained with cytochrome c and Alexa-Phalloidin. The data showed that LatB-treated wild type MEFs did not exhibit any unusual mitochondrial morphology (Fig. 2.10B). We also tested the degree to which LatB treatment could prevent stress-induced mitochondrial fission. Wild type MEFs were pretreated with LatB for 2 min, followed by the addition of Drp1-dependent mitochondrial fission inducer FCCP for 30 min. After treatment, cells were immunostained with anti-cytochrome c mAb and Alexa-Phalloidin, followed by

structured illumination imaging as well. Cells pretreated with LatB showed normal mitochondrial tubules, rather than mitochondrial fragmentation observed in FCCP only treated cells, suggesting that FCCP-induced mitochondrial fission was inhibited by LatB (Fig. 2.10C).

We quantified the percentage of cells with different mitochondrial phenotypes in FCCP, AntA, LatB, LatB+FCCP, and LatB+AntA treated wild type MEFs. Cells with distinct mitochondria phenotype including tubular (white), fragmented (orange) and swollen (blue) were counted. FCCP treatment induced a gradual increase of percentage of cells with fragmented mitochondrial from about 5% to about 70%, likewise AntA treatment led to about 45% of cells exhibiting fragmented mitochondria. While LatB did not affect mitochondrial phenotype after 30 min treatment, pretreatment of LatB followed by additional either 30 min FCCP or AntA dramatically decreased the percentage of cells with fragmented mitochondria (Fig. 2.11). In sum, these data demonstrate that F-actin polymerization is required in the stress-induced mitochondrial fission process.

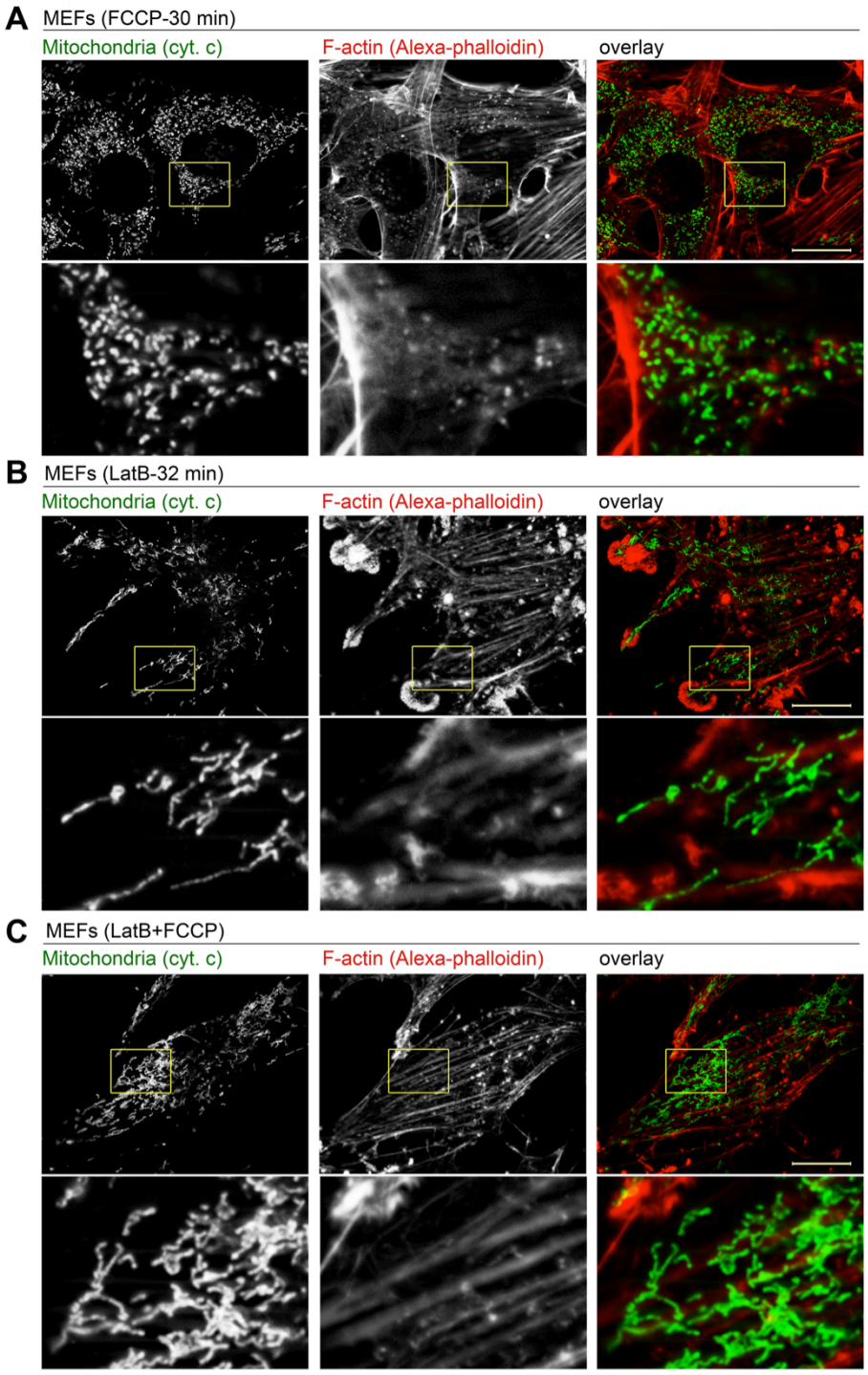

Figure 2.10 LatB pretreatment inhibited FCCP-induced mitochondrial fission. Wild type MEFs (A-C) were treated with FCCP for 30 min (A), LatB for 32 min (B), or pretreated with LatB for 2 min, followed by addition of FCCP for additional 30 min (C). Cells were labeled with Alexa-Phalloidin to detect F-actin (red on overlay image) and immunostained with anti-cytochrome mAb (green on overlay image) to detect mitochondria. Bars: 20 μm; (detail) 5 μm.

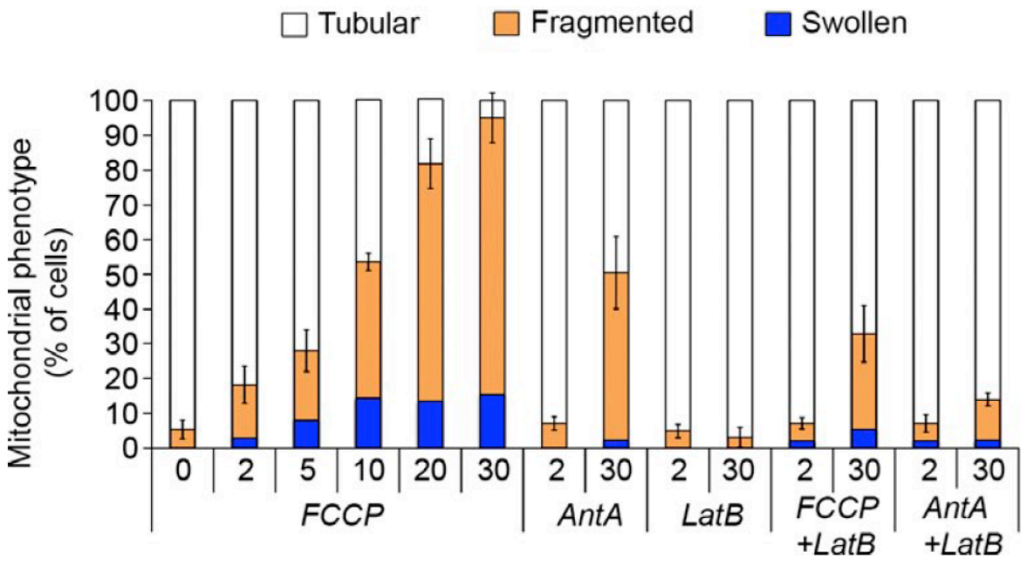

Figure 2.11 Quantitative analysis of mitochondrial morphological phenotypes in FCCP/AntA treated cells with LatB pretreatment. Wild type MEFs with indicated treatment for certain time points as indicated. Means ± AvDev from a representative experiment after triplicate counting of 150 cells/condition are shown.

Subsection 4: Mitochondrial assembly of F-actin in mitotic cells

Apart from stress-induced mitochondrial fission, the possibility that F-actin could also translocate to the mitochondria during physiological non-drug induced mitochondrial fission was also investigated. Interconnected mitochondrial networks become fragmented in mitotic cells in a Drp1-dependent manner, facilitating stochastic mitochondrial segregation into two daughter cells. To test whether mitochondrial accumulation of F-actin also occurs during mitosis, we utilized double thymidine block to synchronize cells in G_1/S phase of the cell cycle. HeLa cells were treated with 2 mM thymidine for 18 hours, and then released to normal growth medium for 9 hours, followed by an additional 18 hours treatment of 2 mM thymidine to synchronize cells to G_1/S checkpoint. Afterwards, cells were released into

thymidine-free medium to restart cell cycle progression, then fixed at different time points after release for up to 10 hours and immunostained with Alexa-Phalloidin, anti-cytochrome c mAb, and DAPI (4'6-diamidino-2-phenylindole) to detect DNA, followed by structured illumination imaging. Spatial relation of F-actin and mitochondria of cells in different stages of mitosis were analyzed. Cells in anaphase (Fig. 2.12A), in which chromosomes are split and the sister chromatids move to opposite poles of the cell, and prophase (Fig. 2.12B), in which chromatin condenses into chromosomes, revealed that F-actin probe Alexa-Phalloidin were aligned along mitochondrial labeled cytochrome c. Percentage of cells with mitochondrial F-actin (grey) and mitochondrial fragmentation (white) were calculated (Fig. 2.13). Although mitochondrial fragmentation was apparent in about 80% of metaphase cells and about 85% of these cells showed mitochondrial association of F-actin cytoskeleton, mitochondrial assembly of F-actin was also detectable in about 95% of prophase cells, about 45% of which displayed mitochondrial fragmentation (Fig. 2.13). Thus, it appears that in a similar manner as in stress-induced mitochondrial fission, mitochondrial assembly of F-actin also precedes mitochondrial division in mitotic cells.

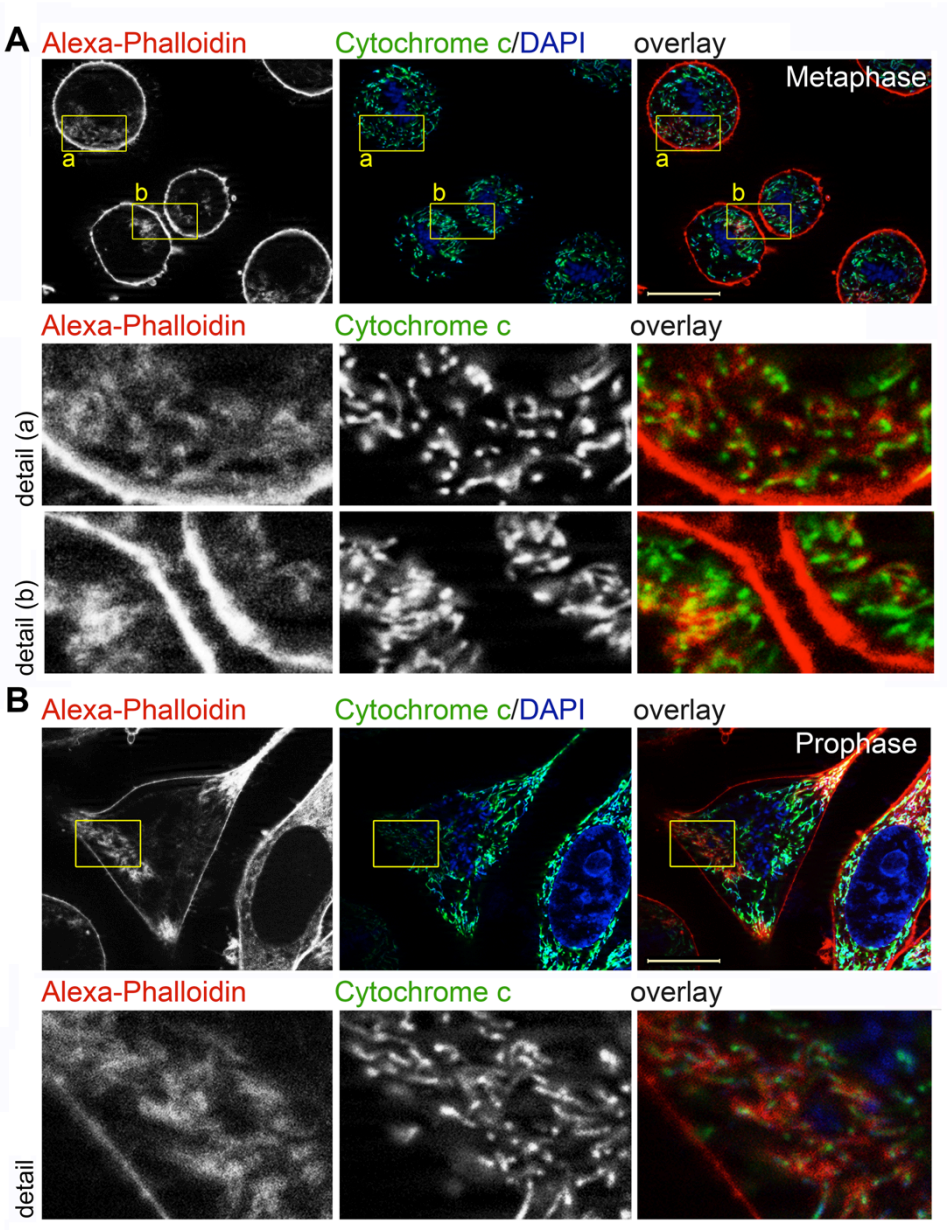

Figure 2.12. Spatial relations of F-actin and mitochondria in mitotic cells. HeLa cells were synchronized in G_1/S phase of the cell cycle using a double thymidine block procedure and subsequently released into thymidine-free medium to restart the cell cycle progression. Cells were fixed at 8.5 hours after release and stained with anti-cytochrome c mAb (A and B overlay images; green; to reveal mitochondria), Alexa-Phalloidin (A and B overlay images; red; to reveal F-actin), and DAPI (A and B overlay images; blue, to reveal DNA), followed by structured illumination imaging. The examples of anaphase (A) and prophase (B) cells that were identified based on the chromosomal status and distribution are shown. Higher magnifications of insets marked with yellow rectangles in A and B are shown in detail images. Bar: 20 μm; (detail) 5 μm.

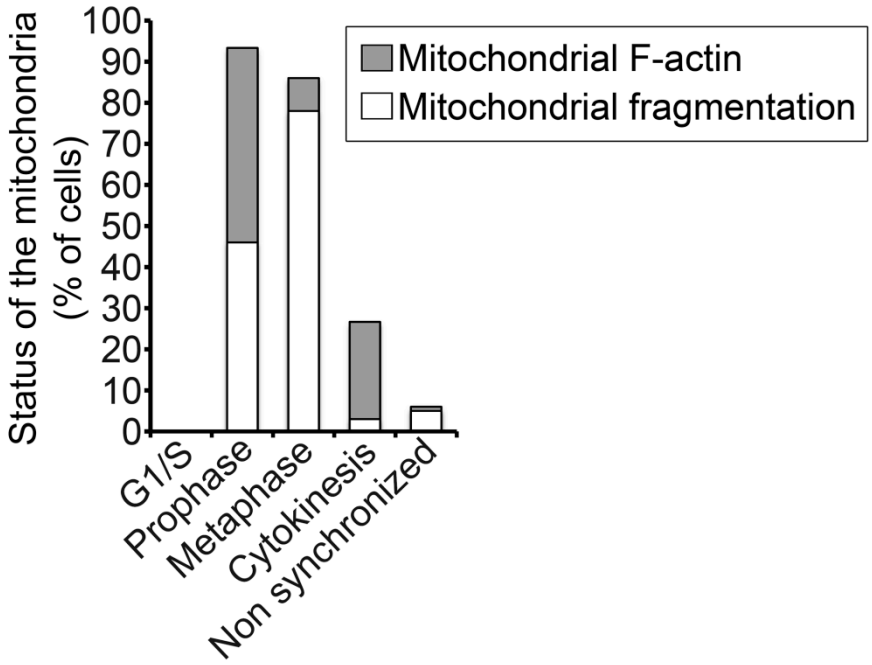

Figure 2.13 Quantitative analysis of the number of cells with mitochondrial assembly of F-actin and mitochondrial morphology in mitotic progression. HeLa cells were synchronized in G_1/S phase of the cell cycle using a double thymidine block procedure and subsequently released into thymidine-free medium to restart the cell cycle progression. Cells in different stages of mitosis were analyzed for mitochondrial F-actin and mitochondrial morphology. Data represent quantification of about 70 cells per mitotic stage.

Subsection 5: Submitochondrial localization of F-actin

In order the further characterize F-actin network colocalizing with the mitochondria, we examined the sub-mitochondrial localization of F-actin, in detail. Wild type, Drp1$^{-/-}$ and Mfn2$^{-/-}$ MEFs were treated with FCCP for 2 min, fixed and immunostained with Alexa-Phalloidin to detect F-actin and anti-cytochrome c mAb to detect mitochondrial intermembrane space, inner mitochondrial membrane (IMM) and mitochondrial cristae. Analyses of FCCP-treated wild type (Fig. 2.14A), Drp1$^{-/-}$ (Fig. 2.14C) and Mfn2$^{-/-}$ (Fig. 2.14E) revealed that F-actin did not colocalize with the cytochrome c-positive IMM, IMS or mitochondrial cristae, but rather formed

cytochrome c circumscribing rings. These results were further confirmed by the fluorescence linescans analysis (Fig. 2.14B, D, F). Considering the patterns of F-actin colocalization with mitochondria are similar in wild type, Drp1$^{-/-}$ and Mfn2$^{-/-}$ MEFs, it appears that Drp1 does not affect F-actin distribution on mitochondria in FCCP-induced mitochondrial fission model. Furthermore, immunofluorescence analysis and fluorescence linescans revealed that Alexa-Phalloidin colocalized with Tom20 (Fig. 2.14G, H), further indicating that mitochondrial F-actin accumulates on the OMM. The OMM localization of F-actin points to a possible crosstalk between F-actin and OMM proteins during mitochondrial fission.

Drp1 and Mff are two essential mitochondrial fission factors. When Drp1 is activated, it is recruited to OMM through the integration with Mff, which acts as a Drp1 receptor on mitochondria (Otera et al. 2010). Mitochondrial Drp1 forms submitochondrial foci with Mff at prospective fission sites. Given the possibility that OMM-localized F-actin could interact with OMM-associated Drp1 and/or Mff, we analyzed the degree to which F-actin colocalized with these proteins Wild type MEFs were treated with FCCP for 2min, fixed and then immunostained with Alexa-Phalloidin and anti-Drp1 or anti-Mff antibodies. While Drp1 and Mff formed submitochondrial foci, Alexa-Phalloidin revealed an equal F-actin distribution along the mitochondria with no specific colocalization with Drp1 and Mff (Fig. 2.15), suggesting that F-actin does not accumulate on Drp1/Mff positive mitochondrial membrane constriction sites.

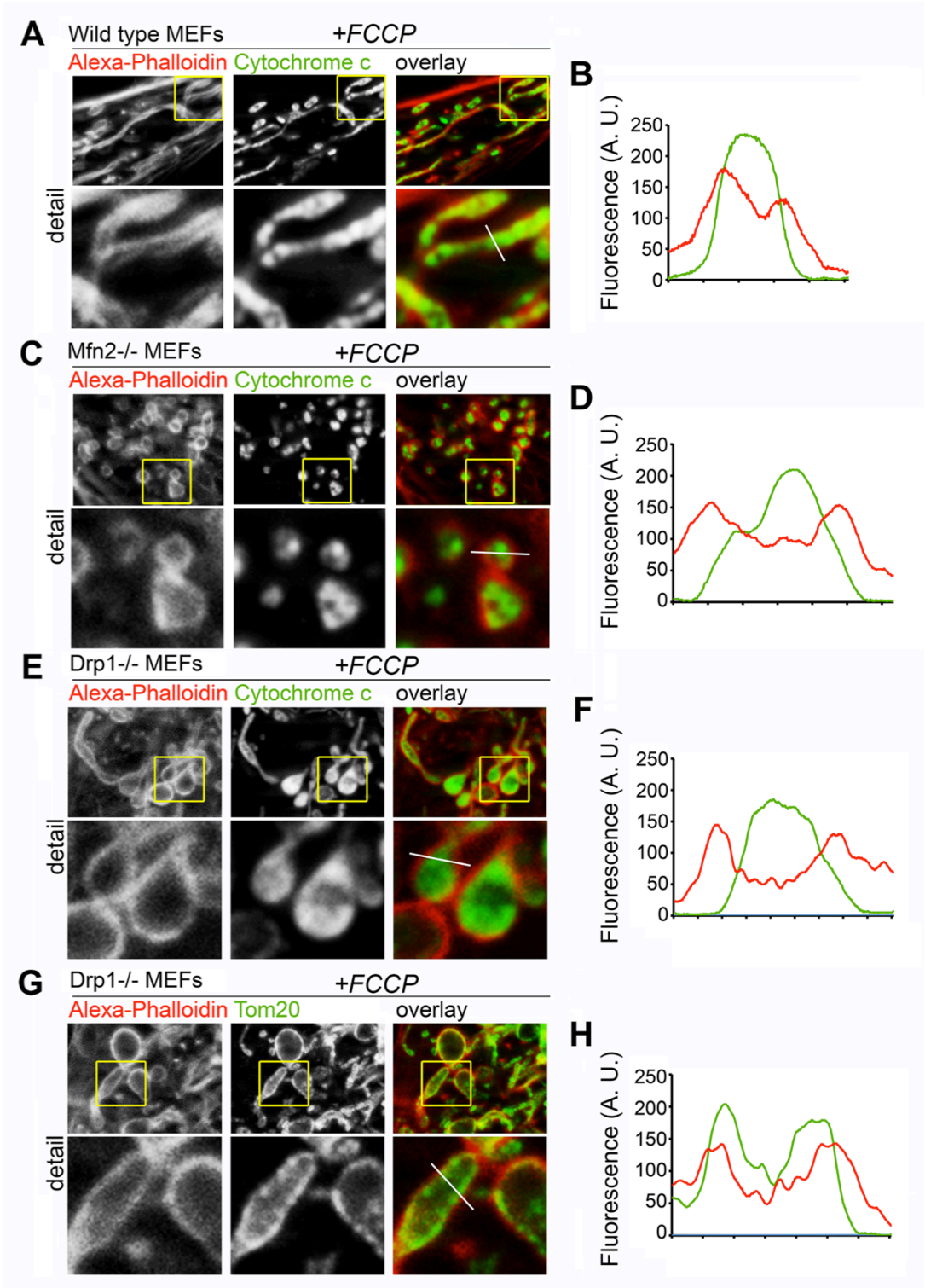

Figure 2.14 Submitochondrial distribution of F-actin networks. Wild type (A), Mfn2$^{-/-}$ (C), and Drp1$^{-/-}$ (E and G) MEFs were treated with FCCP for 2 min, followed by immunostaining with Alexa-Phalloidin to detect F-actin (red on overlay image), anti-cytochrome c mAb to detect mitochondrial intermembrane

(Continued) space, mitochondrial inner membrane and mitochondrial cristae (A, C, E), or anti-Tom20 antibody to detect outer mitochondrial membrane (G) (green on overlay image). Higher magnifications of insets marked with yellow rectangle are shown in detail images. Linescans of fluorescence intensity are shown in B, D, F, H. Bar: 20 μm; (detail) 5 μm.

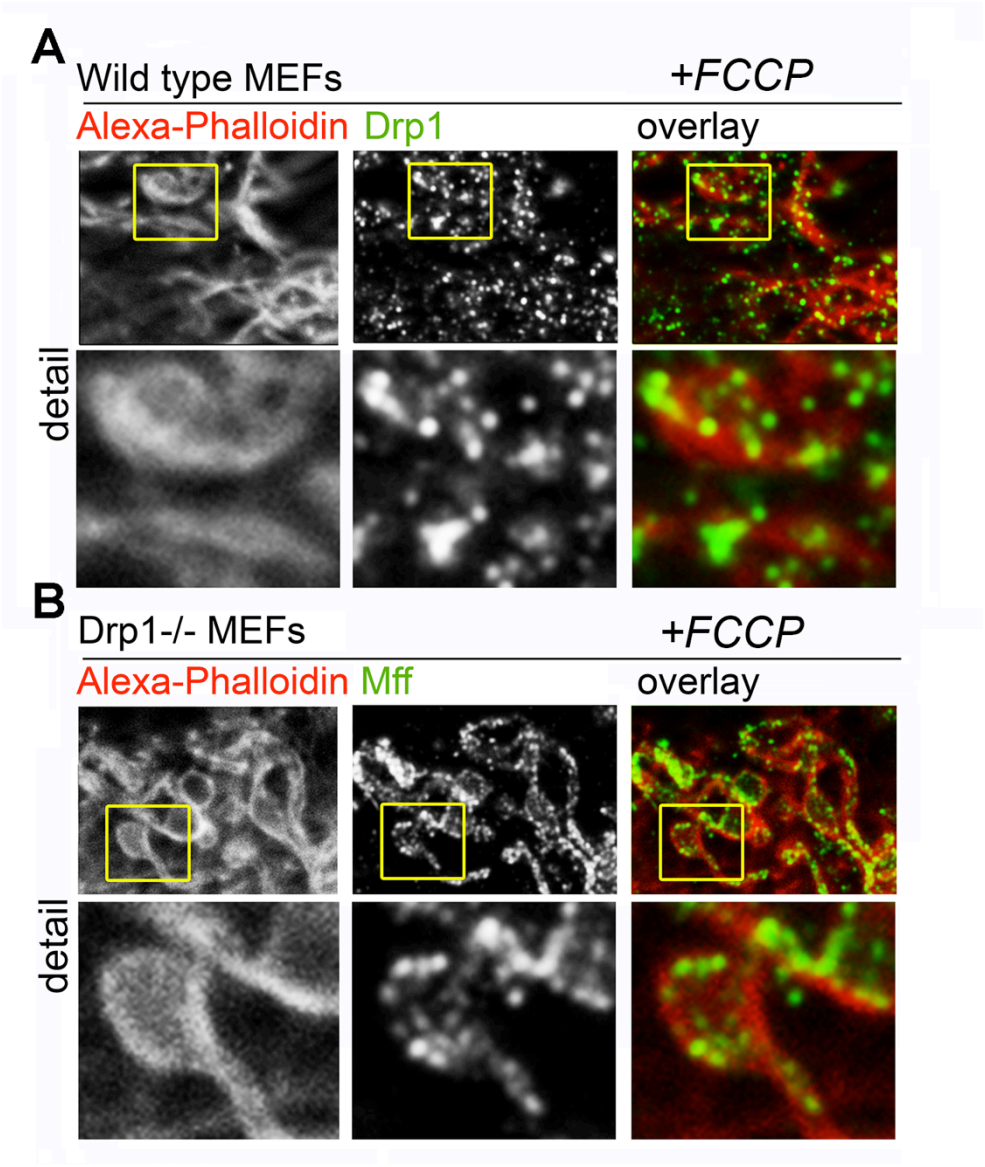

Figure 2.15 F-actin did not form submitochondrial foci. Wild type (A) and Drp1$^{-/-}$ (B) MEFs were treated with FCCP for 2 min, fixed and immunostained with Alexa-Phalloidin (A and B) (red on overlay image), anti-Drp1 (A) or anti-Mff (B) antibodies (green on overlay image), followed by structured illumination imaging. Higher magnifications of insets marked with yellow rectangle are shown in detail images. Bar: 20 μm; (detail) 5 μm.

Subsection 6: Mitochondrial accumulation of F-actin in living cells

To further verify mitochondrial assembly of F-actin independently, we utilized fluorescent actin probes and performed live cell time-lapse imaging. Lifeact is a 17 amino acids peptide derived from the N-terminal domain of actin binding protein 140 (Abp140), which specifically stained F-actin structures in eukaryotic cells and tissues. It has been shown that fluorescent protein-tagged Lifeact interacted with F-actin with about 30 times greater affinity than with G-actin, enabling visualization of local F-actin polymerization associated with various cellular pathways. Another benefit of Lifeact is that it does not interfere with actin dynamics *in vitro* and *in vivo*, which makes it an ideal tool to visualize F-actin cytoskeleton in live cell imaging (Riedl et al. 2008). HeLa cells cotransfected with mRuby-Lifeact and mito-YFP were treated with FCCP to induce mitochondrial fission, followed by time-lapse microscopy. These imaging experiments revealed that mitochondrial accumulation of mRuby-Lifeact was detectable at about 4 min, with a gradual decline in mitochondrial levels of mRuby-Lifeact at about 12 min after initial detection (Fig. 2.16 and 2.17). These data further confirmed the transient nature of the mitochondrial translocation of F-actin. Furthermore, the diffused OMM localization pattern of the mRuby-Lifeact (Fig. 2.18B) was reminiscent of that observed in Alexa-Phalloidin labeled fixed cells. Similar dynamics of F-actin assembly on the OMM was also detected in HeLa cells expressing dominant negative mutant $Drp1^{K38A}$ (Fig. 2.19, Fig. 2.20 and Fig. 2.21). Another live cell actin probe, the caplonin homology domain of utrophin (UtrCH), was also applied to further verify mitochondrial assembly of F-actin. UtrCH is able to bind specifically to F-actin without stabilizing it in *in vitro* dilution assays. It has been

shown that UtrCH interacted with F-actin in both fixed and living cells with no discernible effects on the actin cytoskeleton. HeLa cells cotransfected with mCherry-UtrCH and mito-YFP were treated with FCCP followed by time-lapse imaging. In a similar manner as mRuby-Lifeact, mCherry-UtrCH accumulated on the mitochondria in FCCP-treated cells at ~ 2-4 min after addition of FCCP and disappeared after 16 min FCCP treatment (Fig. 2.22 and Fig. 2.23).

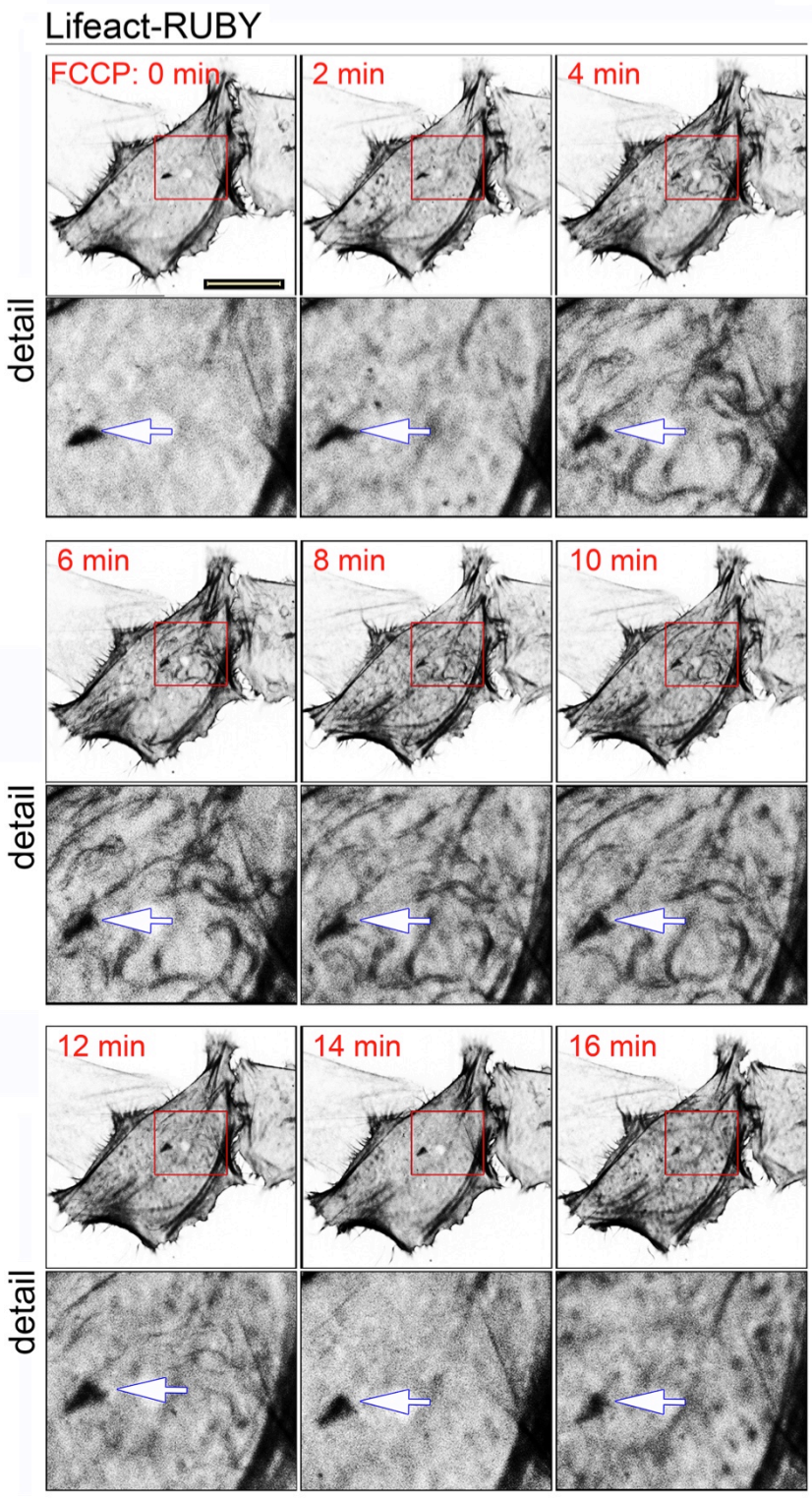

Figure 2.16 Mitochondrial assembly of F-actin in living cells. HeLa cells expressing mRuby-Lifeact and mito-YFP were treated with FCCP as indicated, followed by a time-lapse structural illumination imaging. Fluorescence images of mRuby-Lifeact are shown. To enable easier interpretation of the data, fluorescent images were inverted. Arrows indicate F-actin-positive structures that are not altered by FCCP treatment. Bar: 20 μm; (detail) 5 μm.

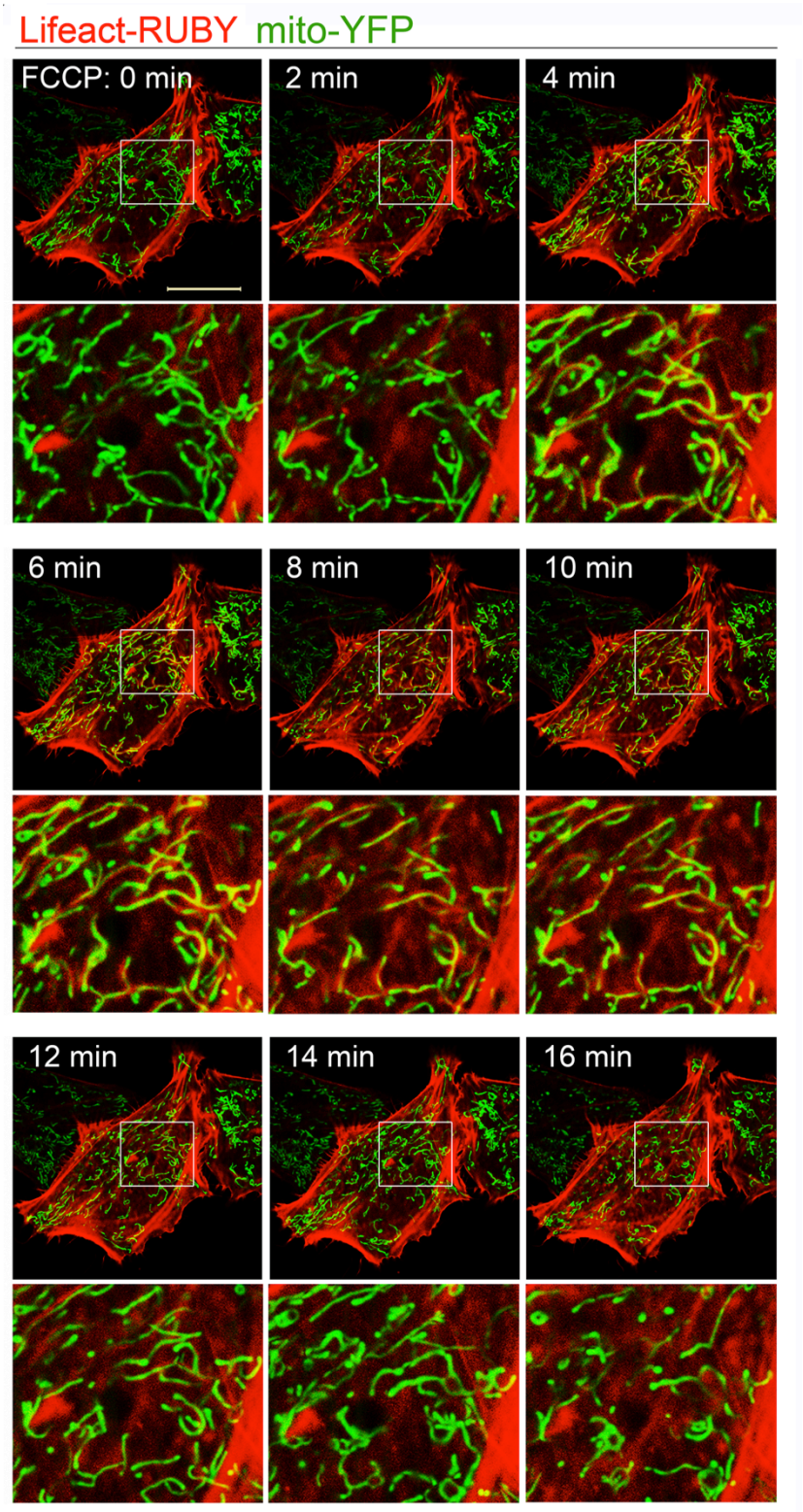

Figure 2.17 Mitochondrial assembly of F-actin in living cells (continued). HeLa cells expressing mRuby-Lifeact (red on the overlay image) and mito-YFP (green on the overlay image) were treated with FCCP as indicated, followed by a time-lapse structural illumination imaging. Bar: 20 μm; (detail) 5 μm.

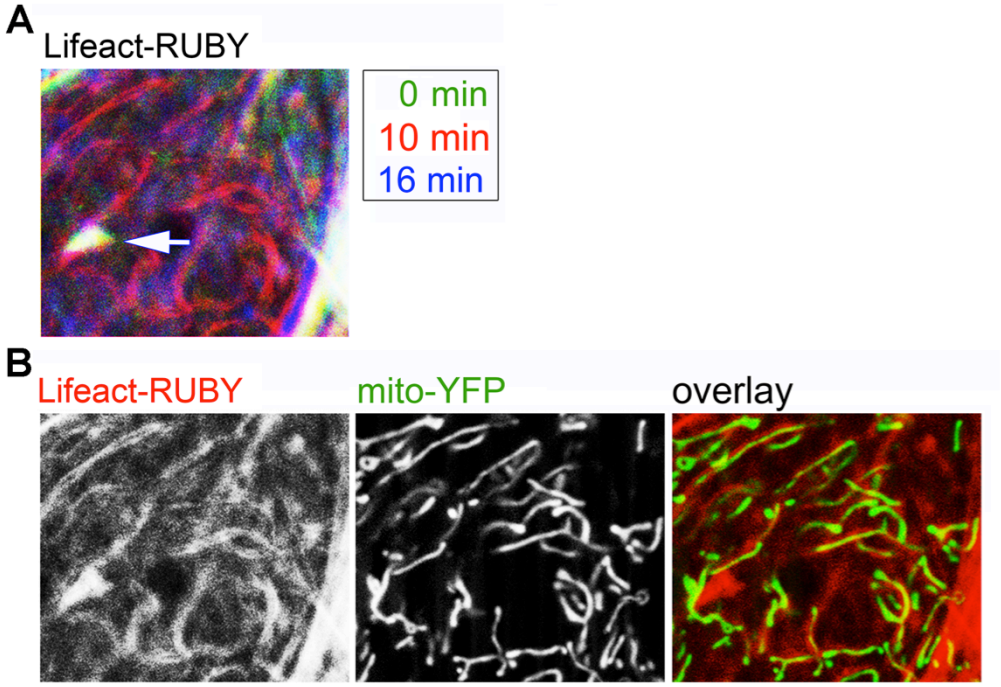

Figure 2.18 Mitochondrial assembly of F-actin in living cells (continued). HeLa cells expressing mRuby-Lifeact (red on the overlay image) and mito-YFP (green on the overlay image) were treated with FCCP as indicated, followed by a time-lapse structural illumination imaging. (A) Pseudocolored images showing the mitochondrial F-actin assembly at 0 min (green), 10 min (red), and 16 min (blue) after addition of FCCP within the red rectangle shown in Fig. 2.17. Arrows indicate F-actin-positive structures that are not altered by FCCP treatment, which shows a white pseudocolored signal. (B) Details from marked area in the image taken at 10 min of FCCP treatment. Bars: 5 μm.

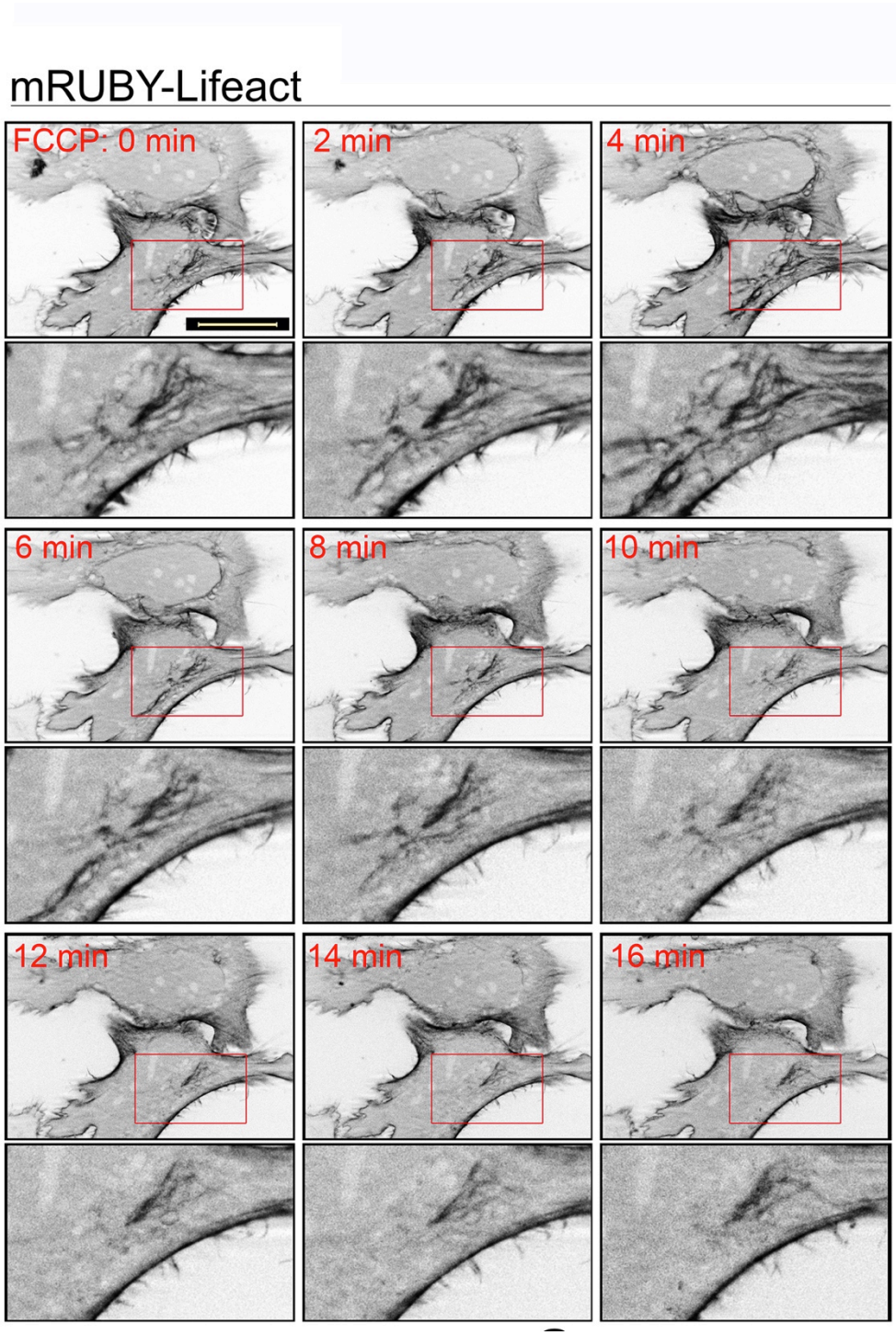

Figure 2.19 Mitochondrial assembly of F-actin in Drp1^{K38A}-expressing living cells. HeLa cells expressing Drp1^{K38A} (determined by mitochondrial morphology), mRuby-Lifeact and mito-YFP were treated with FCCP as indicated, followed by a time-lapse structured illumination imaging. Fluorescence images of mRuby-Lifeact are shown. To enable easier interpretation of the data, fluorescent images were inverted. Bars: 20 μm; (detail) 5 μm.

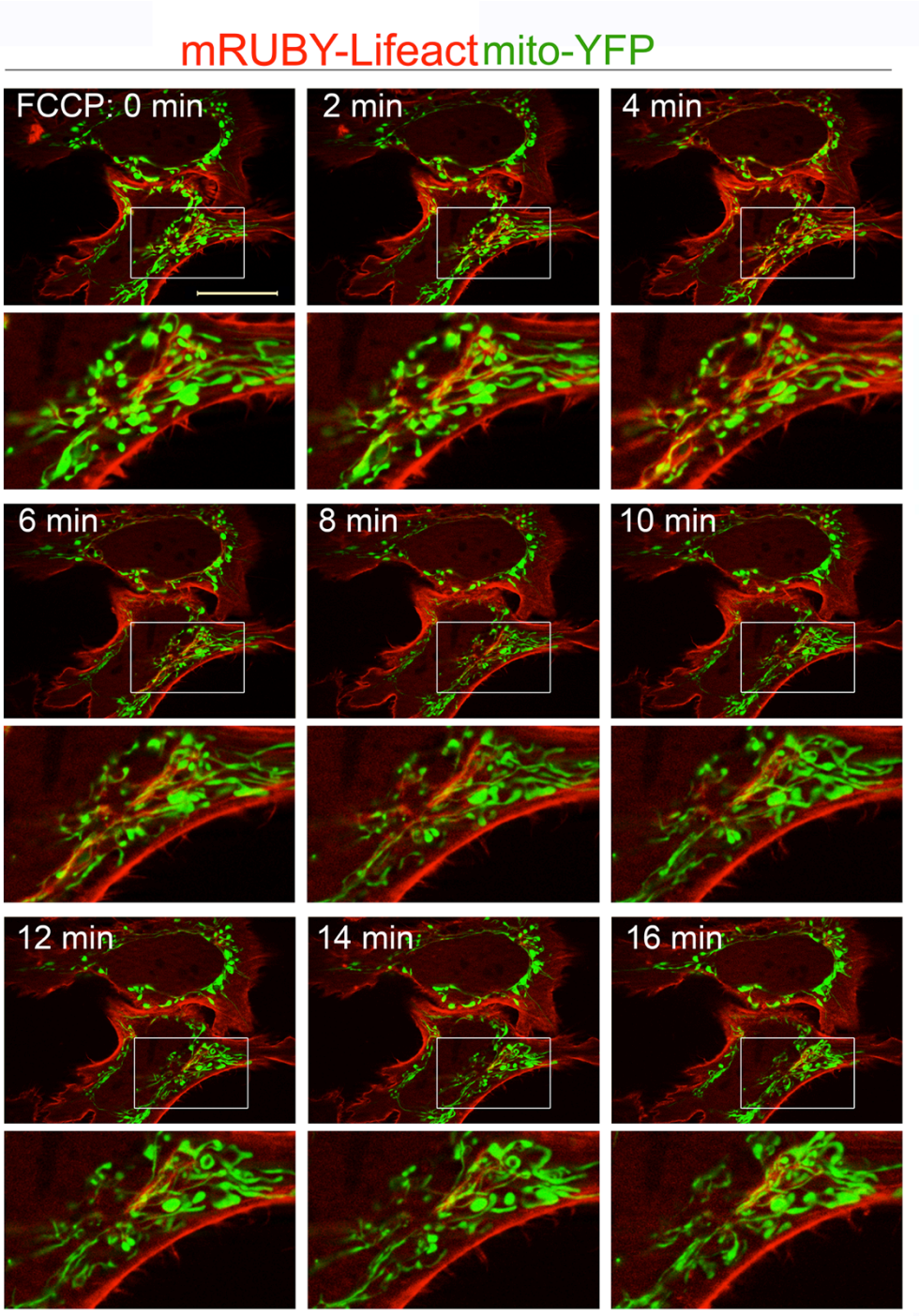

Figure 2.20 Mitochondrial assembly of F-actin in Drp1^{K38A}-expressing living cells (continued). HeLa cells expressing Drp1^{K38A} (determined by mitochondrial morphology), mRuby-Lifeact and mito-YFP were treated with FCCP as indicated, followed by a time-lapse structured illumination imaging. Fluorescence overlayed images of mRuby-Lifeact and mito-YFP are shown. Bars: 20 μm; (detail) 5 μm.

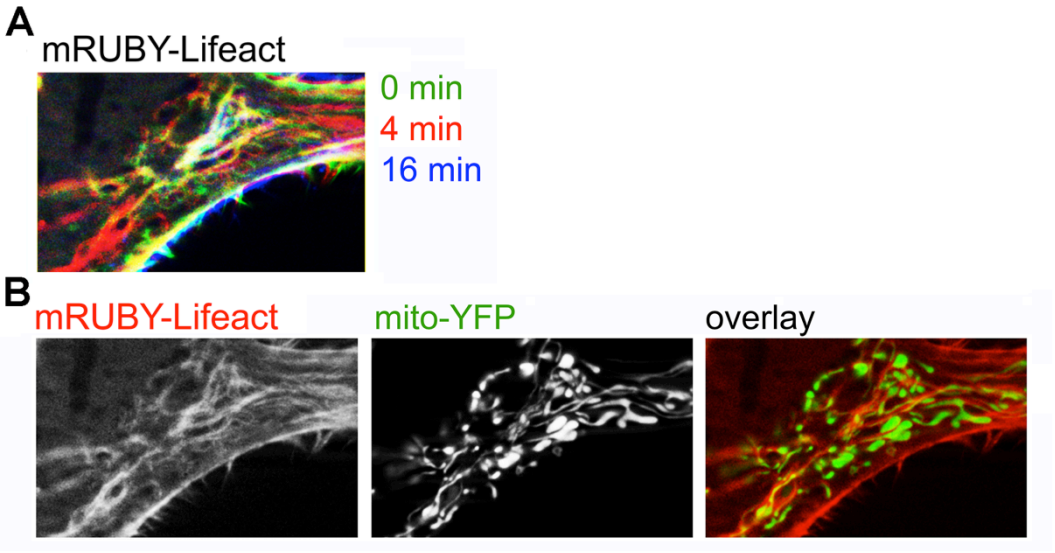

Figure 2.21 Mitochondrial assembly of F-actin in Drp1^{K38A}-expressing living cells (continued). HeLa cells expressing Drp1^{K38A} (determined by mitochondrial morphology), mRuby-Lifeact and mito-YFP were treated with FCCP as indicated, followed by a time-lapse structured illumination imaging. (A) Pseudocolored images showing the mitochondrial F-actin assembly at 0 min (green), 4 min (red), and 16 min (blue) after addition of FCCP within the rectangle area shown in Fig. 2.20. (B) Details from marked area in the image taken at 4 min (shown in Fig. 2.20) of FCCP treatment. Bars: 20 μm; (detail) 5 μm.

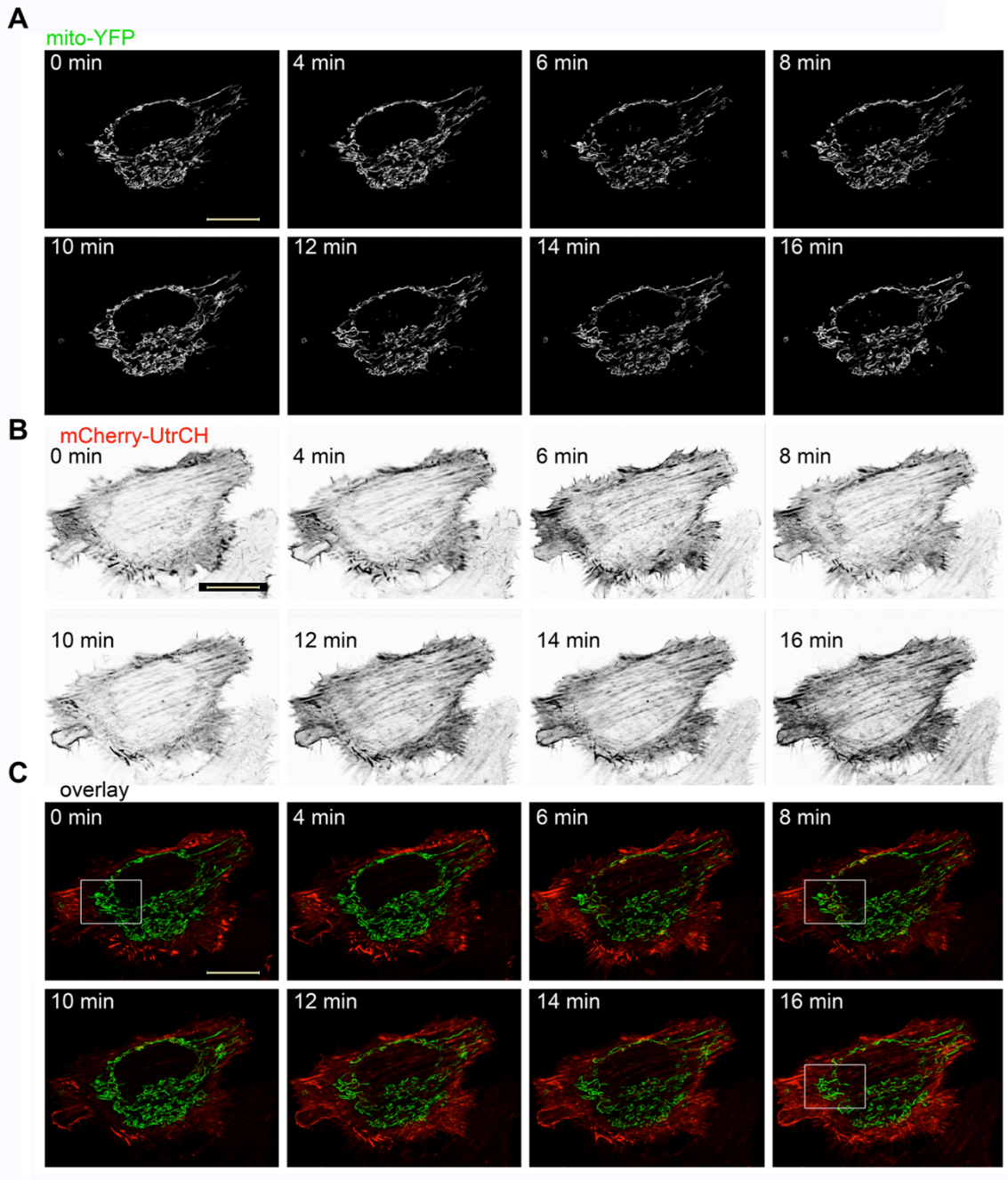

Figure 2.22 Mitochondrial assembly of mCherry-UtrCH in living cells. HeLa cells were transfected with mCherry-UtrCH (red on overlay images) and mito-YFP (green on overlay images) were treated with FCCP as indicated, followed by a time-lapse structured illumination imaging. (A) Fluorescence images of mito-YFP are shown. (B) Fluorescence images of mCherry-UtrCH are shown. To enable easier interpretation of the data, fluorescent images were inverted. (C) Fluorescence overlay images of mRuby-Lifeact and mito-YFP are shown. Bars: 20 μm; (detail) 5 μm.

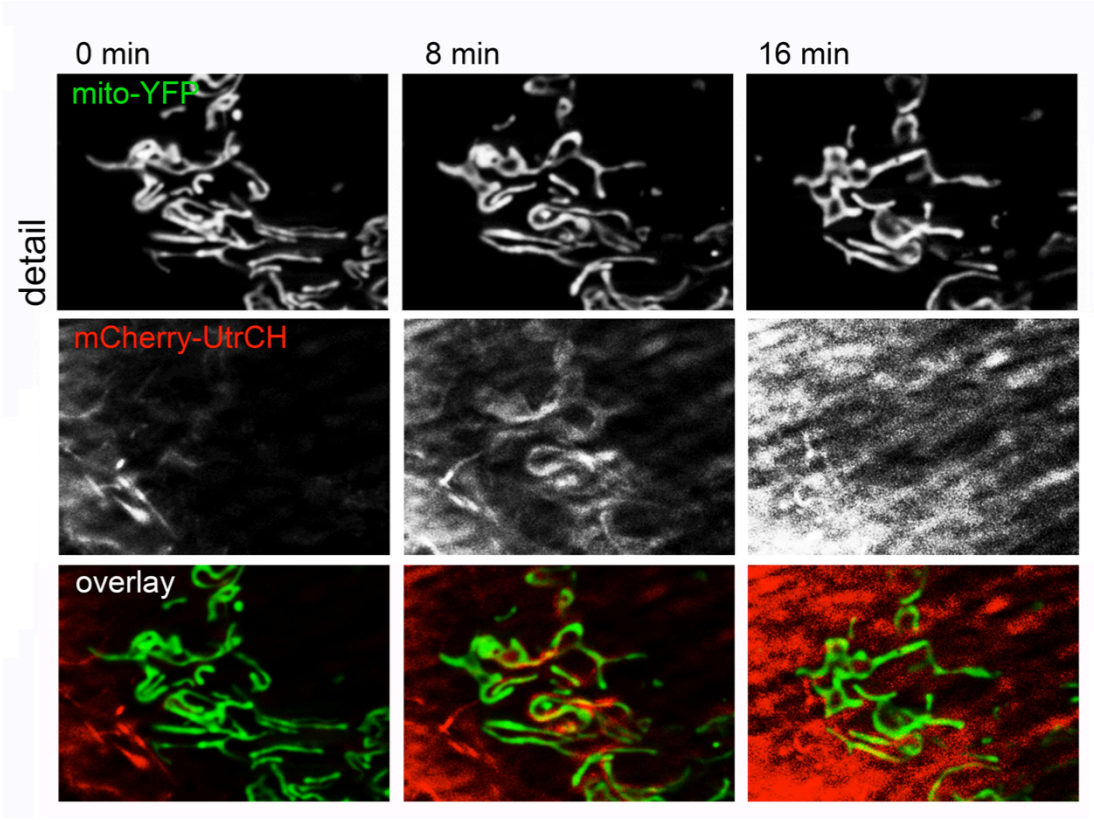

Figure 2.23 Mitochondrial assembly of mCherry-UtrCH in living cells (continued). HeLa cells expressing Drp1^{K38A} (determined by mitochondrial morphology), mRuby-Lifeact and mito-YFP were treated with FCCP as indicated, followed by a time-lapse structured illumination imaging. Detailed fluorescence images of the mitochondrial F-actin assembly at 0 min, 8 min, and 16 min after addition of FCCP within the rectangle area in Fig. 2.22 are shown. Bars: 20 μm; (detail) 5 μm.

Section 4: Discussion

In this chapter, we show that transient assembly of F-actin on the OMM plays a vital role for the control of Drp1-driven mitochondrial division. F-actin polymerization occurs on the OMM upon mitochondrial uncoupler FCCP induced mitochondrial fission in a Drp1-independent manner. Clarifying the molecular mechanism that coordinates mitochondrial assembly of F-actin with Drp1-dependent events of mitochondrial fission is critical. Other than Mff, mitochondrial fission

proteins MiD49/51 directly recruit Drp1 to the mitochondrial surface and high level overexpression of MiD49/51 led to sequestering Drp1 from functioning at mitochondria, resulting in mitochondrial abnormal accumulation of inactive Drp1 and extensive mitochondrial tubules (Palmer et al. 2011b). These data suggest that overexpression of MiD49/51 does not impair the translocation of Drp1, but rather hinders Drp1 activity. In addition, high-level overexpression of MiD51 led to F-actin association with extensive mitochondrial tubules, further suggesting that mitochondrial F-actin disassembly coordinates with mitochondrial Drp1 activity. Supporting this notion, our data showed that F-actin accumulates on mitochondrial elongated tubules generated in cells expressing dysfunctional Drp1 or in the absence of Drp1. Together with previous reports, it is therefore plausible that mitochondrial F-actin dynamics coordinate with Drp1, as well as Drp1 receptors such as Mff and MiD49/51.

As described previously, both fixed-cell and live-cell imaging exhibit a transient mitochondrial F-actin accumulation upon FCCP treatment. A temporal model of actin assembly during FCCP induced Drp1-dependent mitochondrial fission in mammalian cells similar to endocytosis is proposed based on our data. Clathrin-mediated endocytosis is regulated by dynamin, which shares a similar domain organization and function with Drp1. In the early stage of endocytosis, clathrin and adaptors are recruited to the endocytic sites to initiate membrane curvature in the first 1-2 min of the process. Afterwards, it takes about 15-25 seconds for the actin network and its nucleators to accumulate at the bud, then the invagination elongates, followed by dynamin recruitment and membrane fission (Mooren et al. 2012). In our study, we

found that F-actin polymerizes on mitochondria upon 2 min FCCP treatment, in a similar timeframe of actin network polymerization in endocytic sites. While the initiation of membrane curvature may not be dependent on actin according to EM studies, it is still unclear whether mitochondrial fission sites are determined and generated prior to actin polymerization. Upon initial polymerization, mitochondrial F-actin patterns were presented for about 10 min before deploymerization, compared with only around 20 second of F-actin appearance at endocytic sites during clathrin-mediated endocytosis. While a complete operation of clathrin-mediated endocytosis takes only a few minutes, the time duration of FCCP-induced mitochondrial fission process is usually 20-30 min. This temporal deviation may be due to the size difference between cargo molecules and organelles. Actin may be needed for multiple stages in mammalian clathrin-mediated endocytosis, including invagination, tubule elongation and membrane fission. According to the time profiles of live-cell imaging and quantification of fixed-cell experiments, mitochondrial F-actin disassembles before the occurrence of Drp1 mediated membrane scission events, further suggesting that F-actin possibly assists Drp1 during tubules elongation and constriction, but not the final step of membrane fission.

The initiation of membrane curvature is sensed by BAR (Bin-Amphiphysin-Rvs) domain superfamily proteins, which contains a highly conserved coil-coil protein dimerization domain and can be further categorized as BAR/N-BAR (N-terminal amphipathic helix preceding the BAR domain) proteins, F-BAR (Fes/CIP4 homology-BAR domain) proteins, and I-BAR (inverse BAR) proteins. During clathrin-mediated endocytosis in mammalian cells, BAR/N-BAR proteins are

recruited to invaginated buds and preferentially bind to highly curved membranes and induce curvature in cells to promote and stabilize tubulation (Frost et al. 2009). In addition, BAR/N-BAR proteins also stimulate Arp2/3-mediated actin network assembly at endocytotic sites. Synaptic enriched BAR-domain containing protein Tuba is able to bind to dynamin, as well as various actin regulatory protein including N-WASP and Ena/VASP and promotes actin assembly through the C-terminal SH3 domain. Another major binding partner of dynamin SNX9 was also reported to directly regulate F-actin nucleation through N-WASP and the Arp2/3 complex and couples actin assembly to phosphoinositide signals in membrane remodeling during endocytosis (Ferguson et al. 2009). Although several BAR domain proteins have been reported to be involved in clathrin-mediated endocytosis, only one BAR domain protein called endophilin B1 is required for the maintenance of mitochondrial morphology. Downregulation of endophilin B1 or overexpression of endophilin B1 lacking the NH_2 terminal lipid-modifying domain alters mitochondrial morphology and distribution. Cytosolic endophilin B1 also translocates to the mitochondria during apoptosis stimuli induced membrane remodeling (Karbowski, Jeong, et al. 2004). Considering the role of BAR-domain proteins in stimulating actin assembly in endocytosis, it is possible that endophilin B1 senses the membrane curvature and subsequently initiate actin polymerization on mitochondria in the very early stage of mitochondrial fission. Double knockdown of endophilin B1 and Drp1 leads to mitochondrial elongation that is identical to Drp1 single knockdown suggesting that Drp1 acts upstream of endophilin B1 (Karbowski, Jeong, et al. 2004), which can be explained by the dual function of BAR-domain proteins during membrane remodeling.

Quantitative analysis of the time profiles for protein recruitment of various proteins revealed that an F-BAR protein FBP17 showed biphasic recruitment and peaked after scission (Mooren et al. 2012), supporting the notion that Drp1 works upstream of endophilin B1 during mitochondrial fission. Considering that BAR domain proteins are able to interact with dynamin and actin regulatory protein N-WASP and the biphasic recruitment profiles, it appears that in mammalian cells BAR-domain proteins contributes to membrane scission beyond initiating membrane curvature.

Mitochondrial membrane constriction and scission during fission occurs through Drp1-dependent oligomerization and GTP hydrolysis (Ingerman et al. 2005). However, how transient F-actin assembly on the mitochondria contributes to mitochondrial fission is still unclear. Biochemical interactions between dynamin and actin cytoskeleton are mediated by actin binding proteins, as well as BAR domain proteins (Gu et al. 2010a; Gu et al. 2014), suggesting that dynamin may couple the actin network to mitochondrial fission. One possible mechanism is that actin cytoskeleton may contribute to membrane constriction and scission. Stalled clathrin pits resulting from actin inhibitors did not recruit dynamin, implying that actin may generate membrane tension to assist dynamin mediated membrane constriction. Further supporting this notion, a role of myosin II in mammalian mitochondrial fission has been reported (Korobova et al. 2014b). Pharmacological inhibition or downregulation of actin motor protein Myosin II increased mitochondrial length in U2OS cells and decreased mitochondrial associated Drp1. Immunofluorescence analysis revealed that Myosin II was present at mitochondrial constriction sites. Considering that Myosin II functions to generate powerful contractile forces, these

data indirectly point to a role of actin and myosin II in assisting Drp1-driven membrane constriction. In addition, myosin I and VI were recruited to sites of clathrin-mediated endocytosis as part of the dynamin module (Geli et al. 1998; Kirchhausen et al. 2014), providing further evidence that actin cytoskeleton may assist dynamin mediated membrane constriction and subsequent scission by myosin generated force. Furthermore, FRET analysis revealed that dynamin oligomerization was inhibited by pharmacological inhibition of actin polymerization (Ferguson & De Camilli 2012), suggesting that mitochondrial actin network polymerization may also promote Drp1 polymerization during fission processes.

Chapter 3: Actin-modifying proteins contributes to Actin cytoskeleton-dependent mitochondrial fission

Publication: Sunan Li, Shan Xu, Brian A. Roelofs, Liron Boyman, W. Jonathan Lederer, Hiromi Sesaki, and Mariusz Karbowski. Transient assembly of F-actin on the outer mitochondrial membrane contributes to mitochondrial fission. 2015. 208(1): 109-123.

Section 1: Introduction

F-actin polymerization requires the appropriate function of actin nucleating proteins. Based on the structure of actin filaments, actin nucleating proteins fall into three main categories: (1) Arp2/3 complex and nucleating promoting factors (NPFs), (2) tandem monomer binding nucleators and (3) formins (Campellone & Welch 2010). Arp2/3 complex consists of actin-related proteins Arp2 and Arp3 and five additional subunits ARPC1-5. Arp2/3 complex activation requires both the binding to the sides of mother actin filaments and NPFs, featuring both G-actin binding WH2 and Arp2/3 complex binding domains. Upon activation, Arp2/3 complex creates a new nucleation core and grows newly synthesized actin filaments on the old ones to form a functional branched actin network (Rotty et al. 2013). Tandem-monomer-binding nucleators, a recently identified group including Spire, Cordon-bleu (Cobl), Leiomodin (Lmod-2), JMY and andenomatous polyposis coli (APC), possess tandem repeats of G-actin binding motifs. These nucleators bring G-actin monomer together to form a polymerization nucleus and stabilize either the actin-monomers along the long-pitch helix or cross-filament interactions along the short-helix of actin filament (Firat-Karalar & Welch 2011). Formins are multi-domain proteins that dimerize to

nucleate and elongate actin filaments. Formins bear conserved formin homology 1 (FH1) and FH2 domains. The homodimeric FH2 domain forms a ring structure to catalyze actin nucleation by stabilizing actin dimers. The proline-rich linear FH1 domain stimulates the elongation of actin filaments by binding to profilin-bound G-actin and deliver it to the barbed end (Zigmond 2004).

Arp2/3 complex and NPFs are the major actin nucleators found at endocytosis sites and various other membrane trafficking events (Mooren et al. 2012; Lanzetti 2007; Grassart et al. 2014). The Arp2/3 complex is the key regulator for actin filament assembly at endocytic sites in yeast and mammalian cells. Loss of WASp inhibits endocytosis and reduces the frequency at which actin accumulates at sites of endocytosis (Benesch et al. 2005), suggesting that activation of Arp2/3 complex at endocytic sites requires the presence of Class I NPF WASp. Class II NPF cortactin binds to the Arp2/3 complex via SH3 domain and actin via tandem cortactin repeats, in order to stabilize Arp2/3 dependent actin filament branching and promote actin filaments growth in clathrin-mediated endocytosis (Weaver et al. 2002). Cortactin can also interact with dynamin via a proline-rich region, serving as a bridge between actin cytoskeleton and the dynamin superfamily (Zhu et al. 2005). In addition, coronin family proteins are known to directly inhibit the Arp2/3 complex *in vitro* and synergize with cofilin to promote actin severing and disassembly (Cai et al. 2007). Cofilin-mediated severing provides positive ends on filament fragments, subsequently destabilizes the filament and preferentially promotes the release of ADP-actin monomer, further enhancing the dynamics of actin filament assembly as a long-lasting effect (De La Cruz 2009).

In the previous chapter, I discussed results supporting the role of transient F-actin assembly on the OMM in Drp1-mediated mitochondrial fission. However, the mechanism of mitochondrial F-actin assembly still remains unclear. In this chapter, I will discuss the evidence that FCCP-induced mitochondrial F-actin polymerization on the OMM is mediated by Arp2/3 complex and Class II NPF cortactin and actin severing protein cofilin.

Section 2: Materials and Methods

Subsection 1: Cell culture

HeLa cells, wild type mouse embryonic fibroblasts (MEFs), and $Drp1^{-/-}$ MEFs were provided by Dr. H. Sesaki from Johns Hopkins University (Wakabayashi et al. 2009). HeLa cells and MEFs were cultured in DMEM supplemented with 10% heat-inactivated fetal bovine serum, 2 mM Glutamax, 1 mM sodium pyruvate, 1 mM nonessential amino acids, 100 U/ml penicillin in 5% CO_2 at 37°C.

Subsection 2: General experimental methods

Transfection, immunofluorescence, image acquisition and live cell imaging were performed as described in Chapter 2 (section 2 Materials and Methods).

Subsection 3: Expression constructs and shRNA

GFP-tagged INF2 and $INF2^{A149D}$ were provided by H. Higgs (Dartmouth Medical School, Hanover, NH) (Korobova et al. 2013). MISSION shRNAi vectors were purchased from Sigma-Aldrich. Cortactin (TRCN0000294181, RNAi#1; TRCN0000294182, RNAi#2; and TRCN0000298256, RNAi#3), cofilin

(TRCN0000381606, RNAi#1; TRCN0000381418, RNAi#2; and TRCN0000381720, RNAi#3), gelsolin (TRCN0000343442, RNAi#1; TRCN0000343443, RNAi#2; and TRCN0000352869, RNAi#3), Arp2 (TRCN0000290833), p34 (TRCN0000379644), Opa1 (TRCN0000303506), and Mfn2 (TRCN0000082686) were downregulated with above-mentioned MISSION shRNAi vectors. eGFP targeting shRNAi construct was used as a control (SHC005). Cells were transfected with respective shRNAi constructs, and then 24 hours after transfection they were incubated with 3 μg/ml puromycin for an additional 4-5 days to select for transfected cells.

Subsection 4: Mitochondrial fusion assay

Mitochondrial matrix-targeted photoactivatable GFP (Mito-PAGFP)-based mitochondrial fusion assay was performed using a confocal microscope (LSM 510 META; Carl Zeiss) equipped with Plan-Apochromat 100x/1.4D oil DIC M27 objective lens (Carl Zeiss) as described previously (Karbowski, Arnoult, et al. 2004; Karbowski et al. 2006). Cells were transfected with mito-PAGFP for 18 hours, then incubated in Phenol-Red DMEM. In brief, after acquisition of a preactivation image, a 5-μm-diameter circular region of interest (ROI) was photoactivated by brief irradiation with 351/364-nm light (using Coherent Enterprise Ion Laser 80.0mW), followed by time-lapse imaging using 488-nm Argon Ion Laser excitation (25.0 mW set at 0.3%). 15 postactivation images were collected with the interval between images set to 2 min. To avoid z-section shift, focus was maintained using the "Multi-time Macro" and the autofocusing system (utilizing linescans to detect the reflection off the coverglass). Images were acquired and analyzed using ZEN 2009 image acquisition software (Carl Zeiss).

The diffusion rates of mito-PAGFP are likely to be similar to mito-GFP diffusion coefficients of 2-3 × 10^{-7} cm^2/s determined by spot photobleaching, which is only three- to fourfold less than that for GFP diffusion in water (Partikian et al. 1998). Due to the fast diffusion of GFP within the mitochondrial matrix, photoactivated PAGFP rapidly diffuses from the activated ROIs. The redistribution and dilution of mito-PAGFP fluorescence from the matrix of "photoactivated" mitochondria into nonactivated mitochondria that occurs as a result of mitochondrial membrane fusion is used to monitor and quantify this process. Images were analyzed by using region measurement tool to collect pixel intensities within activated ROIs as well as in nonactivated areas of the cell from all images in the series. The obtained values can then be plotted as a function of time (Karbowski et al. 2014).

Subsection 5: Western blot

Cells were harvested, and total cell protein lysates were prepared as previously described (Xu et al. 2011). In brief, cells were washed with ice-cold PBS, collected by scrapping, then centrifuged at 0.8rcf for 5 min. Cell pellets were resuspended in 1x SDS PAGE sample buffer, and incubated at 100°C for 10 min. Protein concentrations were measured directly in the samples using NanoDrop 1000 spectrophotometer (Thermo Fisher Scientific). Proteins were separated on 4–20% gradient Tris-Glycine polyacrylamide gels (Invitrogen) at 150 volts for 90 min, transferred onto PVDF membranes (Immubilon-P; Millipore) at 100 volts for 90 min. Blots were blocked with 5% milk in PBS-Tween for 1 hr, incubated with primary antibodies overnight, then washed 3 times with Tween-PBS for 20 min, followed by HRP-conjugated anti–mouse (1:2000; Roche) or anti–rabbit (1:5000; Roche)

secondary antibodies. Before detection, blots were washed 2 times with Tween-PBS for 20 min and 1 time with PBS for 20 min, and then detected with SuperSignal West Pico Chemiluminescent Substrate (Life Technologies) using ImageQuant LAS4000 chemiluminescence imager (GE Healthcare). Antibodies used for Western blot were: anti-cortactin mAb (1:1000; BD Biosciences), anti-cofilin polyclonal antibody (1:1000; clone FL-166; Santa Cruz Biotechnology, Inc.), anti-Arp2 polyclonal antibody (1:500; clone H-84; Santa Cruz Biotechnology, Inc.), anti-ARC/p34 polyclonal antibody (1:1000; Millipore), anti-Tom20 polyclonal antibody (1:5000; clone FL-145; Santa Cruz), anti-Opa1 monoclonal antibody (1:1000; BD Biosciences), and anti-Mfn2 monoclonal antibody (1:1000; Abcam).

Section 3: Results

Subsection 1: Knockdown of actin-modifying proteins resulted in abnormal mitochondrial elongation

To further determine the mechanism of F-actin participating in mitochondrial division, we sought to determine whether actin-regulatory proteins could also regulate the mitochondrial fission process via modifying actin filaments. In order to achieve this, we analyzed the degree to which overexpression or downregulation of a broad range of proteins regulating F-actin nucleation, stabilization and disassembly, including WASp, Arp2/3 complex, gelsolin, cofilin, Abp1, cortactin, formin1, FBP17, coronin, affect mitochondrial network organization (Table 3.1). This selection was based on the established role for each of these factors in the regulation of actin cytoskeleton in membrane trafficking in cellular compartments other than mitochondria, including clathrin-dependent and -independent endocytosis (Mooren et al. 2012; Römer et al. 2010; Egea et al. 2006; Shivas & Skop 2012; Anitei & Hoflack 2012). While overexpression of any of the above-mentioned proteins did not affect mitochondrial network organization, downregulation of Arp2/3 complex, cortactin and cofilin led to dramatic elongation and interconnection of mitochondria, as compared with control RNAi cells (Fig. 3.2 and Fig. 3.4).

First, we investigated the effect of Arp2/3 complex depletion on mitochondrial morphology. As described before, Arp2/3 complex is a seven-subunit protein complex that plays a major role in nucleating branched F-actin cytoskeleton. It consists of actin-related proteins Arp2 and Arp3, p20, p21, p34 and p40. Arp2 and Arp3 closely resemble the structure of monomeric actin and serve as nucleation sties

for actin filaments (Rotty et al. 2013). To knockdown Arp2/3 complex, HeLa cells were transfected with (1) single Arp2 shRNA (achieved by a mix of two Arp2 shRNA constructs), (2) single ARC or p34 shRNA (achieved by a mix of two ARC or p34 constructs) and (3) double Arp2/p34 shRNA (achieved by one independent construct for each target), followed by 4 days puromycin selection before collecting cell lysates. Cells were harvested and cell lysates were subjected to SDS-PAGE followed by Western blotting. Western blots of total cell lysates showed that Arp2 and p34 were successfully downregulated in both single and double shRNAi cells (Fig. 3.1). Notably, single shRNA of Arp2 also reduced the expression level of p34 and *vice versa*. It appears that downregulation of Arp2 and/or p34 was able to decrease other subunits of Arp2/3 complex, leading to a complete knockdown of Arp2/3 complex. To explore the effect of Arp2/3 complex downregulation on mitochondrial morphology, we immunostained Arp2/3 shRNA cells with anti-cytochrome c mAb to reveal mitochondrial structure. Compared to control shRNA cells, immunofluorescence analysis displayed abnormal elongated mitochondrial tubules in cells with reduced Arp2/3 complex expression level (Fig. 3.2). Quantitative analysis also exhibited an increase in the percentage of cells with elongated mitochondria in Arp2/3 complex shRNA cells. While there were only 5% of cells with an interconnected network in control shRNA cells, about 40% of cells showed mitochondrial interconnection in Arp2/3 complex shRNA cells, suggesting that mitochondrial division may be impaired by reduction of Arp2/3 complex (Fig. 3.5). In addition, given that Arp2/3 complex binds to the sides of existing filaments and specifically initiates branched actin network, which grows a distinctive new filament

at a 70-degree angle from the mother filament, these data may point to a role of branched F-actin polymerization in mitochondrial fission.

Protein	Function	MW (kD)	Reference
WASp	Activate Arp2/3 complex; stimulate branched F-actin polymerization	65	(Weaver et al. 2002)
Arp2/3 complex	Consists of APRC1-5, Arp2 and Apr3; branched actin nucleation	Varied	(Rotty et al. 2013)
cortactin	Recruit Arp2/3 complex to existing actin; facilitating and stabilizing nucleation	85	(Uruno et al. 2001)
cofilin	Disassemble F-actin; sever F-actin without capping and prefer ADP-actin	19	(Pavlov et al. 2007)
gelsolin	Sever and cap F-actin in a Ca^{2+}, pH and phospholipid dependent manner	86	(Méré et al. 2005)
formin1	Promote non-branch F-actin nucleation and bundling	184	(Kobielak et al. 2004)
FBP17	Link formin and dynamin; recruit actin regulatory proteins	71	(Tsuboi et al. 2009)
Abp1	Functionally link the actin cytoskeleton to dynamin	65	(Kessels et al. 2001)
coronin	Coordinate Arp2/3 mediated actin branches and cofilin activity	55	(Cai et al. 2007)

Table 3.1 Selection of actin-modifying proteins.

Other than Arp2/3 complex, downregulation of cortactin or cofilin, two actin regulatory proteins, also affects mitochondrial network organization. Cortactin, a class II nucleating promoting factor, is an essential molecule promoting and stabilizing Arp2/3 complex mediating branched F-actin polymerization, as well as linking F-actin cytoskeleton to dynamin superfamily proteins. The multi-domain

scaffold has an N-terminal acidic domain that binds and stabilizes Arp2/3 complex, six tandem repeats segments in the central region that directly bind to F-actin, a C-terminal SH3 domain that interacts with the proline-rich domain of WASp and dynamin, indicating that cortactin is likely engaged in F-actin participated Drp1-mediated mitochondrial fission process (Orth & McNiven 2003). To test this hypothesis, HeLa cells were transfected with three independent cortactin targeting shRNA constructs, selected by puromycin for 4 days, then analyzed by Western blot. Western blot results showed successfully knockdown of cortactin in all three shRNAi cells (Fig. 3.3). Cortactin shRNAi cells were analyzed by immunofluorescence. Mitochondrial tubules were extensively elongated and interconnected in cortactin shRNAi cells, as compared to control shRNAi cells (Fig. 3.4A and B), and the percentage of cells with elongated mitochondria was increased in cortactin shRNA

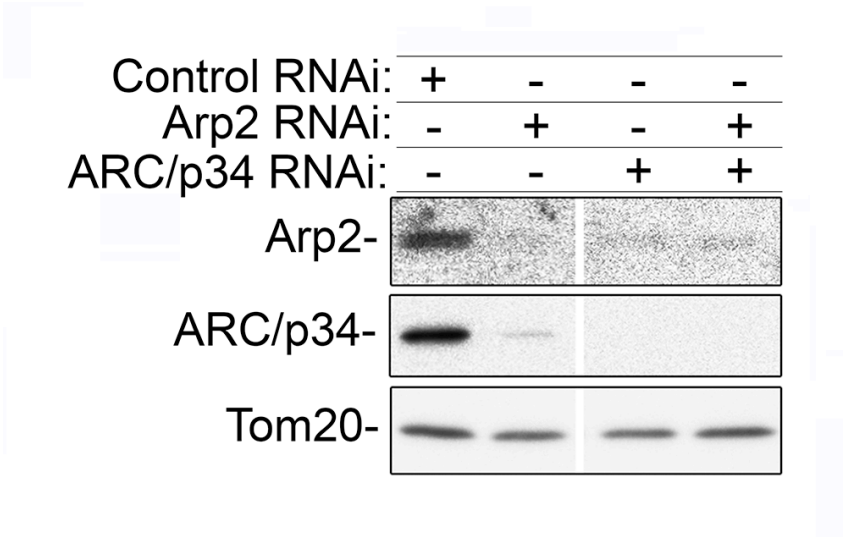

Figure 3.1 Downregulation of Arp2/3 complex in HeLa cells. HeLa cells were transfected with control shRNA (lane 1), Arp2 shRNA (lane 2), ARC/p34 shRNA (lane 3) and double Arp2 and ARC/p34 shRNA (lane 4), then selected by puromycin. Total cell lysates collected from respective shRNA samples were analyzed by Western blotting, blotted with anti-Arp2, anti-p34 and anti-Tom20 antibodies as loading control.

cells as well (Fig. 3.5), suggesting that reduction of cortactin creates conditions supporting mitochondrial elongation. During clathrin-mediated endocytosis, cortactin, together with actin and Arp2/3 complex, are recruited to clathrin-coated pits at the late-phase of dynamin recruitment, in synchrony with endocytic buds invagination. My data implies that cortactin may serve as a mitochondrial F-actin regulatory factor along with Arp2/3 complex in mitochondrial fission. Considering that cortactin recruits and stabilizes Arp2/3 complex, promoting actin filaments extension, the possibility that cortactin stimulates mitochondrial fission by enhancing and stabilizing Arp2/3 complex mediated branched F-actin polymerization is also likely.

The role of cofilin, an actin binding protein to sever and dissemble actin filaments during cellular membrane ruffling, in mitochondrial fission was also examined. As a member of the ADF/cofilin family, cofilin binds to both actin monomers and filaments to reorganize actin filaments. Cofilin depolymerizes actin filaments by two major activities: 1) severing that dissociates G-actin-ADP from the minus end of actin filaments, creating free barbed ends for further polymerization, 2) preventing actin monomers from binding to the pointed end, in order to maintain G-actin/F-actin cycles and promote actin polymerization in long-term effect (Pavlov et al. 2007). To clarify the role of cofilin in mitochondrial dynamics, HeLa cells were transfected with three independent cofilin targeting shRNA constructs, selected by puromycin for 4 days, then analyzed by Western blot. Western blot results showed cofilin expression was downregulated in all three shRNA constructs transfected cells compared with control shRNA cells (Fig. 3.3). Cells with reduced cofilin expression levels were analyzed by immunofluorescence. In contrast to control shRNA cells, the

mitochondrial network was extensively elongated in cofilin shRNA cells (Fig. 3.4A and C), and percentage of cells with mitochondrial elongation was increased (Fig. 3.5), suggesting that reduction of cofilin induces mitochondrial elongation. Although cofilin disassembles actin filaments to create free barbed ends, the prolonged

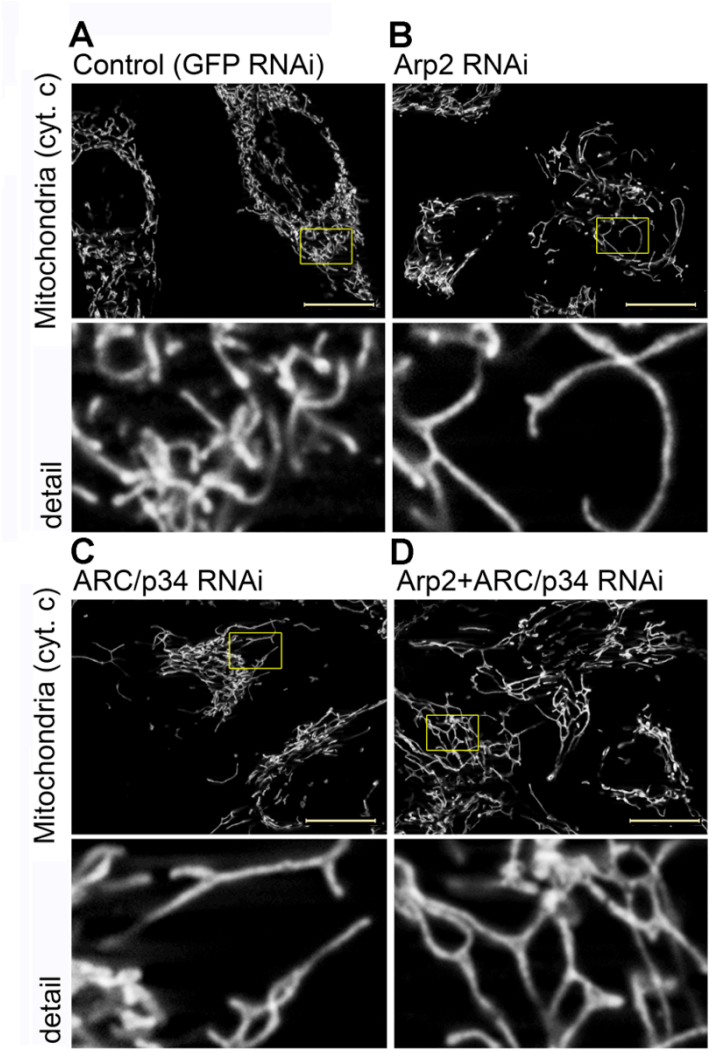

Figure 3.2 Downregulation of Arp2/3 complex resulted in abnormal mitochondrial elongation. HeLa cells were transfected with (A) control shRNA, (B) Arp2 shRNA (achieved by a mix of two independent Arp2 targeting shRNA), (C) ARC/p34 shRNA (achieved by a mix of two independent ARC/p34 targeting shRNA), and (D) Arp2+ARC/p34 shRNA (achieved by one shRNA construct per each target), selected by puromycin, then fixed and immunostained with anti-cytochrome c mAb to detect mitochondria followed by structured illumination imaging. Higher magnifications of area marked with yellow rectangles are shown in detail images. Bars: 20 μm; (detail) 5 μm.

mitochondrial tubules can be explained by the long-term effect of cofilin, which promotes F-actin assembly by providing free G-actin monomers for further nucleation and polymerization.

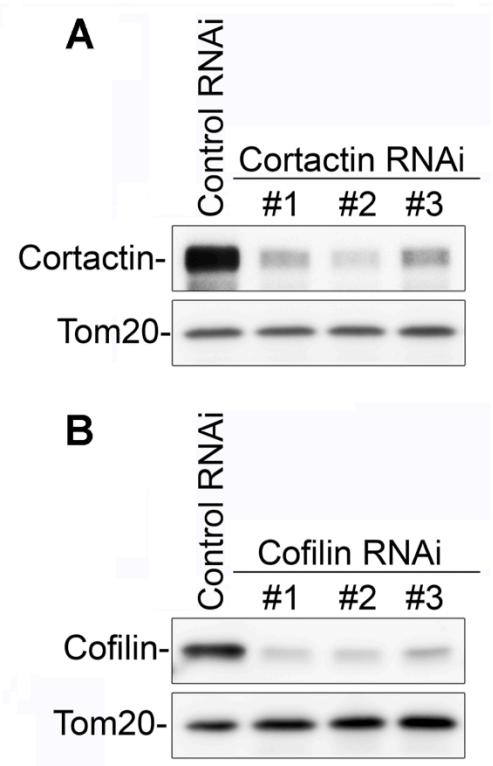

Figure 3.3 Downregulation of cortactin and cofilin in HeLa cells. HeLa cells were transfected with control shRNA (A and B), cortactin shRNA (3 independent cortactin targeting shRNA constructs) (A), cofilin shRNA (3 independent cofilin targeting shRNA constructs) (B), selected by puromycin and subjected to Western blot by anti-cortactin, anti-cofilin and anti-Tom20 antibodies as loading control.

In addition, the effect of another major actin-severing protein gelsolin on mitochondrial morphology was also analyzed. Quantative analysis of immunofluorescence of gelsolin shRNA cells (obtained by three independent gelsolin targeting shRNA constructs) revealed that the percentage of cells with elongated mitochondrial tubules was not altered by the reduction of gelsolin (Fig. 3.5),

suggesting that gelsolin expression level is not related to mitochondrial morphology. These results further support the specificity of the role of Arp2/3 complex, cortactin and cofilin in mitochondrial morphological dynamics, supporting the notion that mitochondrial elongation is induced by the downregulation of Arp2/3 complex, cortactin and cofilin, rather than the cascade signaling effect of impaired actin filaments network in the whole cells. Given the role of Arp2/3 complex, cortactin and cofilin contributing to actin filaments assembly, it is likely that Arp2/3 complex synergizes with cortactin and cofilin to coordinate the mitochondrial specific actin network stimulating mitochondrial division.

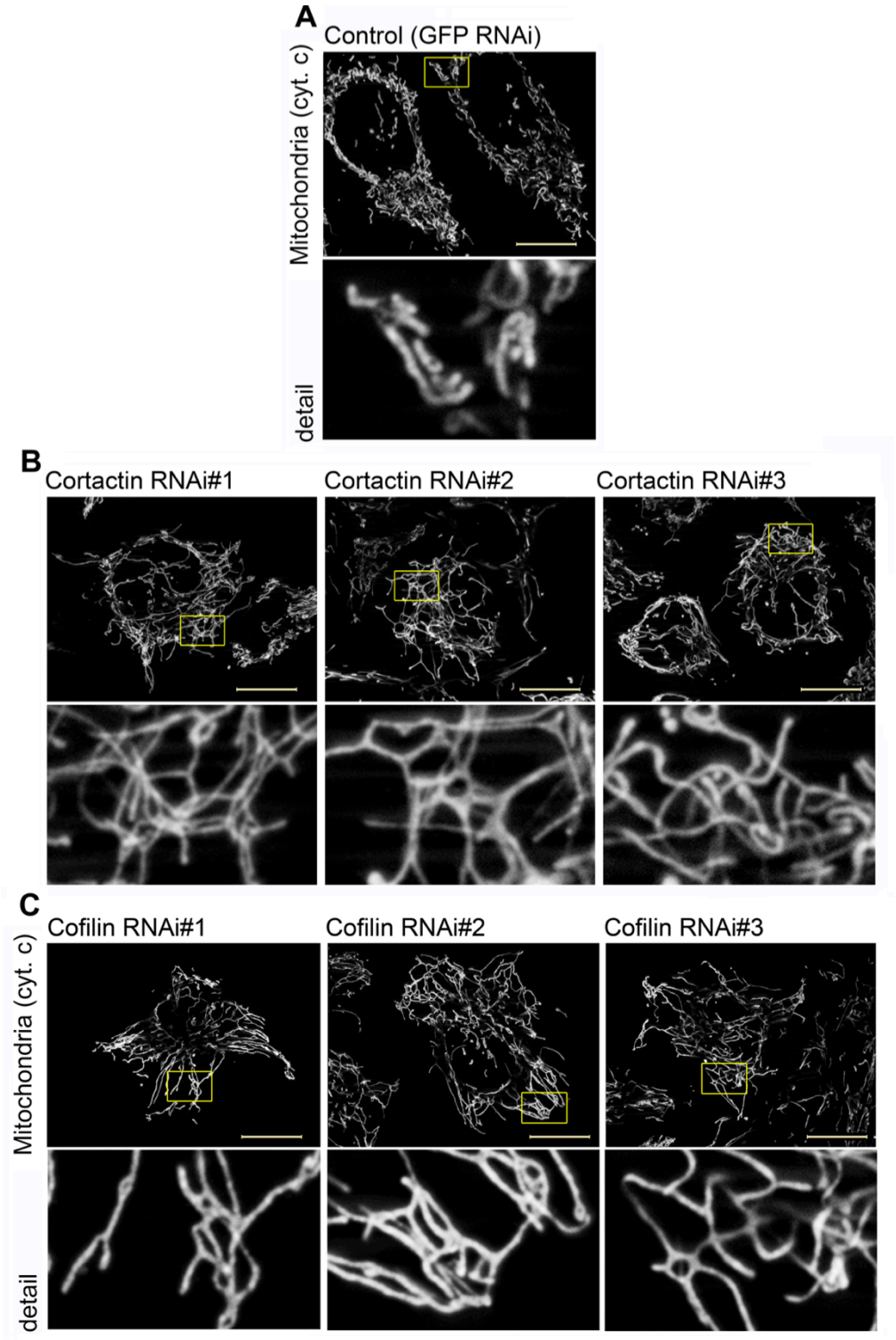

Figure 3.4 Downregulation of cortactin and cofilin resulted in abnormal mitochondrial elongation. HeLa cells were transfected with control shRNA (A), cortactin shRNA (3 independent cortactin targeting shRNA constructs) (B), cofilin shRNA (3 independent cofilin targeting shRNA constructs) (C), selected by puromycin, then fixed and immunostained with anti-cytochrome c mAb to reveal mitochondria. Higher magnifications of areas marked with yellow rectangles are shown in detail images. Bars: 20 μm; (detail) 5 μm.

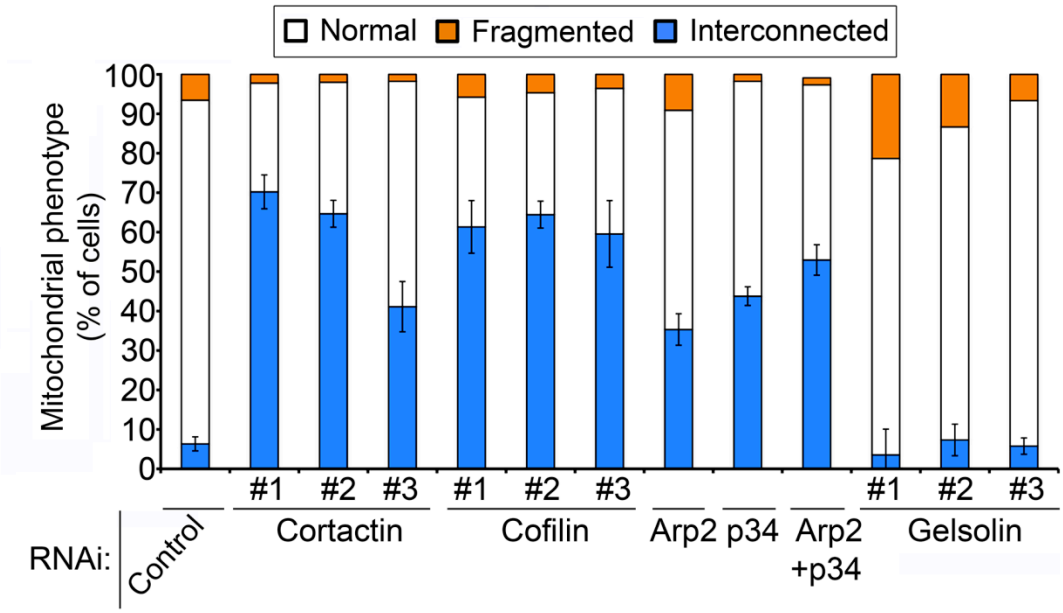

Figure 3.5 Quantitative analysis of mitochondrial morphological phenotype in actin regulatory proteins shRNA cells. HeLa cells were transfected with control shRNA, cortactin shRNA, cofilin shRNA, Arp2 and/or p34 shRNA and gelsolin shRNA, selected by puromycin, fixed and immunostained with anti-cytochrome c mAb as described before, and then quantified as indicated in the figure. Data represent mean ± AvDev from a representative experiment after triplicate counting of 150 cells/condition. Values for the control shRNA cells were obtained by averaging two triplicate counts of 150 cells /condition obtained independently in cortactin/cofilin and Arp2/p34 shRNA experiments. Mitochondrial morphology in gelsolin shRNA cells was also quantified in a similar manner.

Subsection 2: Actin-modifying proteins are required for mitochondrial fission

In the previous section, out data showed that knockdown of actin-modifying proteins including Arp2/3 complex, cortactin and cofilin resulted in mitochondrial elongation, supporting of the possibility that these proteins control the mitochondrial fission process. Hereby, in order to depict the role of F-actin polymerization in the mechanism of mitochondrial fission, we analyzed whether cortactin or cofilin reduction was able to prevent FCCP induced Drp1-dependent mitochondrial division. To this end, HeLa cells were transfected with control shRNA, cortactin shRNA and

cofilin shRNA constructs, selected by puromycin for 4 days, treated with FCCP for 30 min before fixation, and then immunostained with anti-cytochrome c mAb. While in control shRNA cells, 30 min of FCCP treatment induced mitochondrial fragmentation (Fig. 3.6A and B), immunofluorescence and quantitative analysis showed that mitochondria remained interconnected after 30 min FCCP treatment in cortactin shRNA cells and to a lesser degree cofilin shRNA cells (Fig 3.6C and D, and Fig. 3.7), indicating that downregulation of cortactin and cofilin expression levels prevented FCCP-induced mitochondrial fragmentation. Thus, these data indicate that FCCP-induced mitochondrial fission is prevented by reduced cortactin and cofilin, suggesting that these actin-modifying proteins are required for FCCP-induced mitochondrial fission.

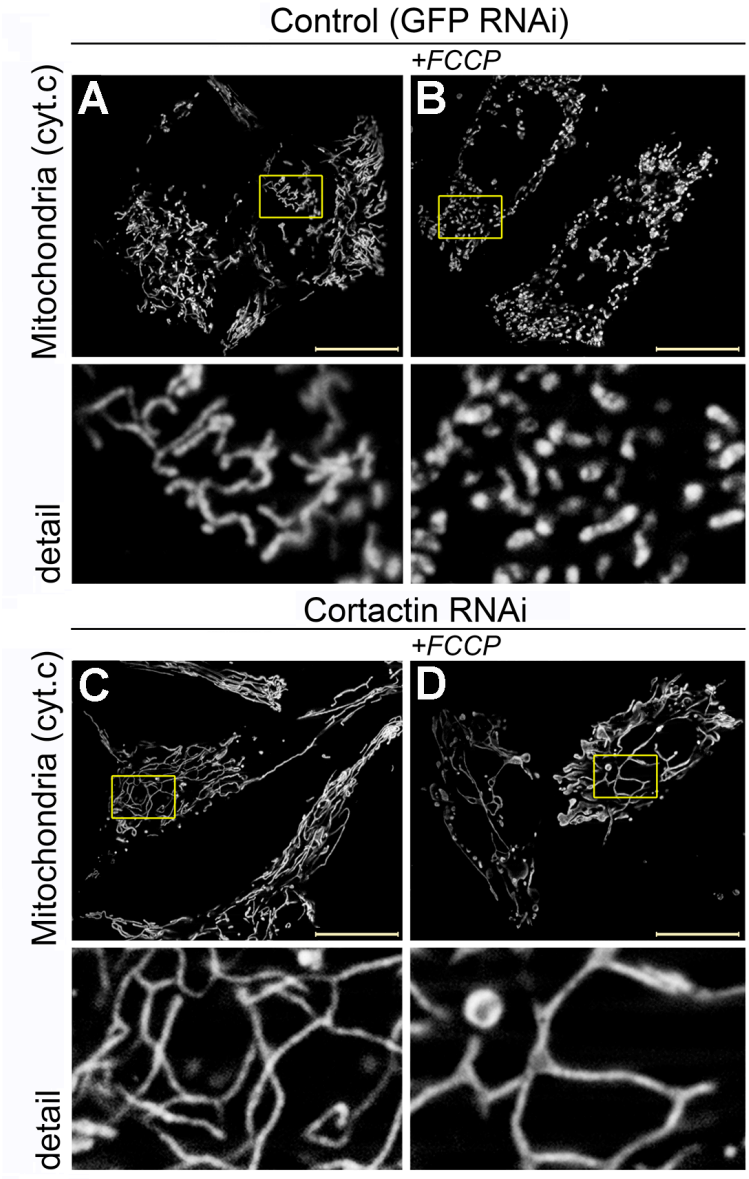

Figure 3.6 Downregulation of cortactin prevented FCCP-induced mitochondrial fragmentation. HeLa cells were transfected with cortactin shRNA, selected by puromycin, then treated with DMSO or 10 uM FCCP before fixation. Cells were then immunostained with anti-cytochrome c mAb to reveal mitochondrial structure. Higher magnifications of areas marked with yellow rectangles are shown in detail images. Bars: 20 μm; (detail) 5 μm.

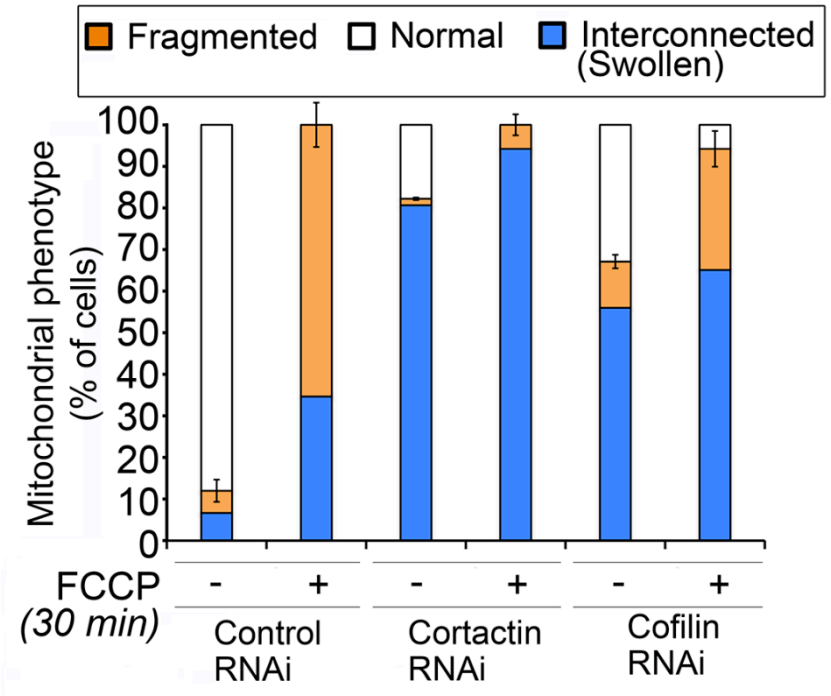

Figure 3.7 Quantitative analysis of mitochondrial morphological phenotype in FCCP-treated cortactin and cofilin shRNA cells. HeLa cells were transfected with control shRNA, cortactin shRNA and cofilin shRNA, selected by puromycin, then treated with FCCP for 30 min before fixation, and immunostained by anti-cytochrome c mAb and quantified as indicated in the figure. Data represent mean ± AvDev from a representative experiment after triplicate counting of 150 cells/condition.

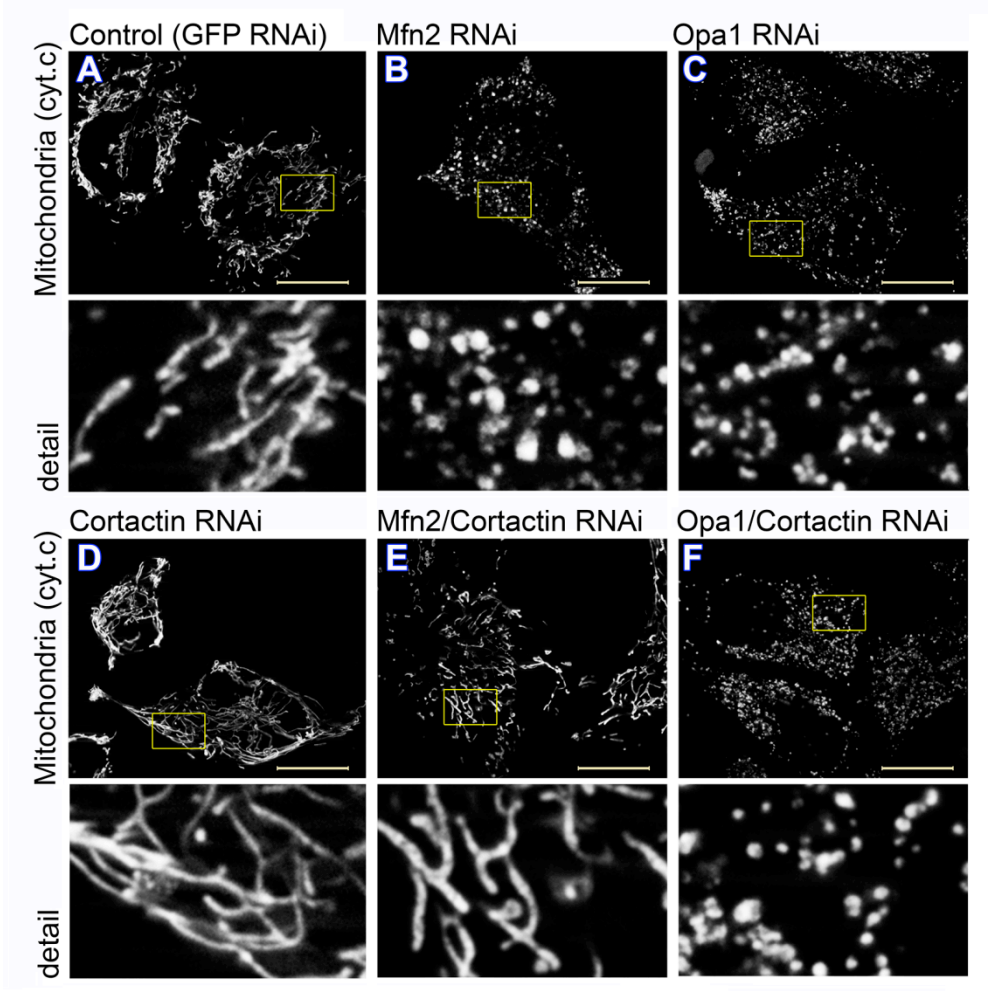

Figure 3.8 Cortactin downregulation restored mitochondrial fragmentation induced by reduced Mfn2 expression. HeLa cells were transfected with control shRNA(A), Mfn2 shRNA(B), Opa1 shRNA(C), cortactin shRNA(D), Mfn2/cortactin shRNA (E) and Opa1/cortactin shRNA (F), selected by puromycin, fixed and immunostained with anti-cytochrome c mAb to detect mitochondrial structure, followed by structured illumination imaging. Higher magnifications of areas marked with yellow rectangles are shown in detail images. Bars: 20 μm; (detail) 5 μm.

To further explore the role of actin-modifying proteins cortactin and cofilin in mitochondrial fission, we also examined whether cortactin and cofilin controls non-FCCP induced mitochondrial division. Mfn2 and Opa1 are two essential mitochondrial fusion factors (see chapter 1 for details). Reduction of either Mfn2 or

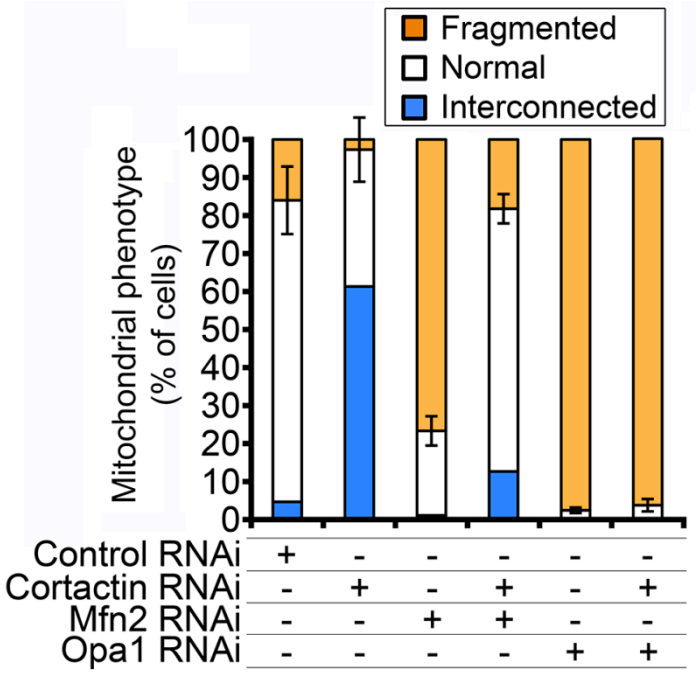

Figure 3.9 Quantitative analysis of mitochondrial morphological phenotype in cortactin/Mfn2 and cortactin/Opa1 double shRNA cells. HeLa cells were transfected with control shRNA, Mfn2 shRNA, Opa1 shRNA, cortactin shRNA, Mfn2/cortactin shRNA and Opa1/cortactin shRNA, selected by puromycin, fixed and immunostained with anti-cytochrome c to detect mitochondria, followed by structured illumination imaging. Mitochondrial morphologies were quantified as indicated in the figure. Data represent mean ± AvDev from a representative experiment after triplicate counting of 150 cells/condition.

Opa1 expression level led to formation of fragmented mitochondria networks as shown in Fig. 3.8B, C and Fig. 3.9, resulting from the inhibition of fusion activity. In order to analyze if cortactin and/or cofilin knockdown can also reverse the mitochondrial fragmentation in Mfn2 and Opa1 knockdown cells, HeLa cells were cotransfected with either cortactin/Mfn2 or cortactin/Opa1 shRNA constructs, selected by puromycin, fixed and immunostained with anti-cytochrome c mAb. Notably, downregulation of Mfn2 alone led to formation of fragmented mitochondrial networks in 76.7 ± 3.9% of the cells (Fig. 3.8B and Fig. 3.9), while cortactin/Mfn2 double shRNA displayed mitochondrial fragmentation in only 18.2 ± 3.8% of the

cells (Fig. 3.8E and Fig.3.9). Furthermore, there was no detectable effect of cortactin shRNA on mitochondrial fragmentation induced by downregulation of Opa1 (Fig. 3.8C, F and Fig. 3.9). Considering that Mfn2 depletion results in partial inhibition of mitochondrial fusion, it is likely that restoration of mitochondrial tubules observed in cortactin/Mfn2 double shRNA cells is due to the compensation of Mfn1-dependent mitochondrial fusion activity. The failure to rescue mitochondrial fragmentation induced by Opa1 could be explained by the complete fusion inhibition caused by loss of Opa1. Western blot analysis confirmed an efficient knockdown of cortactin, Mfn2 and Opa1 expression level (Fig. 3.10). In sum, these results indicate that reduction of cortactin and/or cofilin reverse both FCCP- and Mfn2 depletion-induced mitochondrial fragmentation, further supporting roles for cortactin and cofilin in mitochondrial fission.

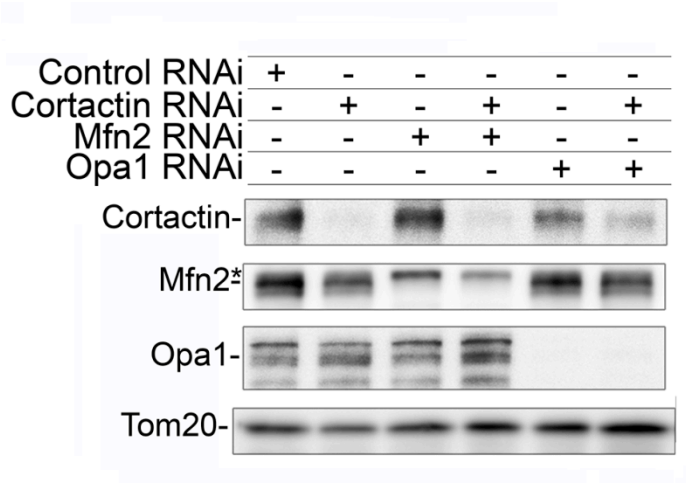

Figure 3.10 Protein expression levels in cortactin, cortactin/Mfn2, and cortactin/Opa1 shRNA cells. HeLa cells were transfected with control shRNA, Mfn2 shRNA, Opa1 shRNA, cortactin shRNA, Mfn2/cortactin shRNA and Opa1/cortactin shRNA, selected by puromycin, harvested and subjected to Western blot analysis. Blots were immunolabeled with anti-cortactin, anti-Mfn2, anti-Opa1 and anti-Tom20 antibodies as loading control.

Mitochondrial elongation and interconnection are induced not by inhibition of mitochondrial division, but rather through the activation of mitochondrial fusion in a process called SIMH (Stress-induced Mitochondrial Hyperfusion) (Tondera et al. 2009). To examine whether the extensive mitochondrial tubules induced by

A

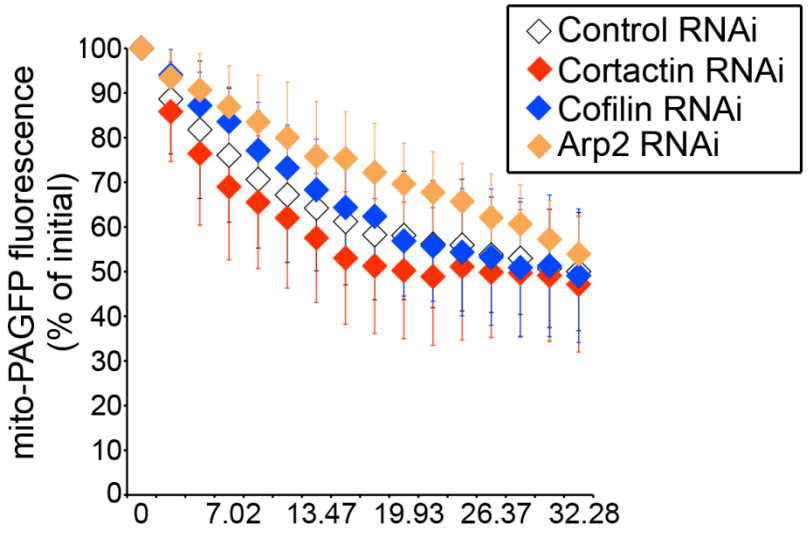

B

Cell type	Time (min)	mito-PAGFP fluorescence (% of initial)	P-value (vs. control)
Control RNAi	15	62.21+/-14.20	NA
	30	50.03+/-13.25	NA
Cortactin RNAi	15	53.03+/-14.84	0.14
	30	47.16+/-15.16	0.70
Cofilin RNAi	15	64.36+/-11.01	0.46
	30	49.10+/-14.96	0.88
Arp2 RNAi	15	75.33+/-10.45	0.16
	30	53.95+/-8.51	0.65

Figure 3.11 Quantitative analysis of mitochondrial fluorescence intensities in control, cortactin, cofilin and Arp2/3 complex shRNA cells. (A) Control shRNA, cortactin shRNA, cofilin shRNA and Arp2 shRNA cells were quantified and plotted as a function of time as shown in the figure. Initial postactivation values were normalized to 100%. Data represent mean ± AvDev of 32 (control shRNA), 21 (cortactin shRNA), 24 (cofilin shRNA), and 14 (Arp2 shRNA) single cell time-lapse experiments. (B) mito-PAGFP fluorescence intensity and p-value of indicated time are shown.

downregulation of cortactin and cofilin is caused by increased fusion activity, we further analyzed the mitochondrial fusion rates in Arp2/3 complex shRNA, cortactin shRNA and cofilin shRNA cells. To achieve this, we applied a mitochondrial matrix-targeted photoactivatable GFP (mito-PAGFP)-based mitochondrial fusion assay. HeLa cells were transfected with control shRNA, cortactin shRNA, cofilin shRNA and Arp2 shRNA, selected by puromycin for 4 days, then transfected with mito-PAGFP for 18 hours. After transfection, regions of interest (red circles in preactivation; "Pre" images in Fig. 3.12A and B) in mito-PAGFP-expressing control, cortactin, cofilin and Arp2+ARC/p34 shRNA cells were photoactivated by brief irradiation with UV light, followed by time-lapse imaging with 488-nm light every about 2 min, over about 30 min. After mito-PAGFP signal is activated by UV light, the rates of fluorescence signal decreases over time reflect mitochondrial fusion rates as higher mitochondrial fusion activity accelerates the spreading of fluorescence molecules. The profiles of fluorescence images revealed that mito-PAGFP signals decreased in control shRNA and cortactin shRNA cells at a similar time frame. Supporting this notion, quantification of mito-PAGFP fluorescence changes in several time-lapse experiments revealed similar fusion rates in all analyzed cell groups (Fig. 3.11). These data further support the possibility that it is not induction of mitochondrial fusion, but rather inhibition of mitochondrial fission that induced the mitochondrial elongation and interconnection observed in Arp2/3 complex, cortactin and cofilin shRNA cells.

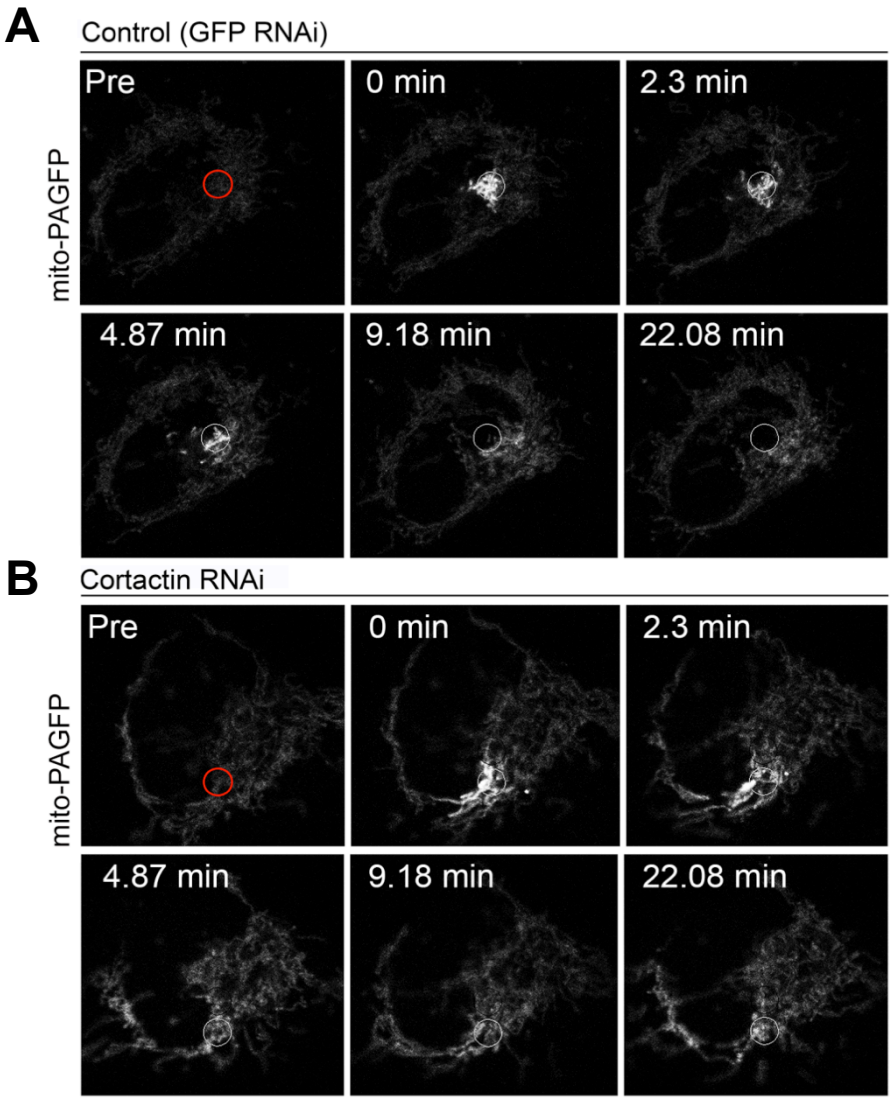

Figure 3.12 Times-lapse series of mito-PAGFP-based mitochondrial fusion assay in control and cortactin shRNA cells. HeLa cells were transfected with control shRNA(A) and cortactin shRNA(B), selected by puromycin for 4 days, then transfected with mito-PAGFP for 18 hours. After transfection, mito-PAGFP-based mitochondrial fusion assay was performed as described in materials and methods section.

Subsection 3: Downregulation of cortactin and cofilin induces mitochondrial accumulation of Drp1

Drp1 is the essential regulator of mitochondrial division, during which Drp1 is recruited from cytosol to mitochondria to stimulate membrane fission events. To gain insight into the mechanism by which cortactin and cofilin regulate mitochondrial division, we analyzed the mitochondrial localization of Drp1. HeLa cells transfected with control shRNA, cortactin shRNA and cofilin shRNA, were immunostained for Drp1 and Tom20 to reveal OMM, followed by structured illumination imaging. We found that downregulation of both cortactin and cofilin led to significant increases in the amount of mitochondria-associated Drp1 (Fig. 3.13). The degree of colocalization of Tom20-labeled mitochondria and Drp1 was quantified and reported as a Mander's correlation coefficient (Rr; Fig. 3.14). The data showed an Rr = 0.44 ± 0.041 in control shRNA cells, as compared with an Rr = 0.58 ± 0.06 in cortactin shRNA cells and Rr = 0.65 ± 0.034 in cofilin shRNA cells. Because Rr = 1 indicates complete colocalization, whereas Rr = 0 indicates random colocalization, Mander's score roughly correlates with percentage of overlap between different fluorescently labeled molecules, therefore the data indicated that about 20% more of total Drp1 colocalized with mitochondria in cortactin or cofilin shRNA cells than in control shRNA cells (Fig. 3.14). Furthermore, a careful examination of images revealed that submitochondrial Drp1 complexes in cortactin and cofilin shRNA cells were larger than those detected in control shRNA cells.

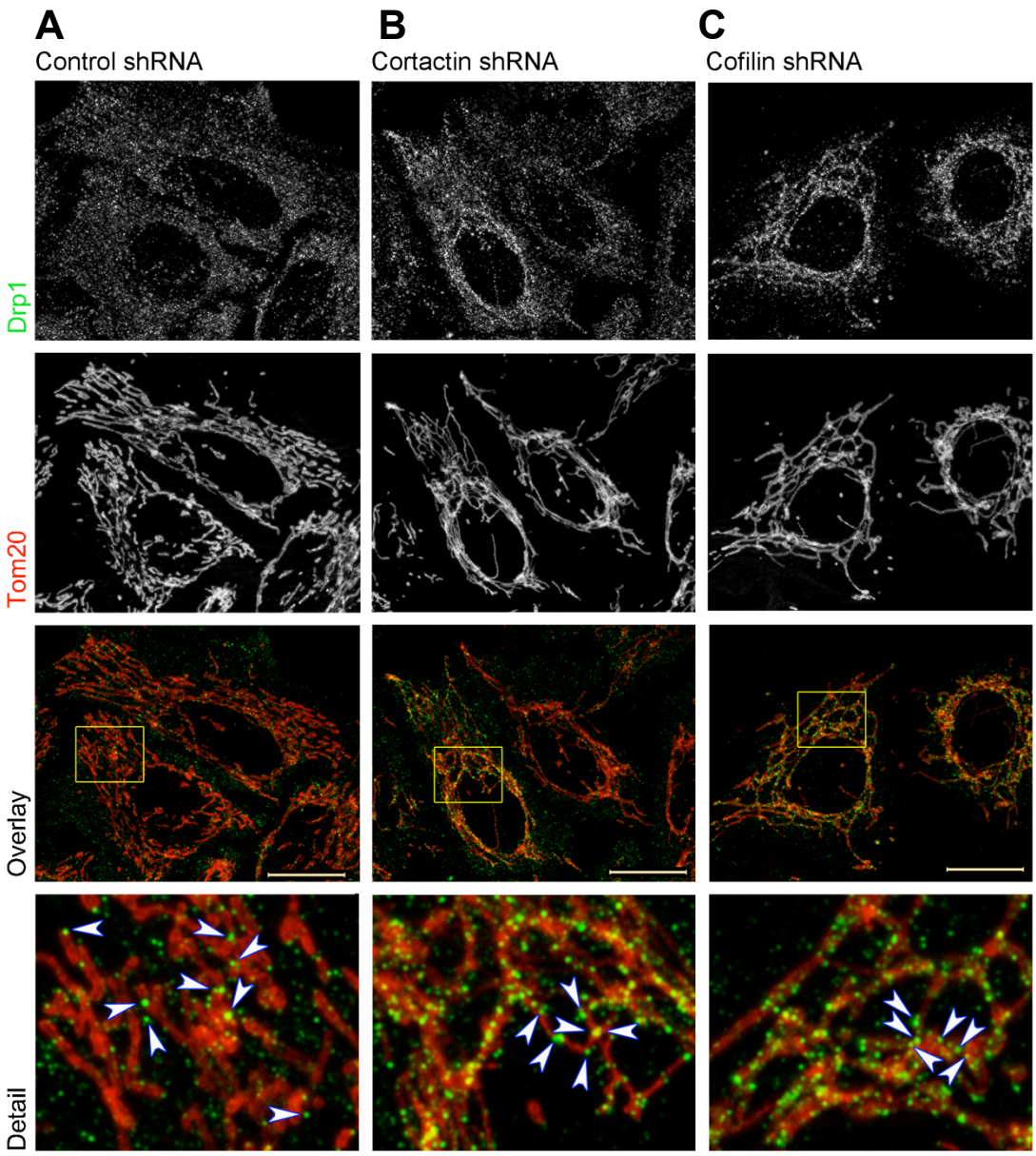

Figure 3.13 Mitochondrial accumulation of Drp1 in control, cortactin and cofilin shRNA cells. HeLa cells were transfected with control shRNA (A), cortactin shRNA (B) and cofilin shRNA (C), then immunostained with anti-Drp1 mAb (green on overlay and detail images) and anti-Tom20 antibody for mitochondria (red on overlay and detail images). Images were acquired using structured illumination imaging. Maximum projections of seven z-sections acquired at 0.25 um intervals starting from the bottom of the cell are shown. Bars: 20 μm; (detail) 5 μm.

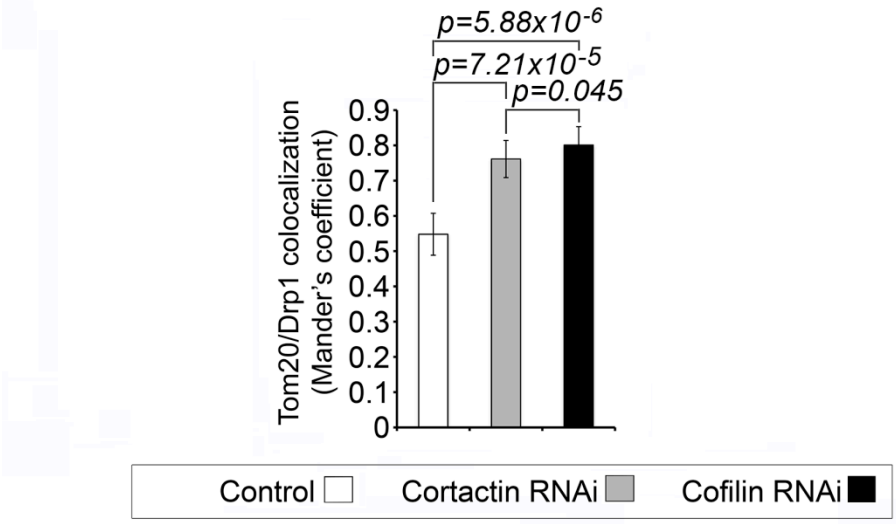

Figure 3.14 Quantitative analysis of mitochondrial accumulation of Drp1 in control, cortactin and cofilin shRNA cells. HeLa cells were transfected with control shRNA, cortactin shRNA, and cofilin shRNA, immunostained for Drp1 and Tom20. Colocalization of Drp1 with mitochondria was analyzed. The values represent Mander's correlation coefficient (Rr) that reveals the degree of association of pixels in different channels of the image. Data represent the mean ± SD of images/condition. Each image used for the analysis contained at least two cells.

We also tested the degree to which cortactin and cofilin could regulate stress-induced mitochondrial accumulation of F-actin. Control shRNA, cortactin shRNA and cofilin shRNA cells were treated with FCCP for 2 min, then fixed and labeled with Alexa-Phalloidin and anti-cytochrome c mAb. Quantification analysis of Mander's coefficient revealed that 25.66% ± 4.22% of cortactin shRNA cells and 23.00% ± 2.66% in cofilin shRNA cells displaying mitochondrial associated F-actin in contrast to 36.67% ± 3.77% of control shRNA cells. FCCP treatment resulted in reduced numbers of cells displaying mitochondrial associated F-actin in both cortactin and cofilin shRNA cells, compared with control shRNA cells (Fig. 3.15), suggesting that mitochondrial associated F-actin polymerization requires the presence

of cortactin and cofilin. Cortactin and cofilin shRNA reduced protein expression level, which is shown in Fig. 3.16. Thus, these data further deepen the understanding of the step at which F-actin functions in mitochondrial fission. Given that Drp1 is recruited from cytosol to mitochondria upon initiation of mitochondrial fission, mitochondrial accumulation of Drp1 in cortactin and cofilin shRNA cells suggested that Drp1 recruitment was not controlled by cortactin and cofilin. Considering that mitochondrial associated F-actin requires the presence of cortactin and cofilin, we can further conclude that mitochondrial F-actin polymerization occurs in parallel with mitochondrial recruitment of Drp1. Taking the accumulation of Drp1 on mitochondria and abnormal interconnected mitochondrial network in cortactin and cofilin knockdown cells together implies that the Drp1-mediated membrane scission event is blocked in the absence of cortactin and cofilin, resulting in mitochondrial fission defects and excessive Drp1 staying on mitochondria. Thereby, it is very likely that mitochondrial F-actin polymerization contributes to Drp1 mediated steps in the late stage of mitochondrial fission, such as membrane constriction and/or GTP-hydrolysis dependent membrane scission.

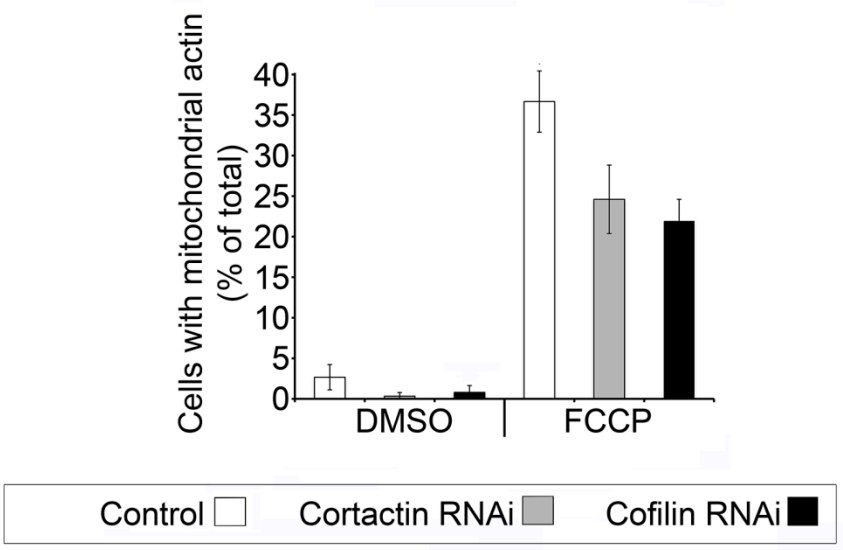

Figure 3.15 Quantitative analysis of mitochondrial assembly of F-actin in FCCP-treated control, cortactin and cofilin shRNA cells. Control shRNA, cortactin shRNA and cofilin shRNA cells were treated with FCCP for 2 min, fixed and then immunostained with Alexa-Phalloidin to detect F-actin and anti-Tom20 antibody to reveal mitochondria. Data represent mean ± AvDev from a representative experiment after triplicate counting of 150 cells/condition.

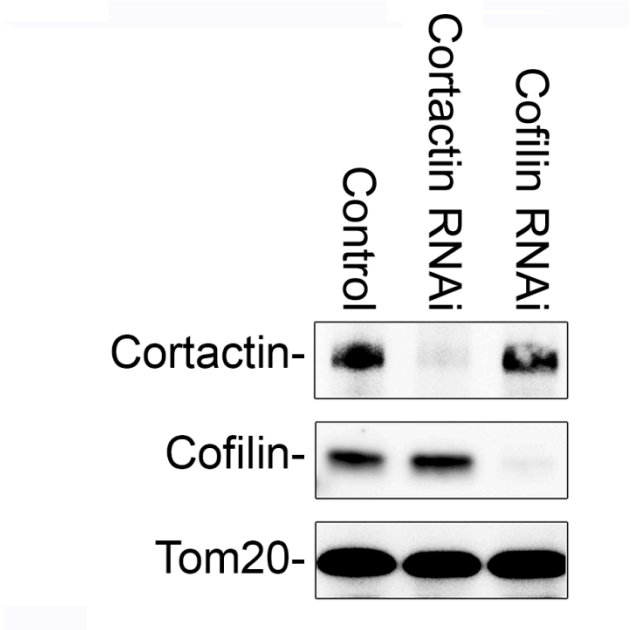

Figure 3.16 Protein expression levels of control, cortactin and cofilin shRNA cells. HeLa cells were transfected with control shRNA, cortactin shRNA and cofilin shRNA, selected by puromycin and analyzed by Western blot. Blots were immunolabeled by anti-cortactin, anti-cofilin and anti-Tom20 antibodies as loading control.

Subsection 4: Mitochondrial association of actin-modifying proteins

Published reports indicate that cortactin, cofilin, Arp2/3 complexes are ubiquitious proteins distributed in the nucleus, cytosol, and membrane compartments of the cell, including the cell membrane, ER, and Golgi complex. Implicating a critical role for actin-modifying proteins in membrane remodeling events, Arp2/3 complex, cortactin and cofilin are recruited to clathrin-coated endocytic buds upon the initial activation of endocytosis. Using structured illumination imaging, we analyzed the spatial relationship between endogenous cortactin, cofilin, or Arp2/3 complex component Arp3 and mitochondria in wild type and Drp1$^{-/-}$ MEFs. Consistent with published data, in wild type MEFs, cortactin (Fig. 3.17), cofilin (Fig. 3.18) and Arp3 (Fig. 3.19) were enriched within the cytosolic boundaries of the cell without showing strong mitochondria colocalization patterns. However a subgroup of these proteins colocalized with or was found in close association with mitochondria. Although these data do not directly convince that cortactin, cofilin, and Arp2/3 complex translocate and act at the OMM, we believe that the mitochondrial localization of these proteins, in combination with previous data, provides evidence suggesting direct mitochondrial roles for cortactin, cofilin and Arp2/3 complex. Further supporting this notion, it appears that additional mitochondrial accumulation of these proteins was apparent in Drp1$^{-/-}$ MEFs. Notably, in many of Drp1$^{-/-}$ cells a mitochondrial pattern of cofilin (Fig. 3.18), Arp3 (Fig. 3.19), and to a lesser degree cortactin (Fig. 3.17) was detectable. Quantitative colocalization analysis of Mander's coefficient also revealed that, in contrast to wild type MEFs, Mander's coefficient (Rr) of cortactin, cofilin, and Arp3 colocalization with mitochondrial markers Tom20

or cytochorome c was significantly increased in Drp1$^{-/-}$ MEFs (Fig. 3.20). Thus, depletion of Drp1 leads to robust mitochondrial accumulation of cortactin, cofilin and Arp3. Considering the increased mitochondrial F-actin polymerization in Drp1$^{-/-}$ MEFs compared to wild type MEFs shown in chapter 2, these data point to the role of increased mitochondrial accumulation of cortactin, cofilin and Arp3 in Drp1$^{-/-}$ MEFs acting on OMM in stimulating mitochondrial F-actin assembly and pertinent mitochondrial fission events. Given that loss of Drp1 enhanced mitochondrial association of actin-modifying proteins, it seems that Drp1 is responsible for the disassembly of F-actin nucleating protein complex. Furthermore, FCCP treatment induces mitochondrial localization of cofilin and Arp3 to some degree in wild type MEFs, implying an FCCP-induced recruitment of cortactin, cofilin and Arp2/3 complex from cytosol to mitochondria in synchrony with the appearance of mitochondrial F-actin upon 2 min of FCCP treatment.

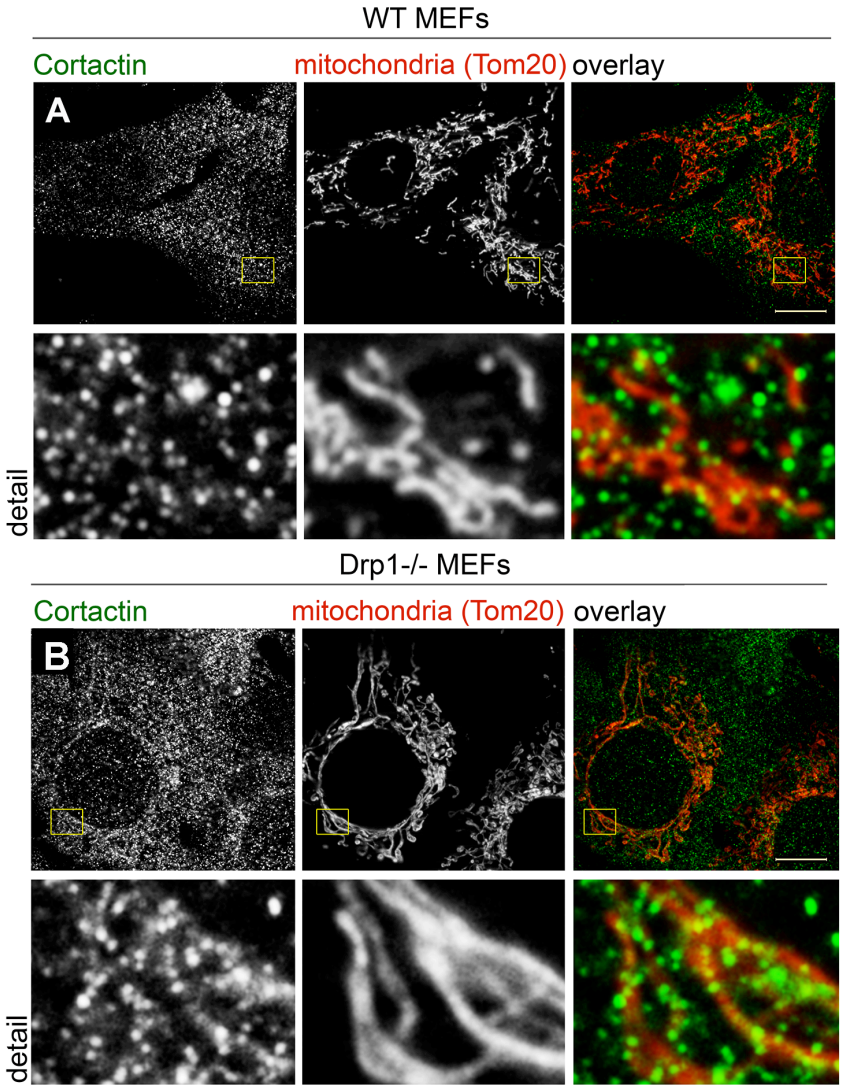

Figure 3.17 Mitochondrial association of cortactin in wild type and Drp1$^{-/-}$ MEFs. Wild type and Drp1$^{-/-}$ MEFs were fixed and immunostained with anti-cortactin mAb and anti-Tom20 antibody, followed by structured illumination imaging. Higher magnifications of areas marked with yellow rectangles are shown in detail images. Bars: 20 μm; (detail) 5 μm.

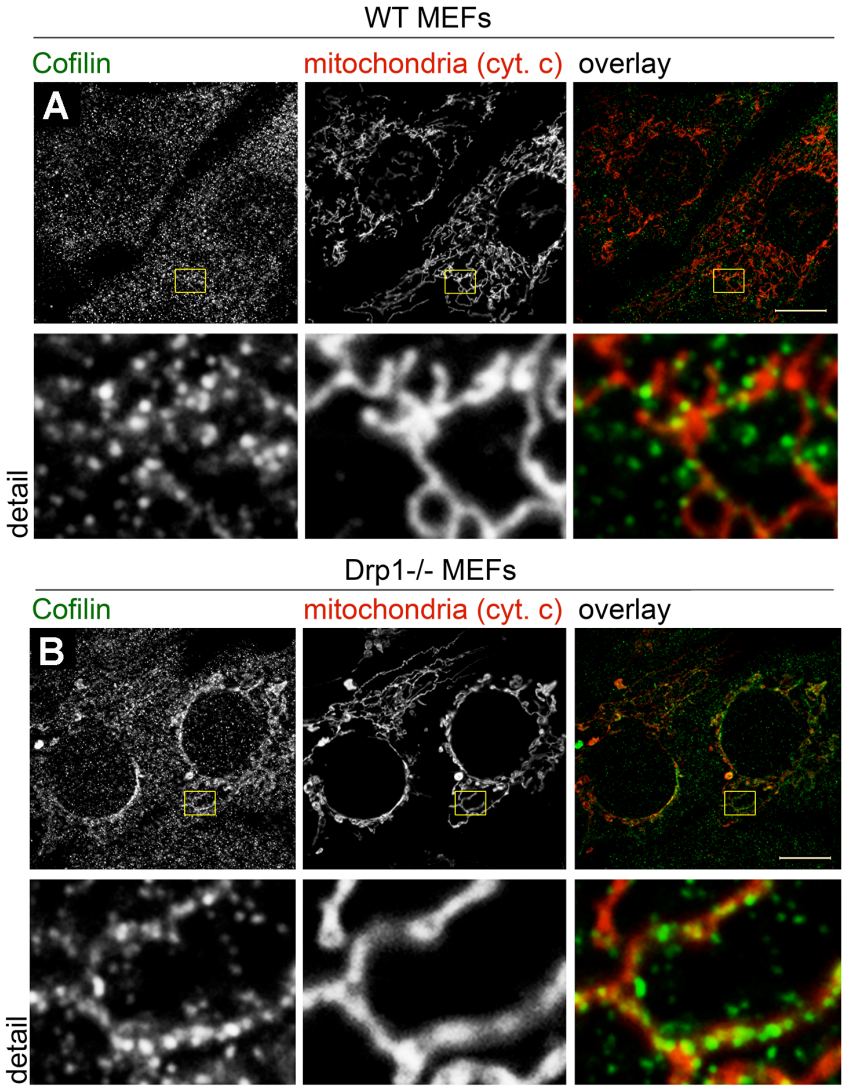

Figure 3.18 Mitochondrial association of cofilin in wild type and Drp1$^{-/-}$ MEFs. Wild type and Drp1$^{-/-}$ MEFs were fixed and immunostained with anti-cofilin antibody and anti-cytochrome c mAb, followed by structured illumination imaging. Higher magnifications of areas marked with yellow rectangles are shown in detail images. Bars: 20 μm; (detail) 5 μm.

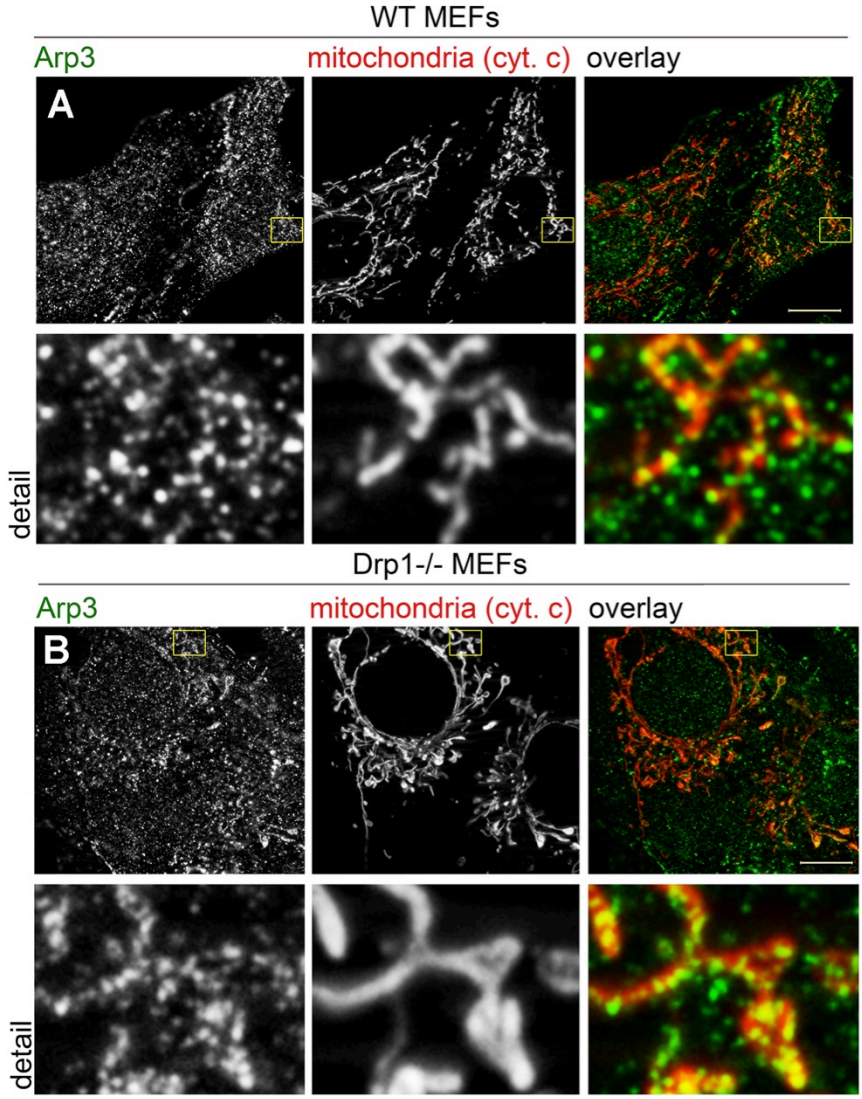

Figure 3.19 Mitochondrial association of Arp3 in wild type and Drp1$^{-/-}$ MEFs. Wild type and Drp1$^{-/-}$ MEFs were fixed and immunostained with anti-Arp3 antibody and anti-cytochrome c mAb, followed by structured illumination imaging. Higher magnifications of areas marked with yellow rectangles are shown in detail images. Bars: 20 μm; (detail) 5 μm.

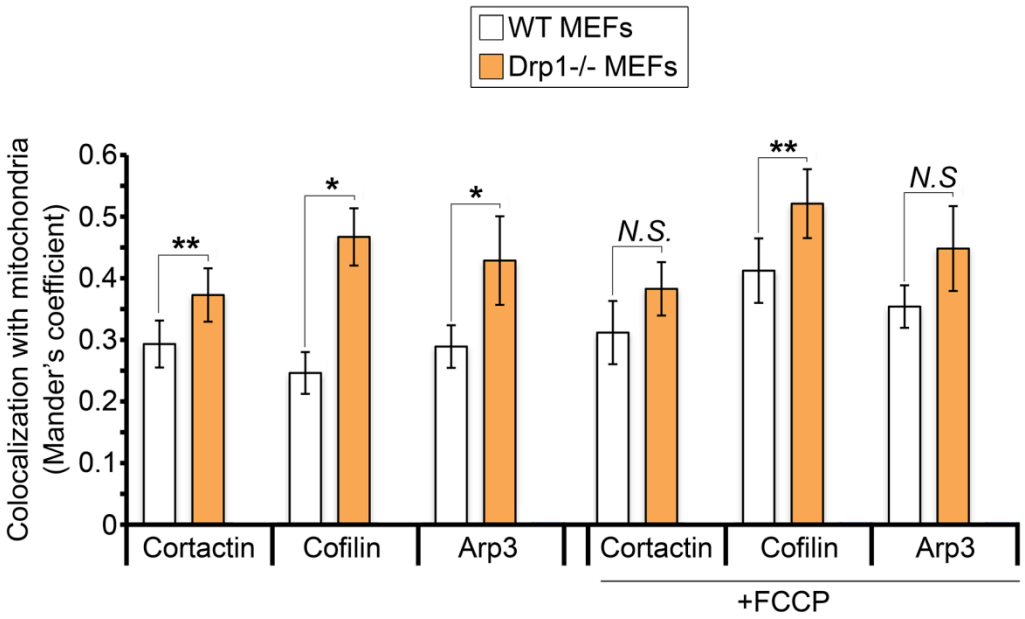

Figure 3.20 Quantitative analysis of mitochondrial association of actin-modifying protein in wild type and Drp1$^{-/-}$ MEFs. Wild type and Drp1$^{-/-}$ MEFs were treated with FCCP for 2 min, fixed, immunostained anti-cortactin, anti-cofilin, anti-Arp3, and anti-Tom20 antibodies. Colocalizations of actin-modifying proteins and Tom20 were analyzed. The values represent Mander's correlation coefficient (Rr) that reveal the degree of association of pixels in different channels of the image. Data represent the mean ± AvDev of 15 images/condition. Each image used for the analyses contained at least two cells. Statistical significance was determined using a two-tailed t test. *, $P<0.001$; **, $P<0.01$; N.S., $P>0.01$.

Section 4: Discussion

While Arp2/3 complex and NPFs mediated branched F-actin polymerization is the major actin nucleating pathway that contributes to mitochondrial fission, actin nucleator formins were reported to promote ER-mediated mitochondrial constriction and fission. Linear F-actin nucleator INF2 has been proposed to be an important mediator of Drp1-dependent mitochondrial fission and enhance actin presence at ER-mitochondrial constriction sites (Korobova et al. 2013). Confirming the published results, we found that overexpression of ER-localizing INF2 and dominant active INF2 mutant INF^{A149D} led to F-actin accumulation on the ER, but not on mitochondria. $INF2^{A149D}$ induced abnormal bundling of F-actin associated with altered morphology of the ER and mitochondrial fragmentation in $INF2^{A149D}$-expressing cells, suggesting that INF2 may mediate ER specific F-actin accumulation, rather than mitochondrial positive F-actin polymerization. Overexpression of either INF2 or INF^{A149D} induces robust F-actin assembly on the ER and $INF2^{A149D}$ induced fragmented mitochondria accumulate along the INF2-positive ER tubules. These data further suggest that INF2 induced mitochondrial fragmentation is specifically mediated by an ER involved mechanism. It is likely that INF2 nucleated actin filaments stay tethered to the ER and form acto-myosin ring with the recruitment of myosin II around the mitochondrial fission sites. In our system we were not able to detect transient assembly of F-actin on the mitochondrial fission sites and effects of INF2 and $INF2^{A149D}$ on mitochondrial assembly of Drp1. Given that the encirclement of mitochondria by acto-myosin network pre-constricts the membrane and orients

Drp1 recruitment to promote subsequent membrane constriction and scission (Korobova et al. 2014a), it is possible that ER-based actin network is not necessary to redistribute to the mitochondrial fission sites during membrane constriction mediated by Drp1. Alternatively, as membrane constriction and scission is an extremely rapid event, the translocation of ER-based actin network to mitochondrial fission sites may be very transient and difficult to capture in our system. Furthermore, INF2 overexpression in HeLa cells did not affect FCCP-induced mitochondrial F-actin assembly. Considering that knockdown of actin-modifying proteins Arp2/3 complex, cortactin and cofilin resulted in mitochondrial elongation and reduce FCCP-induced mitochondrial association of F-actin, we can speculate that INF2- and Arp2/3-cortactin-cofilin- dependent regulation of mitochondrial fission may occur through different mechanisms.

In recent years, F-actin assembly has been linked to dynamin superfamily proteins, assisting various dynamin-mediated actions in membrane remodeling and trafficking (Orth & McNiven 2003; Lanzetti 2007). In our study, we showed that downregulation of cortactin and cofilin led to abnormal accumulation of Drp1 on the elongated mitochondria, suggesting that Drp1 accumulates on mitochondria as an inactive form. It is possible that mitochondrial accumulation of Drp1 observed in cortactin or cofilin shRNA cells are caused by a later-than-recruitment Drp1 regulatory step that was stalled by loss of actin filaments. One possibility is that the actin network regulates Drp1 GTPase activity and its oligomerization status on mitochondria. *In vitro* studies have identified a direct dynamin-actin interaction in the promotion of dynamin oligomerization through a region on the middle domain of

dynamin, implying that actin may bind to Drp1 despite it lacking the C-terminal PRD domain to enhance Drp1 oligomerization into higher order structures on mitochondria. As dynamin's GTPase activity is dependent on its oligomerization status, the local concentration of short actin filaments generated by shearing or actin-severing protein-stimulated dynamin's GTPase activity dependent on dynamin-actin interactions (Gu et al. 2010a). Given that downregulation of cofilin induced elongated mitochondria and abnormal mitochondrial Drp1 accumulation, it is plausible that cofilin may serve as an actin-severing factor to produce short actin filaments at OMM that enhance Drp1 GTPase activity and its oligmerization into contractile ring structures. Alternatively, actin filaments bundling with myosin can trigger contractile force to facilitate membrane constriction and scission. It has been suggested that during apical constriction, actin-myosin networks can be organized into contractile fibers under plasma membrane, driving the shrinkage of membrane and allowing tissue shape changes (Martin et al. 2009). While inhibition of myosin II by pharmacological inhibitor or knockdown of myosin II by shRNA resulted in abnormal mitochondrial elongation (Korobova et al. 2014a), it is likely that mitochondrial F-actin induced by FCCP treatment associates with myosin II to provide the membrane tension force to promote mitochondrial membrane constriction and help position Drp1 at constriction sites.

Understanding the crosstalk between Drp1 and the actin network further clarifies the in depth mechanism of mitochondrial fission. In this chapter, we also showed that Arp2/3 mediated actin filaments accumulate on mitochondria in the absence of functional Drp1. Similarly, cells derived from dynamin1/2 double

conditional knockout mice displayed accumulation of actin filaments at the base of arrested endocytic clathrin-coated pits (Ferguson & De Camilli 2012). Thus, the Arp2/3 dependent F-actin nucleation and polymerization on mitochondria appears to be Drp1-independent. As the disassembly of F-actin requires the presence of functional Drp1 GTPase activity, it is plausible that the depolymerization of mitochondrial actin is initiated by Drp1 mediated GTP hydrolysis. Given the abnormal accumulation of Drp1 on mitochondria in cortactin and cofilin knockdown cells, it suggests that both F-actin polymerization on the OMM and mitochondrial assembly of Drp1 are required to complete Drp1-dependent mitochondrial fission. In addition, dynamin was linked to actin filaments by either direct interaction or actin binding proteins such as profilin, Nck and cortactin (Gu et al. 2010b). The SH3 domain of cortactin is reported to interact with the PRD region of dynamin, forming ring-like structures at membrane remodeling sites in various cellular compartments (Orth & McNiven 2003). However, given the fact that Drp1 lacks a PRD domain on the C-terminus, it is possible that cortactin and Drp1 coordinate to regulate actin filaments by an alternative mechanism.

Chapter 4: Regulation of mitochondrial fission complexes and mitochondrial division by deubiquitinase Usp30

Section 1: Introduction

More than 95 deubiquitinases (DUBs) are encoded by the human genome. DUBs can be further classified into two main categories: cysteine proteases and metalloproteases (Nijman et al. 2005). Cysteine protease Usp30 is the only known mitochondrial associated DUB. Usp30 is anchored to the OMM through a N-terminal transmembrane domain, that is followed by a catalytic domain mediating the DUB activity (Nakamura & Hirose 2008). It has been shown that Usp30 can mediate removal of K-48- and K-63- linked polyubiquitinatin chains. It has been also shown that Usp30 regulates mitochondrial network organization, likely through modifying non-degradative ubiquitination of mitochondrial morphological factors. While overexpression of Usp30 did not affect mitochondrial morphology, knockdown of Usp30 by shRNA resulted in mitochondrial elongation in HeLa cells (Nakamura & Hirose 2008). In addition, Usp30 was able to reverse diterpenoid derivative 15-oxospiramilactone (S3) - induced mitochondrial fragmentation to restore the mitochondrial network in either Mfn1 or Mfn2 knockout cells. The inhibition of Usp30 by S3 led to an increase of non-degradative ubiquitination of Mfn1/2, which enhanced Mfn1 and Mfn2 activity and promoted mitochondrial fusion (Yue et al. 2014). These studies also suggested that Usp30 physically interacted with Mfn1/2 and

decreased non-canonical ubiquitination of Mfn1/2 on cysteine residue, resulting in impaired mitochondrial fusion activity.

Apart from regulating mitochondrial morphology, recent studies showed that Usp30 opposes PINK1/Parkin-mediated mitochondria-specific autophagy (mitophagy) by antagonizing E3 Ub ligase Parkin mediated ubiquitination of various OMM proteins. When overexpressed, Usp30 removed Ub attached to the OMM proteins modified by Parkin on damaged mitochondria and blocked Parkin-driven mitophagy, whereas loss of Usp30 activity rescued defective mitophagy caused by pathogenic mutations in Parkin and improved mitochondrial integrity in Parkin- or PINK1- deficient flies (Bingol et al. 2014). These data suggest that Usp30 and Parkin form a paired system that modulates mitophagy. Global ubiquitination profiling identified multiple mitochondrial substrates oppositely regulated by Parkin and Usp30, including Tom20, MIRO1, VDAC and FKBP8 (Cunningham et al. 2015). Further confirming a Usp30-dependent mechanism of mitochondrial protein deubiquitination, mass spectrometry and peptide quantification showed that Usp30 preferentially removes K-6 and K-11 Ub chains from intact mitochondria upon CCCP treatment (inducer of mitophagy), whereas mitochondrial damage stimulates parkin to assemble K-6-, K-11- and K-63- linked polyubiquitin chains on mitochondria (Cunningham et al. 2015).

It also appears that Usp30-dependent Ub dynamics at the OMM contributes to apoptotic cell death (Liang et al. 2015). Usp30 deletion enhanced CCCP-induced cell death in Parkin overexpressing cells, suggesting that the presence of Usp30 delays CCCP-induced cell death caused by excessive Parkin activation. Moreover, Usp30

deletion by siRNA sensitized cells to BH3-mimetics ABT-737 and ABT-263 independent of Parkin overexpression, suggesting that Usp30 counteracts Bax/Bak-dependent apoptosis.

In this chapter, I report that Usp30 also controls Drp1-mediated mitochondrial division. I found that loss of Usp30 DUB activity resulted in elongated mitochondrial network, stabilization of Drp1-containing mitochondrial fission complexes and actin filaments on mitochondrial surface, suggesting a novel role of Usp30 in regulating mitochondrial fission.

Section 2: Materials and Methods

Subsection 1: Cell culture

HeLa cells were cultured in DMEM medium supplemented with 10% heat-inactivated fetal bovine serum, 2 mM Glutamax, 1 mM sodium pyruvate, 1 mM non-essential amino acids, 100 U/ml penicillin in 5% CO_2 at 37°C. Wild type and $Usp30^{-/-}$ HCT116 cells generated by CRISPR/Cas9 technology were cultured in McCoy's 5A medium supplemented with 10% heat-inactivated fetal bovine serum, 2 mM Glutamax, 1 mM sodium pyruvate, 1 mM non-essential amino acids, 100 U/ml penicillin in 5% CO_2 at 37°C.

Subsection 2: General experimental methods

Cell transfection, immunofluorescence, image acquisition, live cell imaging, and Western blot were performed as described in Chapter 2 (Section 2 Materials and Methods) and Chapter 3 (Section 2 Materials and Methods).

Subsection 3: DNA expression constructs

FLAG-Usp30^{WT}, FLAG-Usp30^{CS} and FLAG-Usp30$^{\Delta TM}$ mammalian expression constructs were described previously (Nakamura & Hirose 2008) and kindly provided by Dr. Nakamura (Tokyo Institute of Technology, Japan). YFP-Drp1 was described before (Karbowski et al. 2007). mRuby-Lifeact construct was also already described before (Riedl et al. 2008) and kindly provided by Dr. T. Blanpied (University of Maryland Baltimore, USA).

Subsection 4: Antibodies

The primary antibodies used for immunofluorescence studies were anti-Tom20 polyclonal antibody (1:2000; Santa Cruz), anti-cytochrome c mAb (1:500; BD Biosciences), anti-Usp30 (1:500; Sigma-Aldrich) and anti-FLAG monoclonal and polyclonal antibodies were from Sigma-Aldrich (St. Louis, MO). The primary antibodies used for Western blot were anti-Usp30 polyclonal antibody (1:1000; Sigma-Aldrich), anti-Drp1 monoclonal antibody (1:1000; BD Biosciences), anti-Tom20 polyclonal antibody (1:5000; Santa Cruz) and anti-FLAG tag antibodies (1:5000; Sigma-Aldrich).

Subsection 5: Fluorescence recovery after photobleaching (FRAP) analysis

FRAP of YFP-Drp1 was performed as described earlier (Karbowski et al. 2007). Briefly, cells were examined through a 40x plan-Neofluar oil immersion objective (NA=1.3) on an inverted microscope (AxioObserver Z1; Zeiss MicroImaging) with a laser scanning confocal microscope (LSM 510) controlled by Zeiss Efficient Navigation (Zen 2009) software. YFP-Drp1 was excited using a 514

nm argon laser, while fluorescent emission was isolated using a 535-590 nm band-pass filter and collected on a photomultiplier tube. Regions of interest (~ 5 μm^2) were bleached by repetitive scanning (50 iterations) with the 514 nm laser (25 mW) at maximal emission over ~5s. Fluorescent recovery was monitored at an acquisition rate of 0.63 frame/s. Focus stability during time-lapse recordings was maintained using the definite focus module, an add-on for the Observer Z1. All FRAP experiments were conducted at room temperature. Image analyses were performed using either Efficient Navigation (Zen 2009) software or AxioVision 4 software, both supplied by Zeiss MicroImaging.

Subsection 6: Super-resolution direct stochastic optical reconstruction microscopy (dSTORM)

The single-molecule-based super-resolution dSTORM determines the precise position of individual fluorophores that are further apart than the minimal distance resolved by the microscope by evaluating their diffraction patterns in the imaging plane, thus, are heavily dependent on the number of detected photons (van de Linde et al. 2011). A super-resolution fluorescence image is finally reconstructed by summing up all localizations. The temporal seperation of fluorophore emission is achieved by the photoactivated or reversibly photoswitched fluorescent proteins and organic fluorophores between OFF state earned by reducting thiol compound that efficiently quenches the fluorophore's triplet state and generates a stable non-fluorescent reduced state (dark) and ON state by spontaneously recovering of fluorophore in aqueous solvents (Heilemann et al. 2009).

dSTORM imaging was accomplished using the ELYRA PS.1 super-resolution platform (Zeiss MicroImaging). (dSTORM), a recently developed super-resolution microscopy technology with typical resolutions of 30-50nm, up to 10 times higher than the resolution of confocal microscopy. Following immunocytochemistry staining, cells were imaged through a 100x alpha Plan-Apochromat oil immersion objective (NA=1.46) on an inverted microscope (AxoObserver Z1). The combination of a strong reducing buffer (dSTORM buffer: 44.4 mM Tris, 9.2 mM NaCl, 8.8% glucose, 0.56 mg/ml Glucose Oxidase, 0.034 mg/ml Catalase, and 100 mM MEA), and a powerful 100mW solid-state 642 nm laser in the total internal fluorescence (TIRF) configuration was used to cause the fluorophore [Alexa 647; in conjugation with anti-Drp1 monoclonal antibody (BD Bioscences) used to detect endogenous Drp1 protein] to continually switch from bright to dark states. Fluorescent emission was acquired by an Andor iXon 897 camera after passing through a 655 nm long-pass filter. Acquisition control and image analysis was completed using Zeiss Efficient Navigation (Zen 2010D) software, which allowed for single molecule localization and drift correction.

Subsection 7: Subcellular fractionation

Cells were harvested, and total cell protein lysates and subcellular fractions were prepared as previously described (Karbowski et al. 2007). Cells were harvested 18 hours after transfection and then suspended in swelling buffer (10 mM HEPEs, 10 mM NaCl, 1.5 mM $MgCl_2$). Cells were disrupted by 15 passages through a 25-gauge needle (with 1-ml syringe). The heavy membrane fraction (HM) was obtained by

centrifugation at 6,000 *g* for 10 min. Protein lysates were analysed by 4-20% SDS-PAGE followed by Western blot.

Subsection 8: Blue Native PAGE, crosslinking and immunoprecipitation

Blue Native PAGE (BN-PAGE) was performed with Native PAGE 3-12% Bis-Tris gel system, using cell lysates obtained by incubation with 1% DDM (n-dodecyl β-D-maltoside; Invitrogen) in BN-PAGE sample buffer for 30 min, following the manufacturer's recommendations (Invitrogen). Immunoprecipitation (IP) was performed as previously described (Benard et al. 2010). Cells were harvested and lysed using IP lysis buffer containing: 25 mM Tris (pH7.4); 0.15 M NaCl; 1 mM EDTA; 1% NP-40; 5 mM N-Ethylmaleimide and protease inhibitors cocktail (Roche), followed by immunoprecipitation using anti-FLAG monoclonal antibody (Sigma-Aldrich). Reversible cross-linking was performed with Dithiobis (Succinimidyl propionate) (DSP; Thermo Scientific). Briefly, cells were washed with PBS, followed by incubation in with 1 mM DSP in PBS containing Ca^{2+} and Mg^{2+}, for 2 hours on ice. The reaction was stopped by addition of 20mM Tris pH 7.4, and then crosslinked cell were collected and processed for IP. Irreversible crosslinking was performed with bismaleimidohexane (BMH; Life technologies). Cells was harvested, washed with PBS, and incubated with in 1 mM BMH in PBS for 30 min on ice.

Subsection 9: Generation of Usp30 knockout cells by CRISPR/Cas9 technology

To generate knockout cells in the Karbowski lab, we adopted a gRNA synthesis protocol generated by the Church lab (Mali et al. 2013), and a protocol

established by Orkin for efficient deletion of desired genomic regions in mammalian cells. Usp30 (Gene ID 84749) is encoded by 4145 nucleotides assembled on chromosome 12 (GRCh38.p2), NC_000012.12 (109023089-109088026). The Usp30 gene consists of 14 exons, and the coding sequence of Usp30 ranges from 110-1663 spreading between exon 1 and exon 14. The DUB domain catalytic site Cys77 is localized on exon 3 (303-485) (109,057,926-109,058,108). In order to deplete Usp30, we designed two gRNA constructs that target both sides of the exon 3 with a 23 bp genomic sites of the form 5'-N^{20}NGG-3', utilizing the online design tool DNA2.0 CRISPR gRNA design tool (https://www.dna20.com/eCommerce/cas9/input). gRNA 1# targets sequence ranging from 109,057,907 to 109,057,929 on minus (-) strand, which localizes upstream of exon 3 with three nucleotides overlapping with 5' of exon 3. The Cas9 cleavage site is at 109,057,912-109,057,913 (Fig. 4.2). gRNA 2# targets sequence ranging from 109,058,060 to 109,058,083 on minus strand, which completely localized inside exon 3 close to the 3'-site. In this case, the Cas9 cleavage site was at 109,058,065-109,058,066 (Fig.4.2). The double-guided Cas9 cleavage led to a double DSB with NHEJ repair, which results in a 100 segments deletion of exon 3. Following gRNA synthesis protocol, we incorporated 19 bp (green region in Fig.4.4 and 4.5) of selected target sequence and its reverse complements into two 60 mer oligonucleotides as shown as step 2 in Fig.4.1 (reverse complements shown as red regions in Fig.4.4 and 4.5). After synthesizing these oligonucleotides, we annealed and extended these two oligonucleotides based on the overlapping region to yield a 100 bp double-stranded DNA fragments by using DNA polymerase. Then, we digested the gRNA cloning vector using AfIII and incorporated the 100 bp DNA

fragments with gRNA cloning vector using Gibson assembly, based on the 20-40 overlapping base-pairs between vector and DNA fragments, to obtain the desired gRNA constructs.

Following a protocol established to generate gene deletion in mammalian cell lines (Bauer et al. 2014), to introduce gRNA into cells we co-transfected gRNA1#, gRNA2#, Cas9 and YFP-tag into parental HCT116 cells by Lipofectamine 2000. YFP-tag was used as a marker to label transfected cells. After 18 hours, the bulk cells were collected, and prepared in a FACS tube. Then the heterogeneous cell mixture was sorted by YFP-positive fluorescence using Fluorescence-activated cell sorting (FACS), then plated one cell at a time to a 96-well plate in order to isolate single cell colonies. Cells in 96-well plates were incubated at 37 degrees for 1-2 weeks. After that, we reseeded the single cell colony that can be visualized under a microscope into cell culture plates for future screening (see Fig. 4.1 for general process).

To screen for the CRISPR/Cas9 clones, we validated the Usp30 deletion by evaluating both genomic DNA sequence and protein expression levels. To verify the DNA depletion, we design one set of internal primers and one set of external primers to validate the monoallelic or biallelic deletion clones (Fig. 4.3). The external primers are 5'-CATGTAGGGGAGAATGAGGA-3' and 5'-GTATCTATTGGGCTCTTGGTG-3', which are localized at about ~300bp upstream (109,057,590-109,056,609) and down stream of Usp30 exon 3 cleavage sites, while the internal primers are 5'-GTTAGGATAAATACTGGTGTGAG-3' and 5'-CTGTTCTCTTGTTCCCCCTG-3', covering the Cas9 cleavage sites sequence at both ends of exon 3 (Fig.4.3). We analyzed the genomic DNA by amplifying them

with these two sets of primers independently. We would be able to categorized the PCR results in three scenarios: (1) non-deletion: the presence of both ~800 bp band (external primers) and ~100 bp band (internal primers); (2) monoallelic deletion: the presence of ~800 bp band (external primers) and the absence of ~100 bp band (internal primers); (3) biallelic deletion: the presence of ~700 bp (external primers) and the absence of ~100 bp band (internal primers). The genome DNA results identified two biallelic deletion clones and one monoallelic clone.

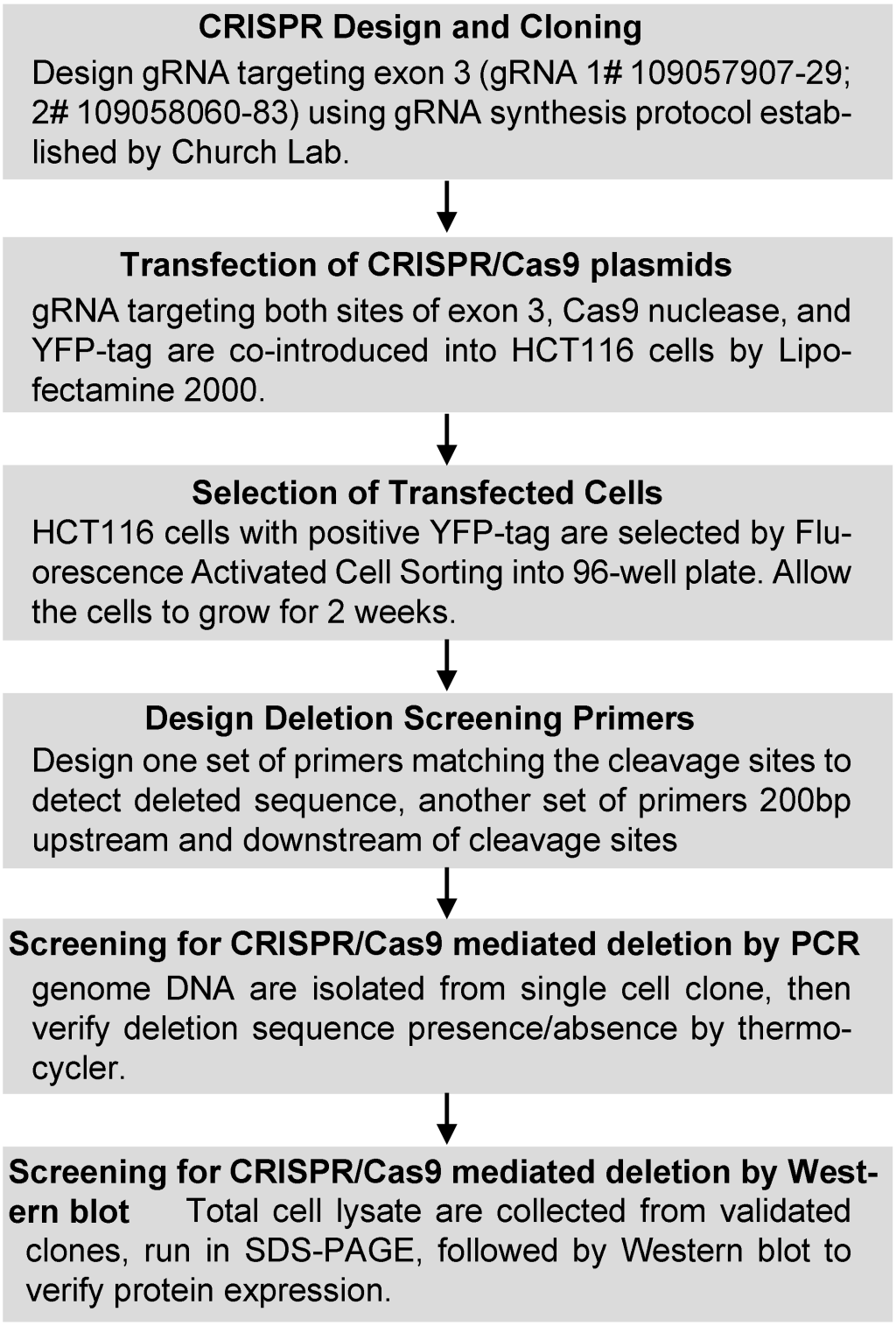

Figure 4.1 Flowchart of CRISPR/Cas9-mediated Usp30 deletion.

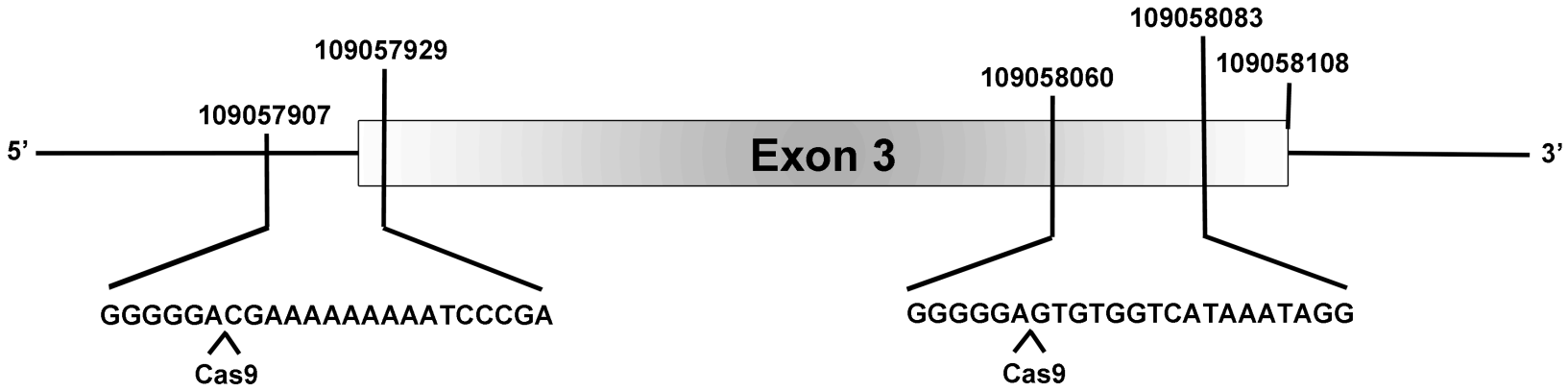

Figure 4.2 guide RNA targeting sequence of Usp30 gene

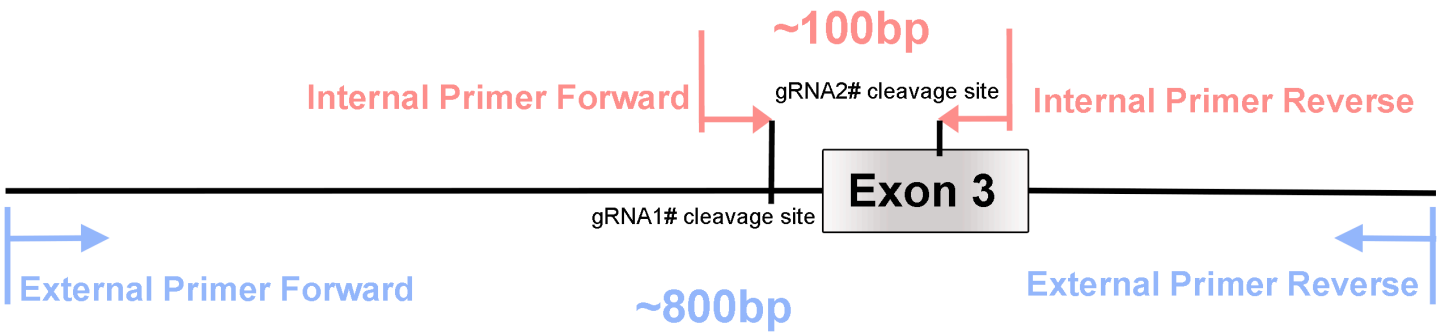

Figure 4.3 Design of validation primers

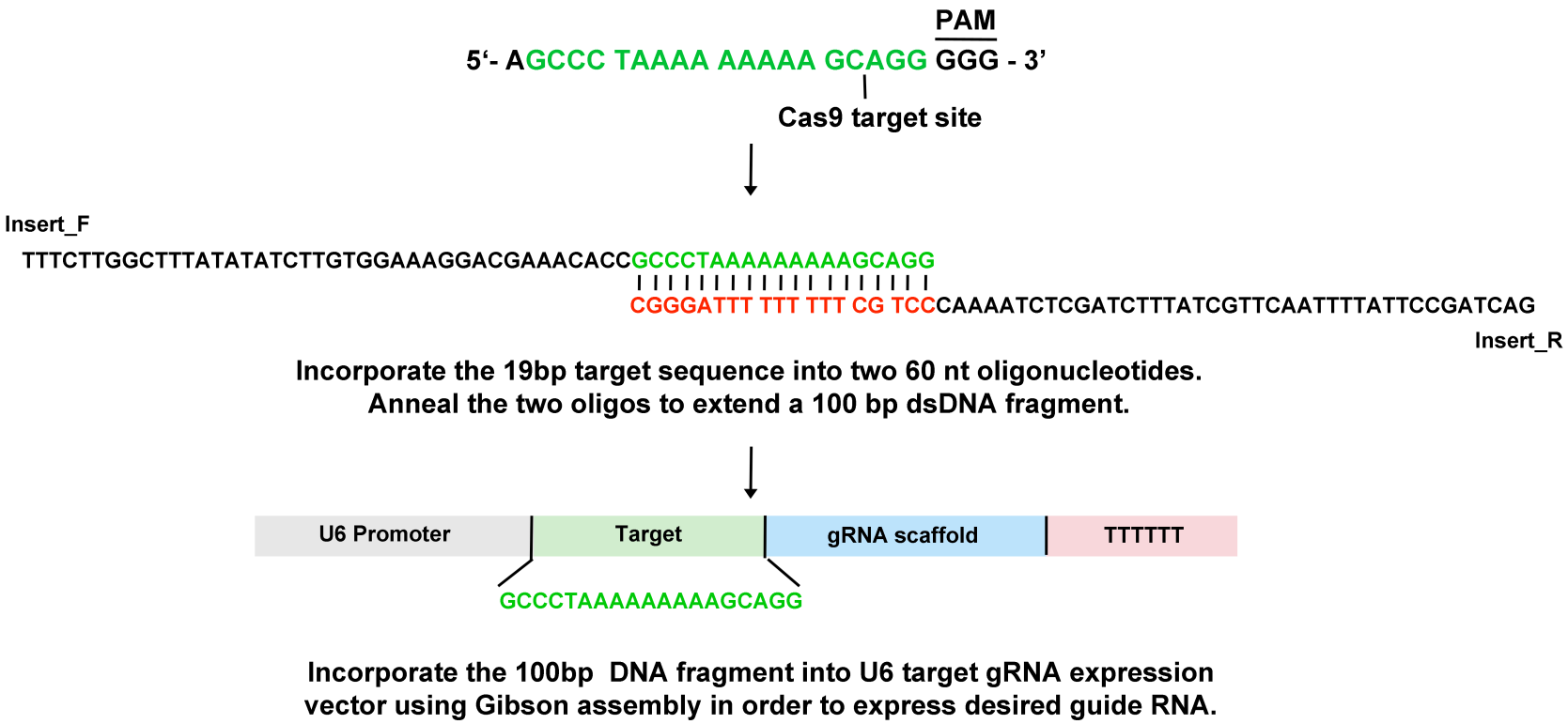

Figure 4.4 Schematic diagram of guide RNA 1# synthesis

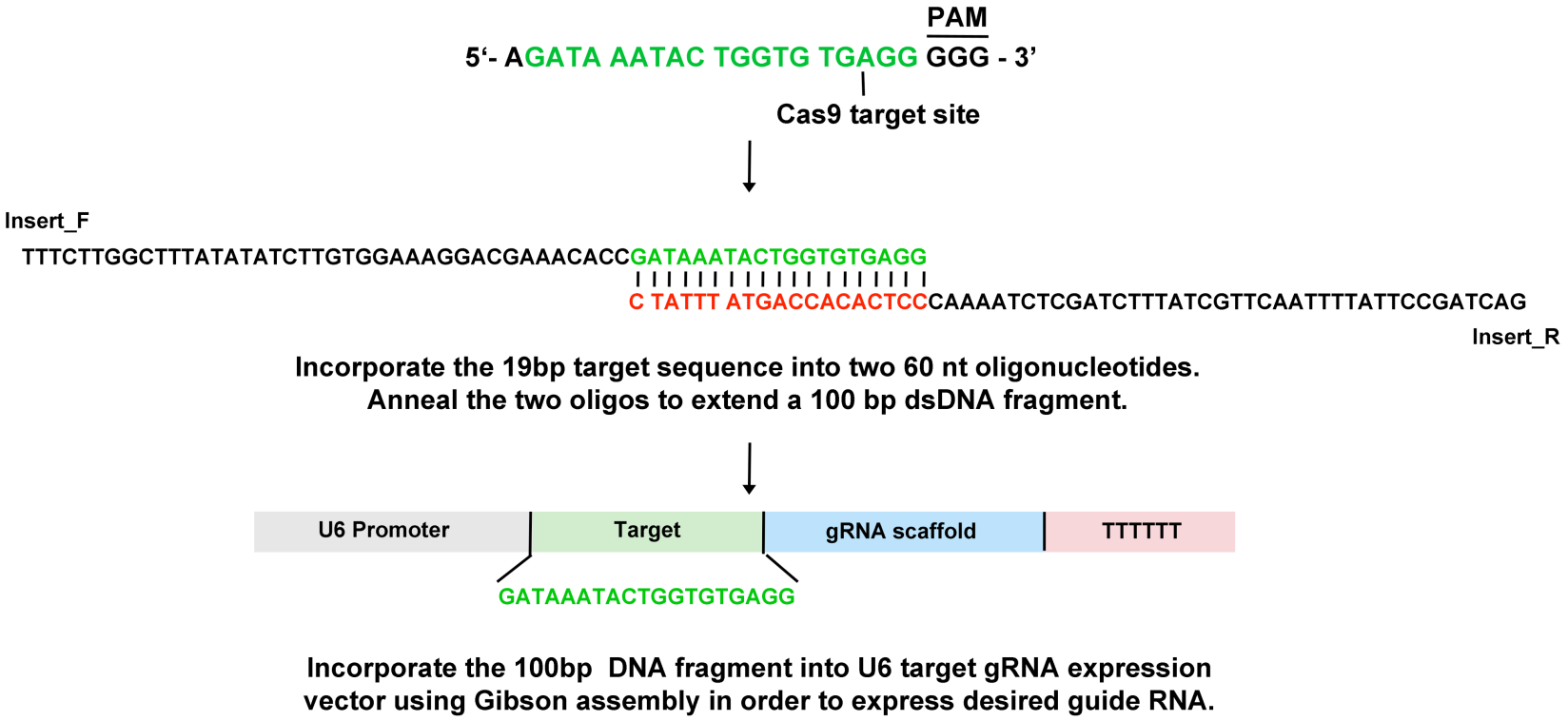

Figure 4.5 Schematic diagram of guide RNA 2# synthesis

Section 3: Results

Subsection 1: Expression of DUB activity-deficient Usp30^{CS} promotes mitochondrial elongation associated with mitochondrial accumulation of Drp1

Usp30 is a 517 amino acid protein, featuring an N-terminal transmembrane domain (residues 35-54), followed by a DUB catalytic domain (residues 69-499) (Figure 4.6) (Nakamura & Hirose 2008). First, we analyzed the subcellular localization of endogenous Usp30. HeLa cells were immunostained for Usp30 and cytochrome c, to reveal mitochondria, followed by structured illumination imaging. Immunofluorescence analysis revealed clear mitochondrial localization of endogenous Usp30 (Fig. 4.7). This result was also confirmed by cell fractionation analysis. Endogenous Usp30 was concentrated in mitochondria-enriched heavy membrane (HM) fractions, but not light membrane (LM) and cytosolic fractions (Fig. 4.8), in a similar manner to the OMM marker Tom20, further confirming that Usp30 is a mitochondrial protein.

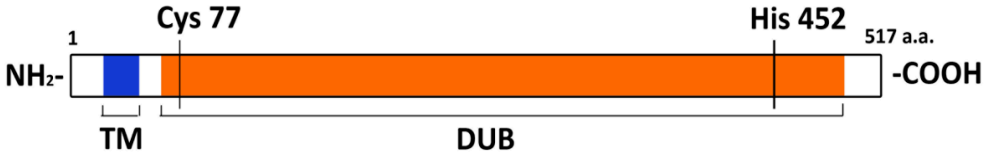

Figure 4.6 Usp30 domain organizations. Usp30 contains 517 amino acids featuring an N-terminal transmembrane domain and a central DUB domain.

A dominant negative mutant was generated by the mutation of the conserved cysteine residue (Cys77 to Ser; Usp30^{CS}) that was shown to abolish Usp30 DUB catalytic activity (Nakamura & Hirose 2008). To test the effect of Usp30^{CS} on

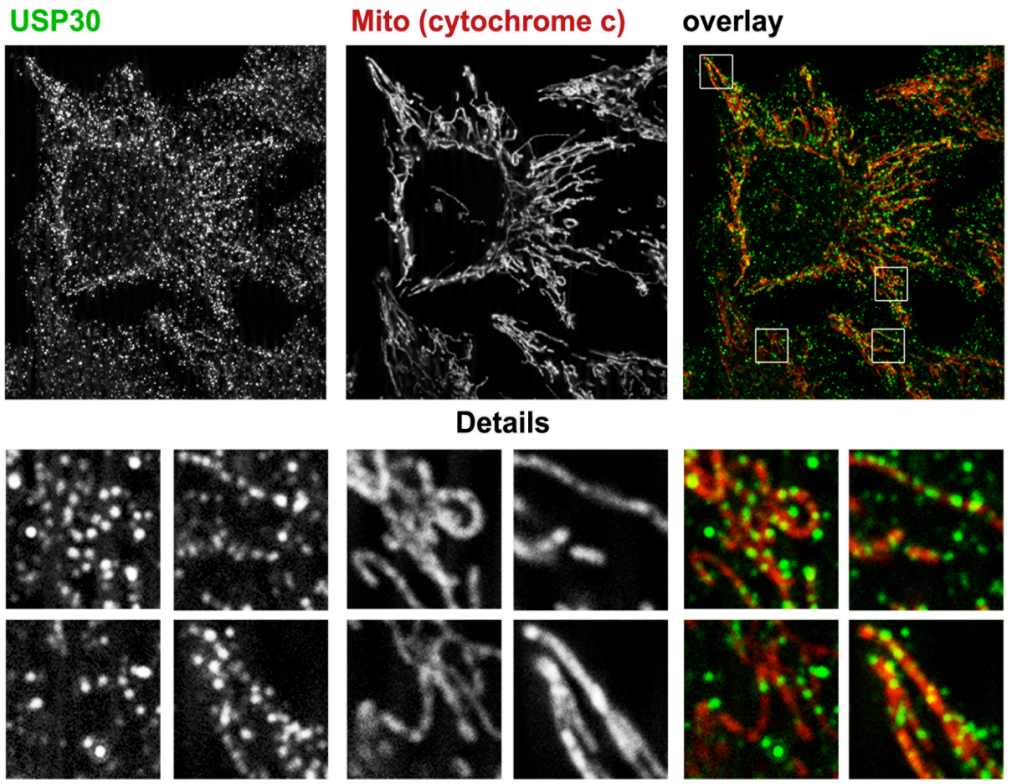

Figure 4.7 Subcellular localization of endogenous Usp30 in HeLa cells. HeLa cells were fixed and immunostained with anti-Usp30 antibody to detect endogenous Usp30 and anti-cytochrome c mAb to reveal mitochondria, followed by structured illumination imaging. Higher magnifications of areas marked with white rectangles are shown in detail images.

mitochondrial network organization, HeLa cells were transfected with FLAG-Usp30^{WT} and FLAG-Usp30^{CS}, fixed and immunostained with anti-FLAG antibody to detect exogenous Usp30 and anti-cytochrome c mAb, to reveal mitochondria followed by structured illumination imaging. While low expression levels of FLAG-tagged Usp30^{WT} or FLAG-Usp30^{CS} did not affect mitochondrial structure, as compared to untransfected control cells, higher expression levels of FLAG-Usp30^{WT} or FLAG-Usp30^{CS} resulted in dramatic differences in mitochondrial network organizations. While overexpression of FLAG-Usp30^{WT} induced mild fragmentation of mitochondrial tubules, expression of FLAG-Usp30^{CS} led to an extensive

mitochondrial tubulation (Fig. 4.9). Interestingly, mitochondrial changes observed in cells expressing higher levels of FLAG-Usp30^{CS}, formation of thin elongated mitochondrial tubules in particular, were highly reminiscent of the mitochondrial alterations induced by overexpression of recently identified mitochondrial fission factors MiD49 and MiD51. Given that overexpression of MiD49/51 led to abnormal accumulation of mitochondrial fission protein Drp1 on mitochondrial tubules, therefore suggesting that MiD49/51 may serve as mitochondrial receptor of Drp1, we also tested the effects of FLAG-Usp30^{WT} and FLAG-Usp30^{CS} on subcellular distribution of Drp1.

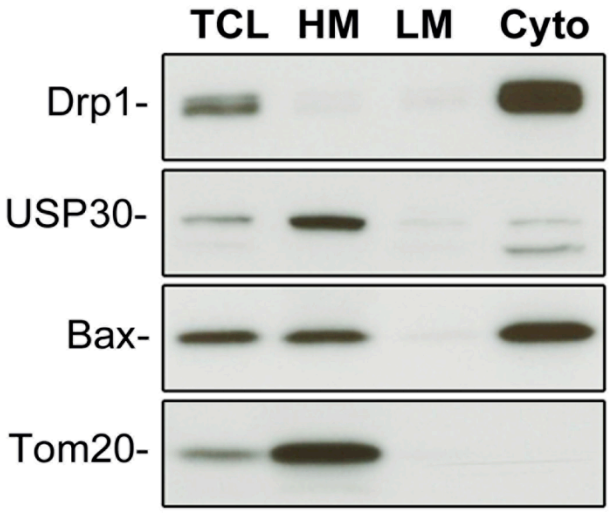

Figure 4.8 Subcellular localization of Usp30. Total cell lysate (TCL), heavy membrane fraction (HM), light membrane fraction (LM), and cytosol fraction were isolated from HeLa cells and analyzed by Western blot. Blots were immunostained with anti-Drp1, anti-Usp30, anti-Bax and anti-Tom20 antibodies.

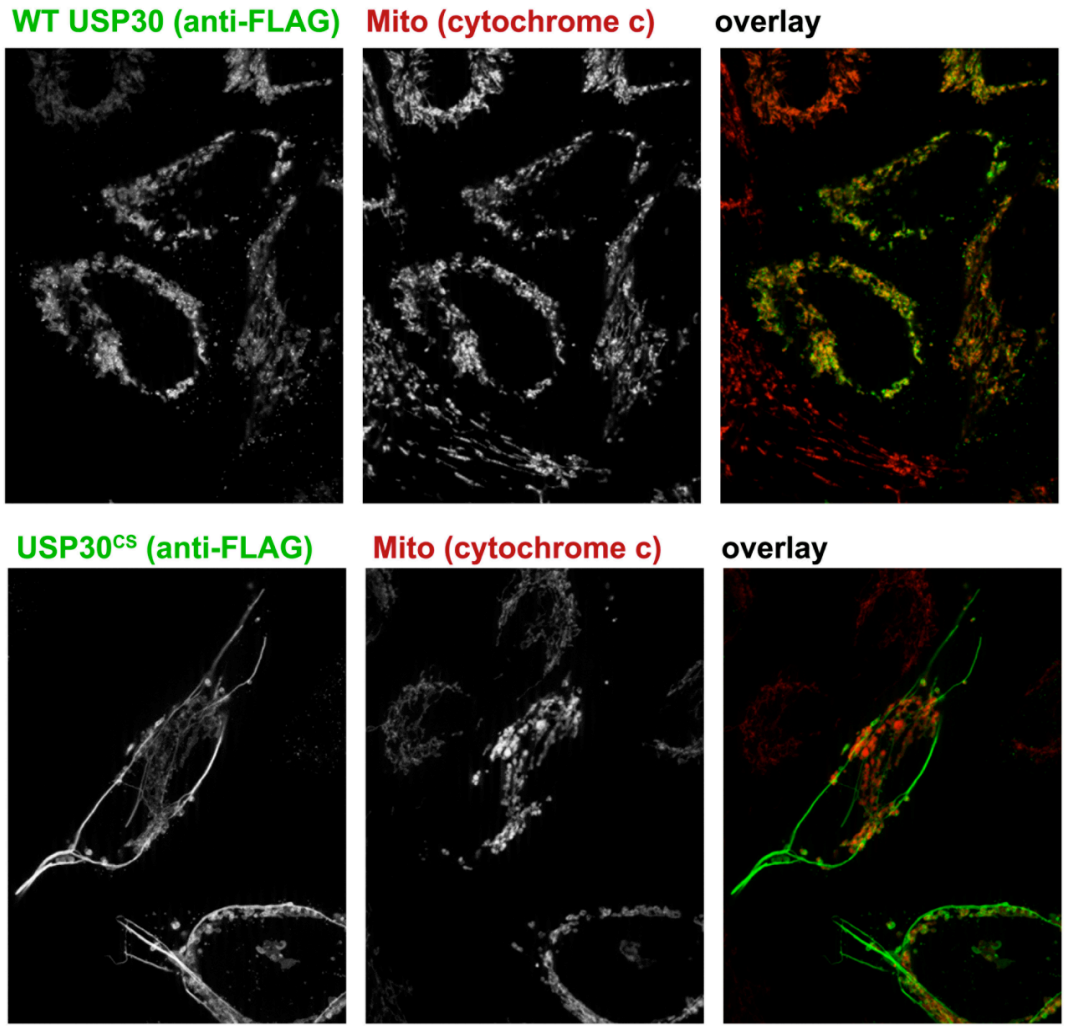

Figure 4.9 The effect in mitochondrial network organization of overexpression of Usp30^{WT} and Usp30^{CS}. HeLa cells were transfected with FLAG-tagged Usp30^{WT} and FLAG-Usp30^{CS}, immunostained with anti-FLAG antibody (green on the overlay image) and anti-cytochrome c mAb (red on the overlay image), followed by structured illumination imaging.

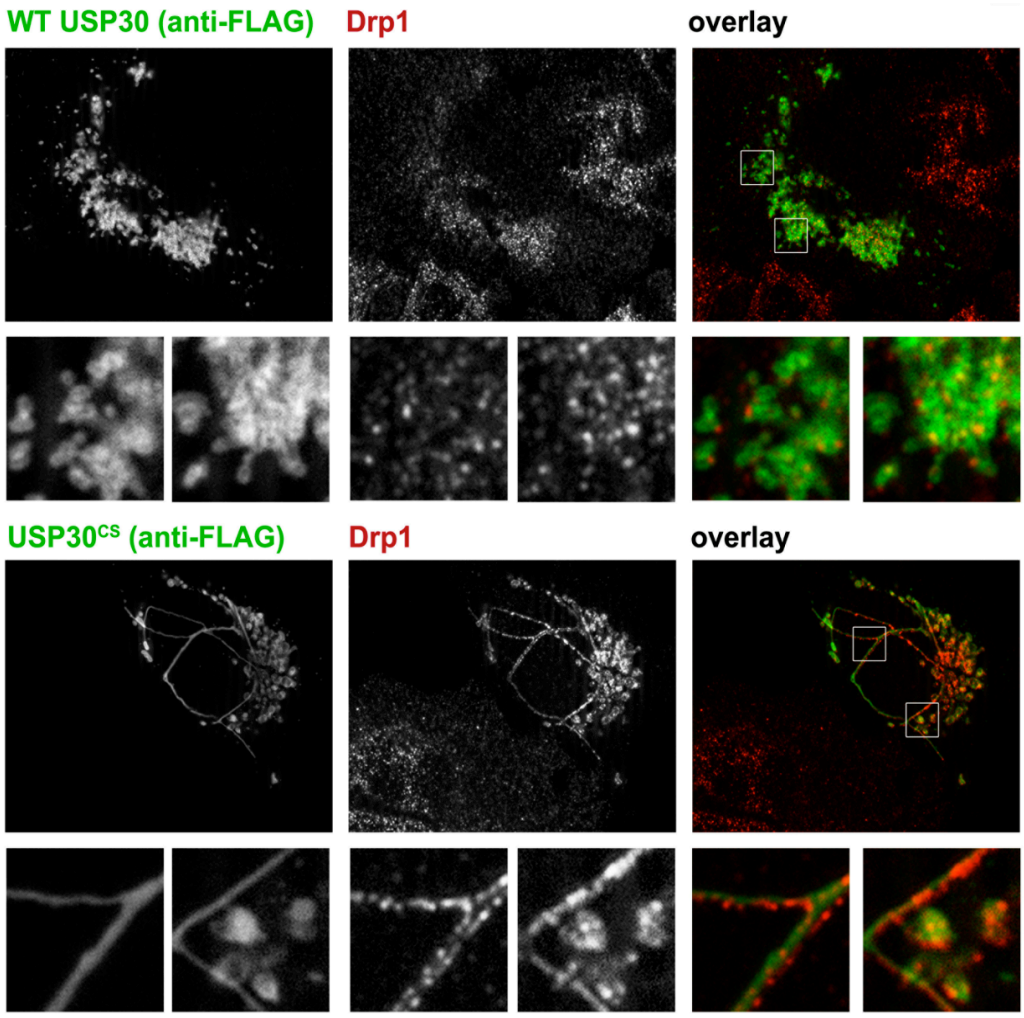

Figure 4.10 Mitochondrial associated Drp1 accumulation in Usp30^{WT} and Usp30^{CS}-expressing cells. HeLa cells were transfected with FLAG-Usp30^{WT} and FLAG-Usp30^{CS}, fixed and immunostained with anti-FLAG to reveal exogenous Usp30 (green on the overlay images) and anti-Drp1 mAb (red on the overlay images).

To achieve this, HeLa cells transfected with FLAG-Usp30^{WT} and FLAG-Usp30^{CS}, were immunostained with anti-FLAG antibody to label exogenous Usp30 and anti-Drp1 antibodies to detect endogenous Drp1, followed by structured illumination imaging. Expression of FLAG-Usp30^{CS} led to a dramatic redistribution of endogenous Drp1 from the cytosol to the mitochondria in a similar manner to

MiD49/51 overexpression, while overexpression of FLAG-Usp30^{WT} did not alter subcellular localization of Drp1 (Fig. 4.10). The degree of mitochondria-associated Drp1 increase appeared to positively correlate with the expression level of Usp30^{CS}. These results were further confirmed by cell fractionation. Subcellular fractions isolated from untransfected HeLa cells and cells transfected with FLAG-Usp30^{WT}, FLAG-Usp30^{CS}, or FLAG-Usp30$^{\Delta TM}$ (transmembrane domain-deficient Usp30 mutant) were analyzed by Western blot. The data showed that Drp1 accumulated in the mitochondria-enriched HM fractions in Usp30^{CS}-expressing cells, but not in Usp30^{WT} or Usp30$^{\Delta TM}$-expressing cells (Fig.4.11). Thus, Usp30^{CS} appears to induce mitochondrial elongation associated with mitochondrial accumulation of Drp1, suggesting that Usp30 may control mitochondrial division via regulating the trafficking of Drp1 between the mitochondria and the cytosol.

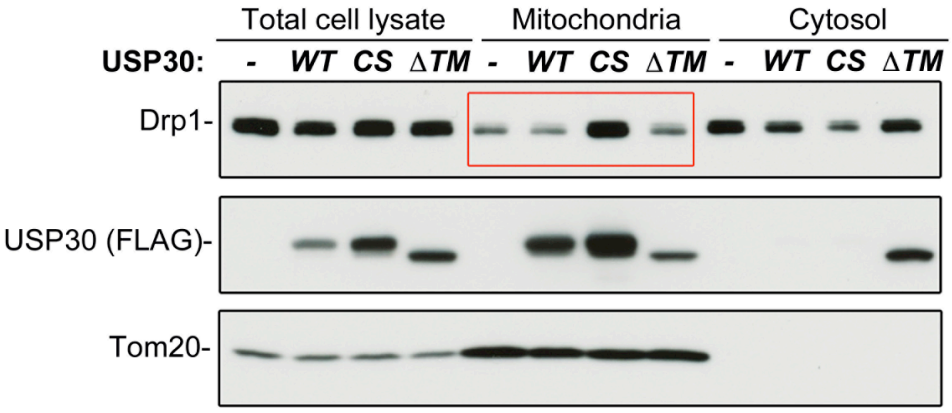

Figure 4.11 Subcellular fractionation of Usp30^{WT}-, Usp30^{CS}- and Usp30$^{\Delta TM}$-expressing cells. HeLa cells transfected with FLAG-Usp30^{WT}, FLAG-Usp30^{CS} and FLAG-Usp30$^{\Delta TM}$, were fractionated and analyzed by Western blot. Blots were immunostained with anti-Drp1 mAb, anti-FLAG antibody to detect exogenous Usp30, and anti-Tom20 antibody as loading control.

Subsection 2: Usp30 deletion results in mitochondrial elongation

To verify the role of Usp30 in the control of mitochondrial division, using CRISPR/Cas9 technology, we generated Usp30 knockout HCT116 cells. The successful Usp30 knockouts were verified by Western blot (Fig 4.12). We investigated the mitochondrial morphology in wild type and Usp30 knockout ($Usp30^{-/-}$) HCT116 cells. Parental cells and 3 different clones of $Usp30^{-/-}$ HCT116 cells were fixed and immunostained with anti-cytochrome c mAb to reveal mitochondrial network morphology. The data showed that $Usp30^{-/-}$ cells exhibited extensively elongated and interconnected mitochondrial tubules (Fig. 4.13), as compared to parental HCT116 cells.

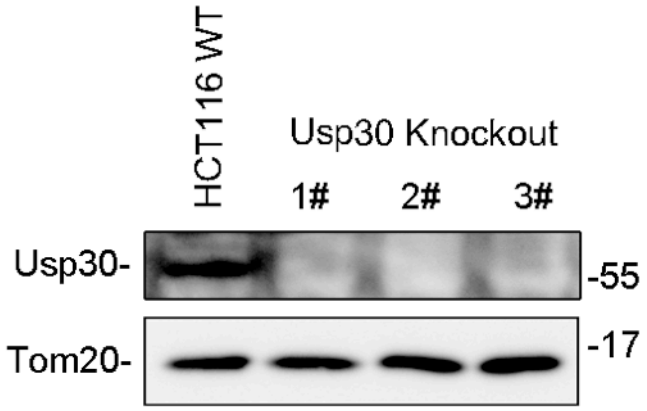

Figure 4.12 Usp30 expression in parental and $Usp30^{-/-}$ HCT116 cells. Total cell lysate from Wild type and three clones of $Usp30^{-/-}$ HCT116 cells were analyzed by Western blot. Blots were immunolabeled with anti-Usp30 antibody to detect endogenous Usp30 expression and anti-Tom20 antibody as a loading control.

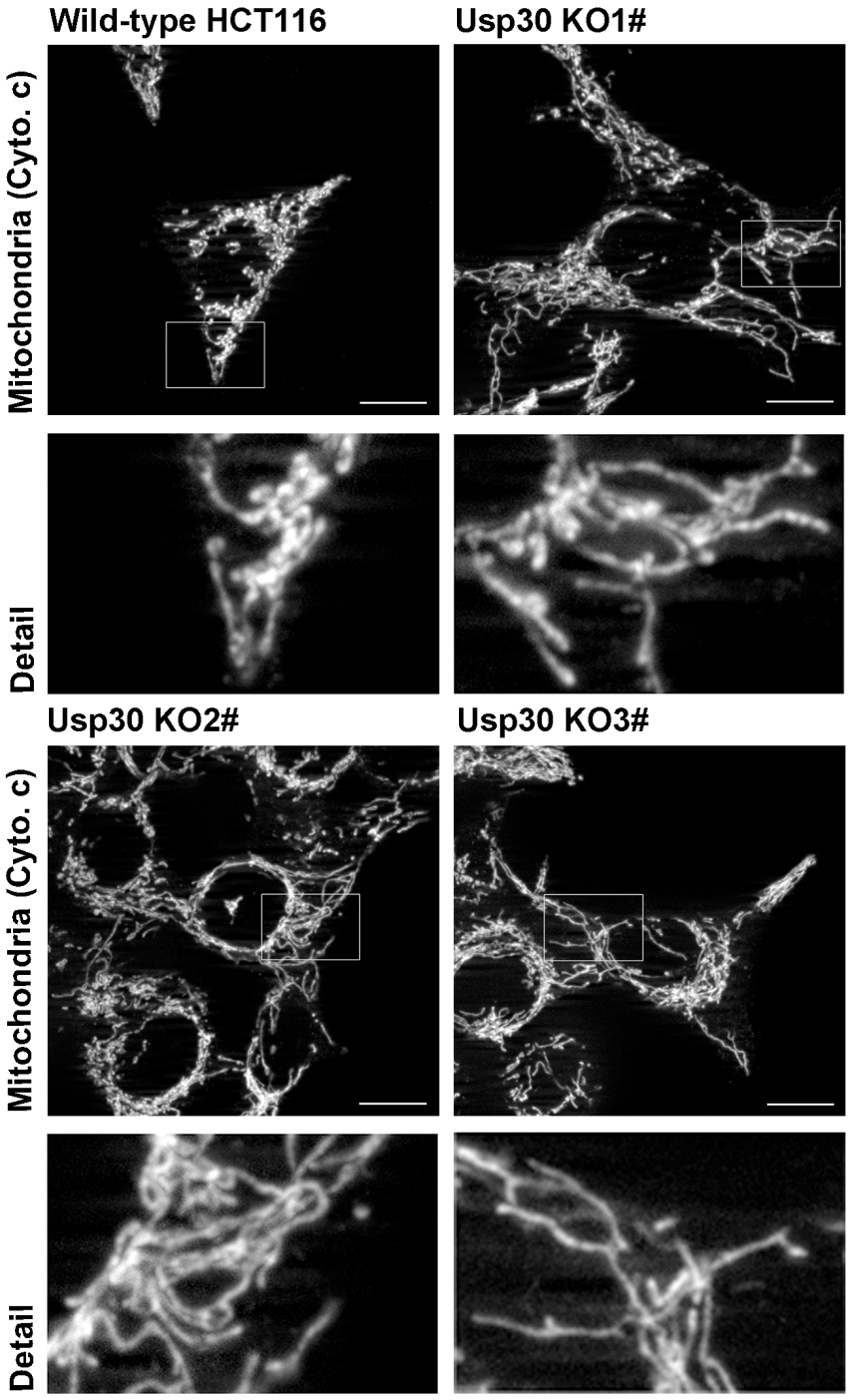

Figure 4.13 Mitochondrial morphology in Usp30$^{-/-}$ HCT116 cells. Wild type and 3 clones of Usp30$^{-/-}$ HCT116 cells were fixed and immunostained with anti-cytochrome c mAb. The mitochondrial-enriched z-sections corresponding to the vertical part of the cells were stacked. Higher magnifications of areas marked with rectangles are shown in detail images.

Subsection 3: Expression of Usp30^{CS} induces high molecular weight Drp1 complex formation

Given that overexpression of Usp30^{CS} led to mitochondrial elongation accompanied by the mitochondrial accumulation of Drp1, it is possible that Usp30 controls mitochondrial fission steps downstream of mitochondrial Drp1 recruitment. Under this scenario, Drp1 would accumulate and oligomerize on the OMM but would not be able to complete mitochondrial membrane scission. To test this hypothesis, we first examined whether Usp30 interacted with Drp1 on the mitochondria. Untransfected cells and cells transfected with FLAG-Usp30^{WT} and FLAG-Usp30^{CS} were lysed, and ectopically expressed Usp30 was immunoprecipitated with anti-FLAG antibody, followed by Western blot analysis. In addition, to increase the chance to reveal the physical interaction between these proteins, a reversible membrane permeable chemical crosslinker Dithiobis(succinimidyl propionate) (DSP) was applied to the cell culture dishes prior to cell lysis and immunoprecipitation. The data showed that while Drp1 coimmunoprecipitated with Usp30^{CS} in both DSP-treated and untreated cells, a detectable coimmunoprecipitation of Drp1 with wild type Usp30 was observed only in DSP-treated cells. Furthermore, application of DSP increased the amount of Drp1 coimmunoprecipitating with Usp30^{CS}, as compared to non-crosslinked samples. These data support the possibility that inactivation of the Usp30 DUB domain led to stabilization of normally transient/weak protein complexes containing Usp30 and Drp1 (Fig. 4.14).

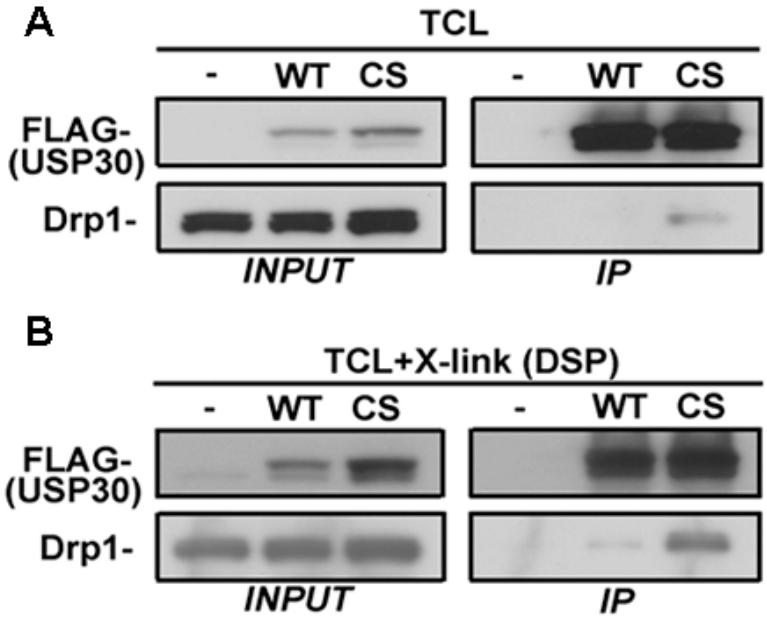

Figure 4.14 Immunoprecipitation of ectopically expressed Usp30 in HeLa cells. Untransfected cells and cells transfected with FLAG-Usp30^{WT} and FLAG-Usp30^{CS} were (A) directly immunoprecipitated by anti-FLAG antibody, (B) incubated with DSP prior to lysis, then immunoprecipitated by anti-FLAG antibody, and analyzed by Western blot. Blots were immunostained by anti-FLAG antibody to detect Usp30, and anti-Drp1 mAb.

Upon recruitment from the cytosol to the mitochondria, Drp1 oligomerizes, and these oligomers are believed to mediate mitochondrial membrane scission. To test whether Usp30 is involved in the regulation of mitochondrial Drp1 oligomerization, we applied Blue Native polyacrylamide gel electrophoresis (BN-PAGE). Consistent with published data, in control cells Drp1 was detected as a ~240 kD complex. While the same Drp1 pattern was also detected in cells expressing Usp30^{WT}, expression of Usp30^{CS} led to formation of higher molecular weight Drp1 complexes, suggesting that Usp30^{CS} either promotes the formation of Drp1 oligomers, or inhibits disassembly of these structures (Fig. 4.15).

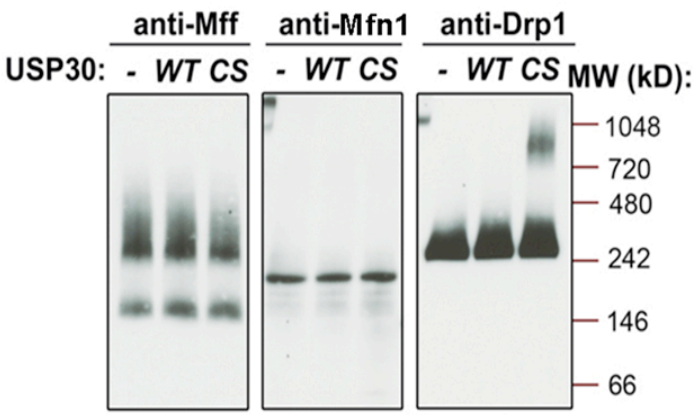

Figure 4.15 Formation of high molecular weight complex of Drp1 in Usp30^{WT}- and Usp30^{CS}- expressing cells. HeLa cells were transfected with Usp30^{WT} and Usp30^{CS}, and analyzed by BN-PAGE followed by Western blot. Blots were immunostained by anti-Mff, anti-Mfn1 and anti-Drp1 antibodies.

Furthermore, non-reversible crosslinker bismaleimidohexane (BMH) was also employed to analyze the oligomeric status of Drp1. Total cell lysates and mitochondria-enriched HM fractions isolated from HeLa cells transfected with either Usp30 or Usp30^{CS} were crosslinked by BMH and then analyzed by Western blot. Confirming BN-PAGE analysis, high molecular weight Drp1 complexes, were detected in crosslinked TCL isolated from the cells expressing Usp30^{CS}. The accumulation of Drp1 oligomers in Usp30^{CS}-expressing cells was even more apparent in HM fractions, suggesting that Usp30^{CS} expression specifically affected oligomerization of the mitochondria-associated subset of Drp1 (Fig. 4.16).

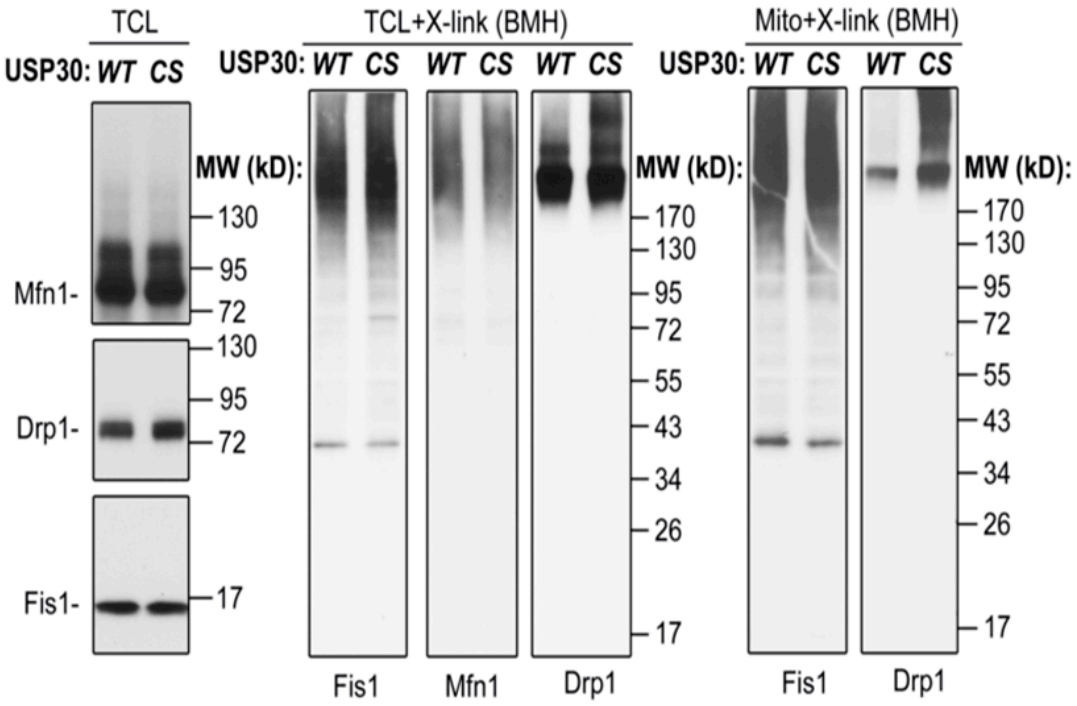

Figure 4.16 BMH crosslinking in total cell lysate and mitochondrial fractionation of Usp30^{WT}- and Usp30^{CS}- expressing cells. HeLa cells were transfected with Usp30^{WT} and Usp30^{CS}, fractionated, crosslinked by BMH, and then analyzed by Western blot. Blots were immunostained by anti-Mfn1, anti-Drp1 and anti-Fis1 antibodies.

Given that oligomeric status of Drp1 is controlled by Usp30 activity, we further tested the assembly status of Drp1 on the mitochondria by taking advantage of dSTORM. Cells transfected with YFP-vector (control), FLAG-Usp30^{WT} and FLAG-Usp30^{CS} were processed for immunofluorescence, using anti-FLAG antibody followed by Alexa-488 secondary antibody (to detect cells expressing Usp30), and anti-Drp1 antibody followed by Alexa-647 secondary antibody. FLAG-Usp30^{WT}- and FLAG-Usp30^{CS}- expressing cells were identifed by green fluorescence signal and followed by STORM anlysis of Alexa-647 fluorescence signal in FLAG tag-postitive cells. While there was no apparent difference in the size and distribution of Drp1 in control and FLAG-Usp30^{WT}-expressing cells, confirming immunofluorescence and biochemical studies, a significant increase in the size of Drp1 clusters was apparent in

FLAG-Usp30^{CS}-expressing cells (Fig. 4.17). Furthermore, Drp1 clusters in FLAG-Usp30^{CS}-expressing cells formed organized assemblies, reminiscent of the Drp1 spirals predicted to be formed before completion of the mitochondrial fission process.

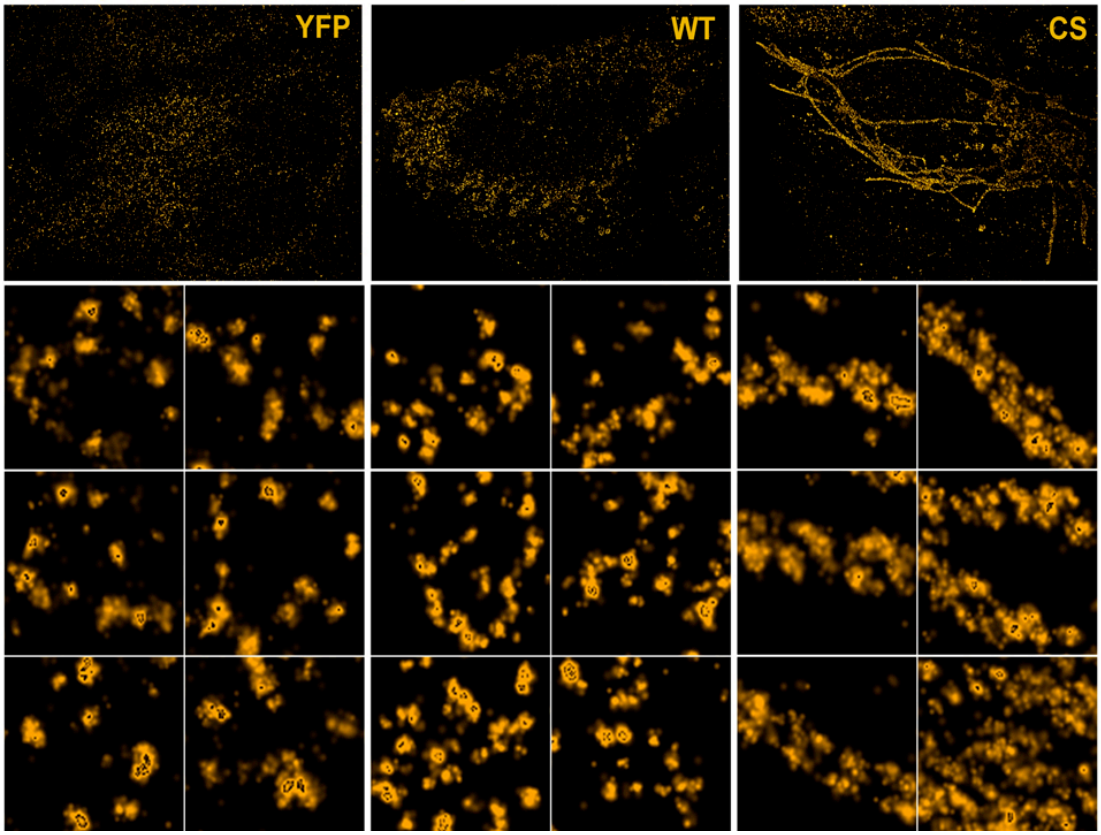

Figure 4.17 dSTORM microscopy of Drp1 organization in Usp30^{WT}- and Usp30^{CS}- expressing cells. HeLa cells were transfected with YFP-vector, Usp30^{WT} and Usp30^{CS}, then immunostained with anti-FLAG antibody followed by Alexa-488 antibody, and anti-Drp1 mAb followed by Alexa-647 antibody. Usp30^{WT}- and Usp30^{CS}- expressing cells were identified by 488 fluorescent signals, and then analyzed by STORM microscopy. Higher magnifications are shown in detail images.

The data showing that expression of Usp30^{CS} has a strong impact on the subcellular localization of Drp1 suggest that Usp30 is involved in the regulation of Drp1 and mitochondrial fission complexes. Drp1 and its yeast homologue Dnm1 cycle between the cytosol and the mitochodnria. It is possible that the abnormal accumulation of Drp1 on the OMM in the response to the expression of Usp30^{CS} is

caused by changes in the subcellular dynamics of Drp1. However, it is also likely that this is caused by anomalous transitions between distinct steps of Drp1-dependent mitochondrial fission, after Drp1 is recruited to the mitochondria in the Usp30-independent manner. The following experiments tested these possibilities. First, the mobility of YFP-Drp1 in cells cotransfected with $Usp30^{WT}$, $Usp30^{CS}$ and YFP-Drp1 (Usp30/Drp1 ratio 6:1) or in YFP-Drp1 only transfected cells was analyzed by fluorescence recovery after photobleaching (FRAP) assay. Like endogenous Drp1, YFP-Drp1 accumulated on the mitochondria in $Usp30^{CS}$-expressing cells. To measure FRAP, regions of interests (ROIs) selected within YFP-Drp1-expressing cells were photobleached by irradiation with a high-power laser and subsequent fluorescence recovery within the ROIs was monitored over ~180 seconds. As shown in Fig.4.18, a distinct decline in the mobility of YFP-Drp1 in cells coexpressing $Usp30^{CS}$ and YFP-Drp1 was evident, as compared to cells expressing YFP-Drp1 only, or Drp1 and wild type Usp30.

In sum, the data described above demonstrate that expression of catalytically inactive Usp30 mutant leads to abnormal stabilization of mitochondrial associated Drp1. Since Drp1 fission complexes in these cells are larger than in control or $Usp30^{WT}$-expressing cells, it is possible that Usp30 participate in late stages of mitochondrial fission, perhaps membrane scission and/or conversion of Drp1 fission complexes.

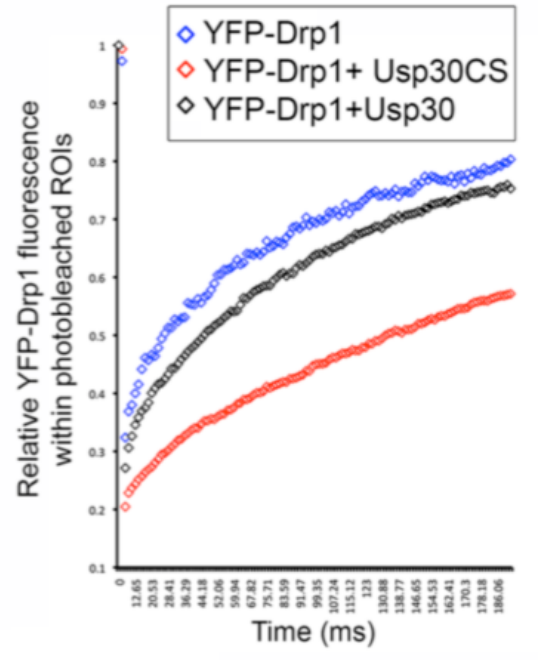

Figure 4.18 The motility of YFP-Drp1 in Usp30^{WT}- and Usp30^{CS}- expressing cells analyzed by FRAP. HeLa cells were cotransfected with YFP-Drp1, YFP-Drp1 and Usp30^{WT}, or YFP-Drp1 and Usp30^{CS}, analyzed by FRAP.

Subsection 4: Mitochondrial and Drp1 remodeling upon forced mitochondrial division

It is well established that mitochondrial uncoupler FCCP or CCCP can induce Drp1-dependent mitochondrial fission. These compounds are commonly used to determine whether mitochondrial phenotypes, most often elongation of mitochondrial tubules, are induced by the activity of Drp1. FCCP/CCCP-induced mitochondrial fragmentation was inhibited in Drp1 knockout cells, or cells with a reduced level of mitochondrial Drp1 receptor Mff or MiD49/51, suggesting that FCCP/CCCP induced mitochondrial fragmentation is Drp1-dependent. Furthermore, the data I discussed in Chapter 3 also support the possibility that actin-modifying proteins are required for

Drp1-dependent FCCP-induced mitochondrial fission. By using FCCP as a trigger for mitochondrial fission, combined with time-lapse microscopy, we tested the submitochondrial remodeling of Drp1 in control, $Usp30^{WT}$- and $Usp30^{CS}$- expressing cells. Cells were cotransfected with $Usp30^{WT}$ or $Usp30^{CS}$ and YFP-Drp1 (Usp30/Drp1 ratio 6:1) or transfected with only YFP-Drp1, treated with FCCP, followed by time-lapse structured illumination imaging. While only minor changes in the subcellular distribution of YFP-Drp1 in control and Usp30-expressing cells were detected, FCCP induced a gradual tubulation of the Drp1-containing structure in $Usp30^{CS}$-expressing cells (Fig.4.19). These thin and elongated structures resembled those formed by the mitochondria in cells expressing higher levels of $Usp30^{CS}$. In addition, treatment with FCCP also induced mitochondrial tubulation in $Usp30^{CS}$-expressing cells, confirming the mitochondrial localization of tubular Drp1 structures. Given that Drp1 oligomerizes on the OMM to mediate mitochondrial fission, we also utilized Blue Native PAGE (BN-PAGE) to determine the oligomeric status of Drp1 upon FCCP treatment. Control, $Usp30^{WT}$- and $Usp30^{CS}$-expressing cells were treated with FCCP, harvested and analyzed by BN-PAGE. The data showed that FCCP treatment led to a further increase in formation of high molecular weight Drp1 complexes in $Usp30^{CS}$-expressing cells, but did not affect Drp1 complexes in control and $Usp30^{WT}$-expressing cells (Fig. 4.20). Thus, unlike in any known situations FCCP induced a dramatic tubulation of the mitochondria, suggesting that although Usp30 appears to regulate Drp1-mediated mitochondrial scission, not an initial mitochondrial assembly of Drp1, but rather steps in mitochondrial fission occurring

after Drp1 assembles into high molecular weight complexes were affected by Usp30 activity.

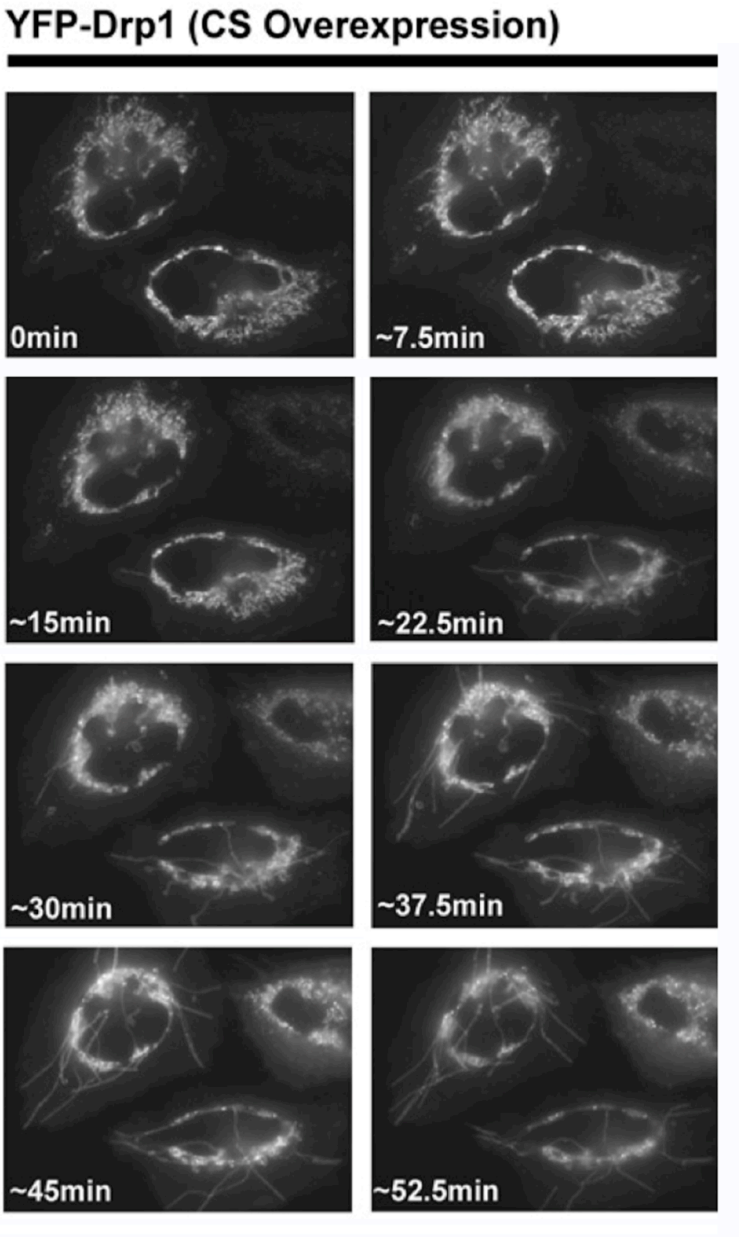

Figure 4.19 Drp1 tubulation induced by FCCP in Usp30^{CS}-expressing cells. HeLa cells were cotransfected Usp30^{CS} and YFP-Drp1, treated with FCCP, and followed by time-lapse structured illumination microscopy.

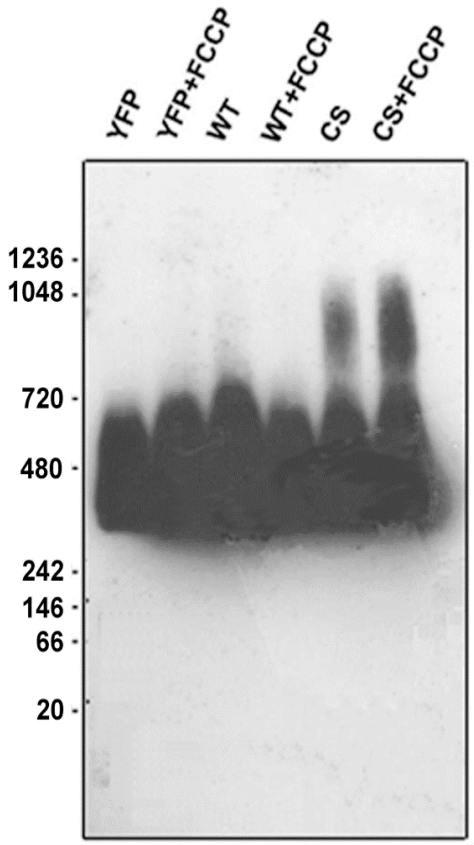

Figure 4.20 Oligomeric status of Drp1 in FCCP-treated control, Usp30^{WT}- and Usp30^{CS}- expressing cells. HeLa cells were transfected with YFP-tag, Usp30^{WT} and Usp30^{CS}, then treated with FCCP and then analyzed by BN-PAGE and Western blot. The blot was then immunolabeled with anti-Drp1 mAb.

Given that mitochondrial Drp1 recruitment and mitochondrial F-actin assembly are two parallel pathways that contributes to Drp1 dependent mitochondrial fission (see Chapter 2 and 3), I further investigated the mitochondrial network organization and mitochondrial F-actin polymerization in control, Usp30^{WT}- and Usp30^{CS}-expressing cells upon FCCP treatment. Cells were cotransfected with Usp30^{WT} or Usp30^{CS} together with YFP-Drp1 and mRuby-Lifeact (ratio 5:1:1), treated with FCCP, and then analyzed by time-lapse structured illumination microscopy. Given that Drp1 is recruited to the OMM when treated with FCCP, it is believed that YFP-Drp1 is able to reveal mitochondrial structure upon FCCP

treatment. The data showed that upon FCCP treatment, a tubular mitochondrial network emerged in Usp30^{CS}-expressing cells. Interestingly, the formation of thin and elongated mRuby-Lifeact-positive structures was also observed in Usp30^{CS}-expressing cells (Fig. 4.21 and Fig. 4.22), but not in control or Usp30^{WT}-expressing cells. These F-actin positive tubular structures colocalized with YFP-Drp1, indicating that, similar to Drp1 forming a mitochondrial tubular structure, F-actin also assembled and accumulated on mitochondria in Usp30^{CS}-expressing cells upon FCCP treatment. It has been shown that in cells overexpressing MiD49/51, the thin and extended mitochondrial tubules, resembling those in Usp30^{CS}-expressing cells, also colocalized with F-actin. Furthermore, upon treatment with actin polymerization inhibitor cytochalasin D, these structures retracted. My data also showed that pretreatment with actin polymerization inhibitor LatB, completely inhibited both F-actin polymerization and mitochondrial tubulation, suggesting the possibility that F-actin polymerization may contribute to the formation of mitochondrial tubules in Usp30^{CS}-expressing cells. The data also showed that Usp30^{CS}-induced remodeling of mitochondrial Drp1 occurred in a similar timeframe as formation of newly assembled F-actin fibers (Fig. 4.21 and Fig. 4.22), providing additional evidence supporting the possibility that Drp1 together with mitochondrial assembly of F-actin contribute to the mitochondrial tubulation observed in Usp30^{CS}-expressing cells.

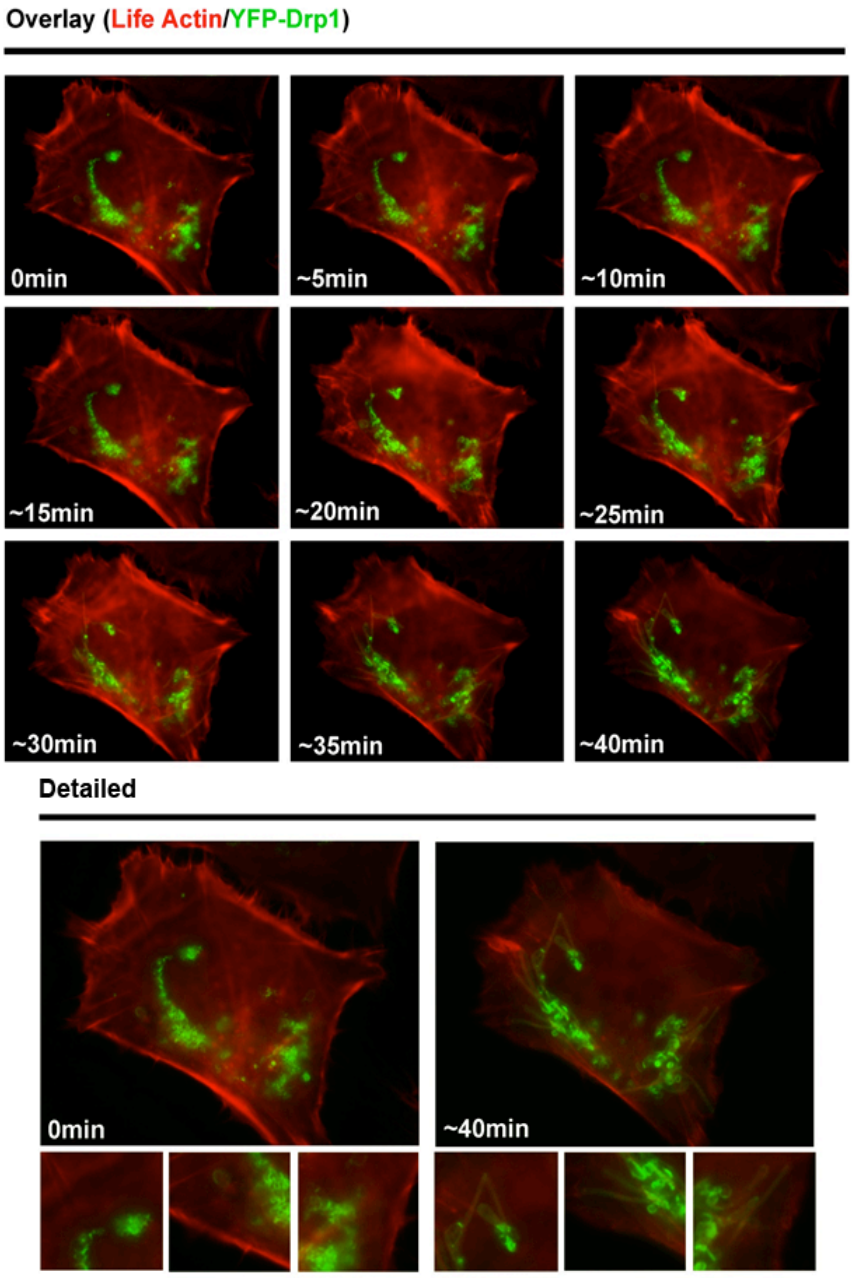

Figure 4.21 Drp1- and F-actin- containing mitochondrial tubule formation in Usp30^{CS}-expressing cells upon FCCP treatment. HeLa cells cotransfected with Usp30^{CS}, YFP-Drp1 (green on overlay images) and mRuby-Lifeact (red on overlay images), treated with FCCP, followed by time-lapse structured illumination microscopy. Detail images of 0 min and 40 min treatment are shown.

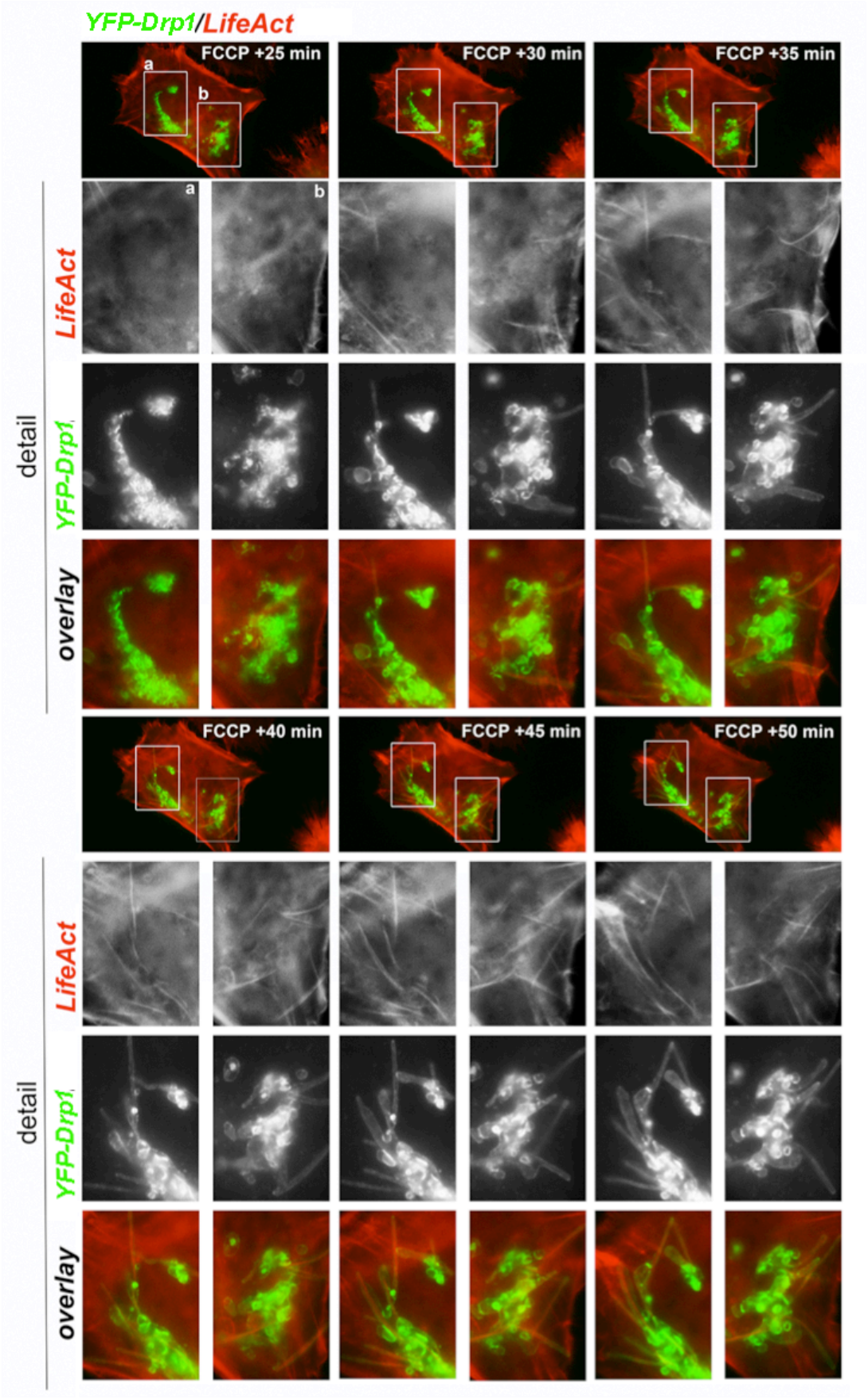
YFP-Drp1/LifeAct
FCCP +25 min
FCCP +30 min
FCCP +35 min
a
b
detail
LifeAct
YFP-Drp1
overlay
FCCP +40 min
FCCP +45 min
FCCP +50 min

Figure 4.22 Drp1- and F-actin- containing mitochondrial tubule formation in Usp30^{CS}-expressing cells upon FCCP treatment (continued). HeLa cells cotransfected with Usp30^{CS}, YFP-Drp1 (green on overlay images) and mRuby-Lifeact (red on overlay images), treated with FCCP, followed by time-lapse structured illumination microscopy. Higher magnifications of areas marked with rectangles are shown in detail images.

Section 4: Discussion

In this chapter, I presented data supporting the possibility that Usp30, an OMM anchored DUB, contributes to the control of Drp1-mediated mitochondrial division. I found that Usp30 inhibition in Usp30$^{-/-}$ HCT116 cells and HeLa cells expressing Usp30^{CS} mutant resulted in extensive mitochondrial tubulation. The BN-PAGE, crosslinking and superresolution imaging support the possibility that Usp30 activity is required for the late stage of Drp1-mediated mitochondrial fission, perhaps the remodeling of the oligomeric fission complexes. Furthermore, I found that mitochondrial-associated F-actin was stabilized in cells expressing Usp30^{CS}, suggesting that Usp30 activity also controls mitochondrial fission-dependent transient F-actin polymerization on the OMM.

Recently, Chen and colleagues proposed a novel mechanism by which Usp30 could regulate mitochondrial dynamics (Yue et al. 2014). They showed that, Usp30 physically interacted with Mfns and thereby reduced ubiquitination of Mfn1 and Mfn2, whereas Usp30^{CS} did not affect ubiquitination levels of Mfns. Consistent with this report, I also found that Usp30^{CS} expression induced interconnected mitochondria. However, rather than regulating Mfns, we found that Usp30 interacted with Drp1 and controlled the oligomeric status of Drp1 on the mitochondria. However, we were not able to observe any difference in Drp1 protein expression in Usp30^{WT}- and USP30^{CS}-

expressing cells, indicating that Usp30 does not regulate Drp1 degradation, but rather the activity of Drp1. Thus, Usp30 may serve as a multi-target OMM deubiquitinase that modifies the function of mitochondrial fusion and fission proteins without affecting their stability.

Interestingly, mitochondrial changes observed in cells expressing higher levels of $Usp30^{CS}$ were highly reminiscent of the mitochondrial alterations induced by overexpression of recently identified mitochondrial Drp1 receptor MiD49/51. Therefore it is likely that Usp30 controls MiD49/51 proteins. Studies addressing this possibility are currently being conducted in the Karbowski lab.

FCCP-induced transient F-actin assembly on the OMM appears to be a required step that contributes to Drp1-dependent mitochondrial fission. Mitochondrial F-actin polymerization acts as a parallel event to Drp1 assembly and likely influence Drp1-driven membrane constriction and scission. Following $Usp30^{CS}$ expression, we found that actin filaments assemble on mitochondria tubules in synchrony with Drp1 translocation from the cytosol to the mitochondria upon FCCP treatment. As FCCP-induced actin nucleation is independent of Drp1, it is likely that F-actin polymerization in $Usp30^{CS}$-expressing cells occurs in a similar timeframe to, but is not coupled to Drp1 recruitment. The independence of mitochondrial F-actin assembly from Drp1 recruitment points to a role for Usp30 in regulating the F-actin-dependent step of mitochondrial fission. Alternatively, given that actin filaments disassembly is dependent on Drp1 GTPase activity, the accumulation of mitochondrial F-actin may also be a consequence of the inhibition of the Drp1-mediated membrane scission event.

Chapter 5: Summaries

In summary, I reported a novel mechanism by which F-actin controls Drp1-dependent mitochondrial fission. I found that F-actin assembled on the OMM upon stress (FCCP and AntA)-induced and mitotic mitochondrial fission. Mitochondrial disassembly of F-actin upon FCCP/AntA treatments was delayed in cells deficient in mitochondrial fission ($Drp1^{-/-}$ and $Mff^{-/-}$ MEFs), as compared to wild type MEFs. Furthermore, actin polymerization inhibitor LatB inhibited mitochondrial toxin-induced mitochondrial fission, suggesting that *de novo* F-actin polymerization is required for mitochondrial fission. Mitochondria-associated F-actin colocalized with the OMM marker Tom20, rather than with cytochrome c labeled IMM and IMS, suggesting that F-actin localized to the OMM and did not specifically localize on the mitochondrial constriction sites. Furthermore, I showed that rather than linear actin filaments, Arp2/3 complex-mediated branched F-actin nucleator, as well as other related factors, including cortactin and cofilin, controlled F-actin dependent mitochondrial fission. Moreover, I also discovered that Usp30, a mitochondrial membrane anchored deubiqutinase-dependent control of mitochondrial fission involved mitochondrial assembly of F-actin. In conclusion, this study reveals a novel mechanism of transient F-actin assembly on mitochondria that contributes to Drp1-mediated mitochondrial fission.

Based on these data, we propose a working model of how F-actin could participate in mitochondrial fission. Upon stress-induced or mitotic mitochondrial fission, G-actin molecules assemble into F-actin on the OMM in a Drp1-independent

manner. The assembly of mitochondrial associated F-actin is initiated by Arp2/3 complex, a class II nucleating promoting factor cortactin and actin severing factor cofilin. Under this model, Drp1 can be recruited from the cytosol to the mitochondria in an actin-independent manner. Therefore, mitochondrial actin polymerization and Drp1 recruitment act as two parallel events, which are both, required for the completion of mitochondrial fission. Either the disassociation of mitochondrial actin or Drp1 containing fission complex activity requires the activity of each other. In the absence of mitochondrial assembly of F-actin, Drp-1 mediated mitochondrial fission can not be completed, resulting in increasing mitochondrial, accumulation of Drp1, whereas loss of functional Drp1 results in accumulation of mitochondrial F-actin accompanied by reduced mitochondrial fission activity.

Since Drp1 translocation and F-actin polymerization did not correlate with each other temporally, the functional and molecular relationship between Drp1 and OMM-associated F-actin needs to be further investigated. As revealed by *in vitro* studies, dynamin (a founding member of dynamin protein family) can interact with actin cytoskeleton and align F-actin into bundles (Gu et al. 2010b). It is necessary to examine the degree to which Drp1, a dynamin family member, mediates mitochondrial fission through interacting with OMM-associated F-actin. Mitochondrial Drp1 receptors such as Mff, Fis1 and MiD49/51 may also control the assembly of F-actin on the OMM and thereby contribute to F-actin-dependent mitochondrial membrane remodeling during mitochondrial fission.

Mitochondrial fission occurs through the membrane constriction and scission by Drp1 assembly-dependent GTP hydrolysis (Ingerman et al. 2005). One possible

mechanism is that mitochondrial F-actin provides the mechanical force that contributes to membrane constriction at membrane curvature. While myosin II was reported to assist mitochondrial fission (Korobova et al. 2014b), it is possible that mitochondrial F-actin associates with myosin II to provide membrane tension force to promote mitochondrial membrane constriction and help position Drp1 at mitochondrial constriction sites.

The factors controlling initiation of F-actin polymerization on the OMM during mitochondrial fission are also unknown. It has been reported that during clathrin-mediated endocytosis BAR domain superfamily proteins are recruited to invaginated buds to sense membrane curvature by preferentially binding to highly curved membranes (Ferguson et al. 2009). Given that a cytosolic BAR domain protein endophilin B1 (Bif-1) can associate with the mitochondria (Karbowski, Jeong, et al. 2004), it is appealing to explore the role of endophilin B1 and other BAR domain proteins in initiation of F-actin polymerization on the OMM during mitochondrial fission. In addition, phosphoinositide lipids promote Arp2/3 mediated F-actin polymerization by binding to nucleating promoting factors WASP and inhibit actin capping protein cofilin and G-actin binding protein profilin (Bezanilla et al. 2015). Mitochondrial assembly of F-actin network may also be regulated by membrane phosphoinositides by regulating actin-modifying proteins activity.

My work showed that a transient branched F-actin polymerization initiated by Arp2/3 complex is vital for mitochondrial fission. The role of branched F-actin polymerization has been established in membrane remodeling during clathrin-mediated endocytosis (Mooren et al. 2012). Meanwhile, INF2 promotes Drp1-

dependent mitochondrial fission by modifying linear F-actin network that was suggested to assemble at the mitochondrial constriction sites along with the ER-mitochondria contact sites (Korobova et al. 2013). However, INF2 was not found to affect stress-induced mitochondrial fission (see Chapter 3). Thus, it is critical to clarify the mechanism by which linear and branched F-actin network co-regulate mitochondrial fission in response to different physiological conditions through distinct mechanism.

Bibliography

Anand, R. et al., 2014. The i-AAA protease YME1L and OMA1 cleave OPA1 to balance mitochondrial fusion and fission. *The Journal of Cell Biology*, 204(6), pp.919–929. Available at: http://www.jcb.org/cgi/doi/10.1083/jcb.201308006 [Accessed March 11, 2014].

Anitei, M. & Hoflack, B., 2012. Bridging membrane and cytoskeleton dynamics in the secretory and endocytic pathways. *Nature cell biology*, 14(1), pp.11–9. Available at: http://www.ncbi.nlm.nih.gov/pubmed/22193159 [Accessed December 16, 2013].

Archer, S.L., 2013a. Mitochondrial Dynamics - mitochondrial fission and fusion in human diseases. *New England Journal of Medicine*, 369, pp.2236–2251.

Archer, S.L., 2013b. Mitochondrial dynamics--mitochondrial fission and fusion in human diseases. *The New England journal of medicine*, 369(23), pp.2236–51. Available at: http://www.ncbi.nlm.nih.gov/pubmed/24304053 [Accessed July 11, 2014].

Bauer, D.E., Canver, M.C. & Orkin, S.H., 2014. Generation of Genomic Deletions in Mammalian Cell Lines via CRISPR/Cas9. *Journal of Visualized Experiments*, (83), pp.1–10. Available at: http://www.jove.com/video/52118/generation-of-genomic-deletions-in-mammalian-cell-lines-via-crisprcas9.

Beal, M.F. & Ferrante, R.J., 2004. Experimental therapeutics in transgenic mouse models of Huntington's disease. *Nature reviews. Neuroscience*, 5(5), pp.373–384.

Beck, H. et al., 2012. PNAS Plus: Serum Response Factor (SRF)-cofilin-actin signaling axis modulates mitochondrial dynamics. *Proceedings of the National Academy of Sciences*, 109(38), pp.E2523–E2532.

Benard, G. et al., 2010. IBRDC2, an IBR-type E3 ubiquitin ligase, is a regulatory factor for Bax and apoptosis activation. *The EMBO journal*, 29(8), pp.1458–1471. Available at: http://dx.doi.org/10.1038/emboj.2010.39.

Benesch, S. et al., 2005. N-WASP deficiency impairs EGF internalization and actin assembly at clathrin-coated pits. *Journal of cell science*, 118(Pt 14), pp.3103–3115.

Bezanilla, M. et al., 2015. Cytoskeletal dynamics: A view from the membrane. *The Journal of Cell Biology*, 209(3), pp.329–337. Available at: http://www.jcb.org/cgi/doi/10.1083/jcb.201502062.

Bingol, B. et al., 2014. The mitochondrial deubiquitinase USP30 opposes parkin-mediated mitophagy. *Nature*, 509(7505), pp.370–5. Available at: http://www.ncbi.nlm.nih.gov/pubmed/24896179.

Van Der Bliek, A.M., 1999. Functional diversity in the dynamin family. *Trends in Cell Biology*, 9(3), pp.96–102.

Bossy, B. et al., 2010. S-Nitrosylation of DRP1 Does Not Affect Enzymatic Activity and is Not Specific to Alzheimer's Disease. *J Alzheimers Dis*, 20(Suppl 2), pp.s513–s526.

Boulant, S. et al., 2011. Actin dynamics counteract membrane tension during clathrin-mediated endocytosis. *Nature cell biology*, 13(9), pp.1124–1131. Available at: http://dx.doi.org/10.1038/ncb2307.

Braschi, E., Zunino, R. & McBride, H.M., 2009. MAPL is a new mitochondrial SUMO E3 ligase that regulates mitochondrial fission. *EMBO reports*, 10(7), pp.748–754.

De Brito, O.M. & Scorrano, L., 2008. Mitofusin 2 tethers endoplasmic reticulum to mitochondria. *Nature*, 456(7222), pp.605–610.

Burkel, B.M., Von Dassow, G. & Bement, W.M., 2007. Versatile fluorescent probes for actin filaments based on the actin-binding domain of utrophin. *Cell Motility and the Cytoskeleton*, 64(11), pp.822–832.

Cai, L. et al., 2007. Coronin 1B Coordinates Arp2/3 Complex and Cofilin Activities at the Leading Edge. *Cell*, 128(5), pp.915–929.

Campanella, M., Pinton, P. & Rizzuto, R., 2004. Mitochondrial Ca2+ homeostasis in health and disease. *Biological research*, 37(4), pp.653–660.

Campellone, K.G. & Welch, M.D., 2010. A nucleator arms race: cellular control of actin assembly. *Nature reviews. Molecular cell biology*, 11(4), pp.237–251.

Cereghetti, G.M. et al., 2008. Dephosphorylation by calcineurin regulates translocation of Drp1 to mitochondria. *Proceedings of the National Academy of Sciences of the United States of America*, 105(41), pp.15803–15808.

Cerveny, K.L. et al., 2007. Regulation of mitochondrial fusion and division. *Trends in Cell Biology*, 17(11), pp.563–569.

Chaturvedi, R.K. & Beal, M.F., 2013. Mitochondrial diseases of the brain. *Free Radical Biology and Medicine*, 63, pp.1–29. Available at: http://dx.doi.org/10.1016/j.freeradbiomed.2013.03.018.

Chen, H. et al., 2003. Mitofusins Mfn1 and Mfn2 coordinately regulate mitochondrial fusion and are essential for embryonic development. *Journal of Cell Biology*, 160(2), pp.189–200.

Chen, H. & Chan, D.C., 2005. Emerging functions of mammalian mitochondrial fusion and fission. *Human Molecular Genetics*, 14(SUPPL. 2), pp.283–289.

Chen, H. & Chan, D.C., 2009. Mitochondrial dynamics-fusion, fission, movement, and mitophagy-in neurodegenerative diseases. *Human Molecular Genetics*, 18(R2), pp.169–176.

Chen, H., McCaffery, J.M. & Chan, D.C., 2007. Mitochondrial Fusion Protects against Neurodegeneration in the Cerebellum. *Cell*, 130(3), pp.548–562.

Cho, D.-H. et al., 2009. S-Nitrosylation of Drp1 Mediates β-Amyloid: Related Mitochondrial Fission and Neuronal Injury. *Science*, 324(5923), pp.102–105. Available at: http://www.jstor.org/stable/20493645.

Cribbs, J.T. & Strack, S., 2007. Reversible phosphorylation of Drp1 by cyclic AMP-dependent protein kinase and calcineurin regulates mitochondrial fission and cell death. *EMBO reports*, 8(10), pp.939–944.

Cunningham, C.N. et al., 2015. USP30 and parkin homeostatically regulate atypical ubiquitin chains on mitochondria. *Nature Cell Biology*, 17(2), pp.160–169. Available at: http://www.nature.com/doifinder/10.1038/ncb3097.

Dietmeier, K. et al., 1997. Tom5 functionally links mitochondrial preprotein receptors to the general import pore. *Nature*, 388(6638), pp.195–200.

DuBoff, B., Götz, J. & Feany, M.B., 2012. Tau Promotes Neurodegeneration via DRP1 Mislocalization In Vivo. *Neuron*, 75(4), pp.618–632.

Egea, G., Lázaro-Diéguez, F. & Vilella, M., 2006. Actin dynamics at the Golgi complex in mammalian cells. *Current opinion in cell biology*, 18(2), pp.168–78. Available at: http://www.ncbi.nlm.nih.gov/pubmed/16488588 [Accessed December 16, 2013].

Ehses, S. et al., 2009. Regulation of OPA1 processing and mitochondrial fusion by m-AAA protease isoenzymes and OMA1. *Journal of Cell Biology*, 187(7), pp.1023–1036.

Faelber, K. et al., 2012. Structural insights into dynamin-mediated membrane fission. *Structure*, 20(10), pp.1621–1628.

Ferguson, S. et al., 2009. Coordinated Actions of Actin and BAR Proteins Upstream of Dynamin at Endocytic Clathrin-Coated Pits. *Developmental Cell*, 17(6), pp.811–822. Available at: http://dx.doi.org/10.1016/j.devcel.2009.11.005.

Ferguson, S.M. & De Camilli, P., 2012. Dynamin, a membrane-remodelling GTPase. *Nature reviews. Molecular cell biology*, 13(2), pp.75–88. Available at: http://www.pubmedcentral.nih.gov/articlerender.fcgi?artid=3519936&tool=pmcentrez&rendertype=abstract [Accessed December 16, 2013].

Firat-Karalar, E.N. & Welch, M.D., 2011. New mechanisms and functions of actin nucleation. *Current Opinion in Cell Biology*, 23(1), pp.4–13. Available at: http://dx.doi.org/10.1016/j.ceb.2010.10.007.

Flotho, A. & Melchior, F., 2013. Sumoylation: a regulatory protein modification in health and disease. *Annual review of biochemistry*, 82, pp.357–85. Available at: http://www.ncbi.nlm.nih.gov/pubmed/23746258.

Frezza, C. et al., 2006. OPA1 Controls Apoptotic Cristae Remodeling Independently from Mitochondrial Fusion. *Cell*, 126(1), pp.177–189.

Frost, A., Unger, V.M. & De Camilli, P., 2009. The BAR Domain Superfamily: Membrane-Molding Macromolecules. *Cell*, 137(2), pp.191–196.

Gandre-Babbe, S. & van der Bliek, A.M., 2008. The Novel Tail-anchored Membrane Protein Mff Controls Mitochondrial and Peroxisomal Fission in Mammalian Cells. *Molecular biology of the cell*, 19(1), pp.2402–2412.

Geli, M.I., Wesp, A. & Riezman, H., 1998. Distinct functions of calmodulin are required for the uptake step of receptor-mediated endocytosis in yeast: The type I myosin Myo5p is one of the calmodulin targets. *EMBO Journal*, 17(3), pp.635–647.

Gilkerson, R.W., Selker, J.M.L. & Capaldi, R. a., 2003. The cristal membrane of mitochondria is the principal site of oxidative phosphorylation. *FEBS Letters*, 546(2-3), pp.355–358.

Giorgi, C. et al., 2012. Mitochondrial Ca2+ and apoptosis. *Cell Calcium*, 52(1), pp.36–43. Available at: http://dx.doi.org/10.1016/j.ceca.2012.02.008.

Grassart, A. et al., 2014. Actin and dynamin2 dynamics and interplay during clathrin-mediated endocytosis. *The Journal of cell biology*, 205(5), pp.721–35. Available at: http://www.ncbi.nlm.nih.gov/pubmed/24891602 [Accessed July 17, 2014].

Griffin, E.E., Graumann, J. & Chan, D.C., 2005. The WD40 protein Caf4p is a component of the mitochondrial fission machinery and recruits Dnm1p to mitochondria. *Journal of Cell Biology*, 170(2), pp.237–248.

Gu, C. et al., 2010a. Direct dynamin-actin interactions regulate the actin cytoskeleton. *The EMBO journal*, 29(21), pp.3593–606. Available at: http://www.pubmedcentral.nih.gov/articlerender.fcgi?artid=2982766&tool=pmcentrez&rendertype=abstract [Accessed December 16, 2013].

Gu, C. et al., 2010b. Direct dynamin-actin interactions regulate the actin cytoskeleton. *The EMBO journal*, 29(21), pp.3593–3606. Available at: http://dx.doi.org/10.1038/emboj.2010.249.

Gu, C. et al., 2014. Regulation of dynamin oligomerization in cells: The role of dynamin-actin interactions and its GTPase activity. *Traffic*, 15(8), pp.819–838.

Guo, C. et al., 2013. SENP3-mediated deSUMOylation of dynamin-related protein 1 promotes cell death following ischaemia. *The EMBO journal*, 32(11), pp.1514–28. Available at: http://www.pubmedcentral.nih.gov/articlerender.fcgi?artid=3671254&tool=pmcentrez&rendertype=abstract.

Harder, Z., Zunino, R. & McBride, H., 2004. Sumo1 conjugates mitochondrial substrates and participates in mitochondrial fission. *Current Biology*, 14(4), pp.340–345.

Hatakeyama, S. et al., 2001. U Box Proteins as a New Family of Ubiquitin-Protein Ligases. *Journal of Biological Chemistry*, 276(35), pp.33111–33120.

Haun, F., Nakamura, T. & Lipton, S. a., 2013. Dysfunctional mitochondrial dynamics in the pathophysiology of neurodegenerative diseases. *Journal of Cell Death*, 6(1), pp.27–35.

Head, B. et al., 2009. Inducible proteolytic inactivation of OPA1 mediated by the OMA1 protease in mammalian cells. *Journal of Cell Biology*, 187(7), pp.959–966.

Heilemann, M. et al., 2009. Super-resolution imaging with small organic fluorophores. *Angewandte Chemie - International Edition*, 48(37), pp.6903–6908.

Herrmann, J., Lerman, L.O. & Lerman, A., 2007. Ubiquitin and ubiquitin-like proteins in protein regulation. *Circulation Research*, 100(9), pp.1276–1291.

Van den Heuvel, L. & Smeitink, J., 2001. The oxidative phosphorylation (OXPHOS) system: nuclear genes and human genetic diseases. *BioEssays : news and reviews in molecular, cellular and developmental biology*, 23(6), pp.518–525.

Hsu, Y.T. & Youle, R.J., 1998. Bax in murine thymus is a soluble monomeric protein that displays differential detergent-induced conformations. *Journal of Biological Chemistry*, 273(17), pp.10777–10783.

Ingerman, E. et al., 2005. Dnm1 forms spirals that are structurally tailored to fit mitochondria. *Journal of Cell Biology*, 170(7), pp.1021–1027.

Inoue, S. et al., 2013. Mule/Huwe1/Arf-BP1 suppresses Ras-driven tumorigenesis by preventing c-Myc/Miz1-mediated down-regulation of p21 and p15. *Genes and Development*, 27(10), pp.1101–1114.

Inuzuka, H. et al., 2011. SCF(FBW7) regulates cellular apoptosis by targeting MCL1 for ubiquitylation and destruction. *Nature*, 471(7336), pp.104–109. Available at: http://dx.doi.org/10.1038/nature09732.

Ishihara, N. et al., 2006. Regulation of mitochondrial morphology through proteolytic cleavage of OPA1. *The EMBO journal*, 25(13), pp.2966–2977.

Itoyama, A. et al., 2013. Mff functions with Pex11pβ and DLP1 in peroxisomal fission. *Biology open*, 2(10), pp.998–1006. Available at: http://www.pubmedcentral.nih.gov/articlerender.fcgi?artid=3798195&tool=pmcentrez&rendertype=abstract.

James, D.I. et al., 2003. hFis1, a novel component of the mammalian mitochondrial fission machinery. *Journal of Biological Chemistry*, 278(38), pp.36373–36379.

Jiang, X. et al., 2014. Activation of mitochondrial protease OMA1 by Bax and Bak promotes cytochrome c release during apoptosis. *Proceedings of the National Academy of Sciences*, 111(41), pp.14782–14787. Available at: http://www.pnas.org/cgi/doi/10.1073/pnas.1417253111.

Jornayvaz, F. & Shulman, G., 2010. Regulation of mitochondrial biogenesis. *Essays Biochem*, 47, pp.69–84. Available at: http://essays.biochemistry.org/bsessays/047/bse0470069.htm.

Kao, S.-H. et al., 2015. Changes in mitochondrial morphology and bioenergetics in human lymphoblastoid cells with four novel OPA1 mutations. *Investigative Ophthalmology & Visual Science*. Available at: http://www.iovs.org/cgi/doi/10.1167/iovs.14-16288.

Karbowski, M., Arnoult, D., et al., 2004. Quantitation of mitochondrial dynamics by photolabeling of individual organelles shows that mitochondrial fusion is blocked during the Bax activation phase of apoptosis. *Journal of Cell Biology*, 164(4), pp.493–499.

Karbowski, M. et al., 2006. Role of Bax and Bak in mitochondrial morphogenesis. *Nature*, 443(7112), pp.658–662.

Karbowski, M. et al., 2002. Spatial and temporal association of Bax with mitochondrial fission sites, Drp1, and Mfn2 during apoptosis. *Journal of Cell Biology*, 159(6), pp.931–938.

Karbowski, M., Cleland, M.M. & Roelofs, B.A., 2014. *Methods in ENZYMOLOGY. Chapter Four: Photoactivatable Green Fluorescent Protein-Based Visualization and Quantification of Mitochondrial Fusion and Mitochondrial Network Complexity in Living Cells*,

Karbowski, M., Jeong, S.Y. & Youle, R.J., 2004. Endophilin B1 is required for the maintenance of mitochondrial morphology. *Journal of Cell Biology*, 166(7), pp.1027–1039.

Karbowski, M., Neutzner, A. & Youle, R.J., 2007. The mitochondrial E3 ubiquitin ligase MARCH5 is required for Drp1 dependent mitochondrial division. *Journal of Cell Biology*, 178(1), pp.71–84.

Kessels, M.M. et al., 2001. Mammalian Abp1, a signal-responsive F-actin-binding protein, links the actin cytoskeleton to endocytosis via the GTPase dynamin. *Journal of Cell Biology*, 153(2), pp.351–366.

Kirchhausen, T., Owen, D. & Harrison, S.C., 2014. Molecular Strcuture, Function, and Dynaics of Clathrin-Mediated Membrane Traffic. *Cold Spring Harb Perspect Biol*, 6(a016725).

Klein, C.J. et al., 2011. Large Kindred Evaluation of Mitofusin 2 Novel Mutation, Extremes of Neurologic Presentations, and Preserved Nerve Mitochondria. *Archives of Neurology*, 68(10), pp.1295–1302.

Kobielak, A., Pasolli, H.A. & Fuchs, E., 2004. Mammalian formin-1 participates in adherens junctions and polymerization of linear actin cables. *Nature cell biology*, 6(1), pp.21–30.

Korobova, F., Gauvin, T.J. & Higgs, H.N., 2014a. A role for myosin II in mammalian mitochondrial fission. *Current biology : CB*, 24(4), pp.409–14. Available at: http://www.ncbi.nlm.nih.gov/pubmed/24485837.

Korobova, F., Gauvin, T.J. & Higgs, H.N., 2014b. A role for myosin II in mammalian mitochondrial fission. *Current biology : CB*, 24(4), pp.409–14. Available at: http://www.ncbi.nlm.nih.gov/pubmed/24485837.

Korobova, F., Ramabhadran, V. & Higgs, H.N., 2013. An Actin-Dependent Step in Mitochondrial Fission Mediated by the ER-Associated Formin INF2. *Science*, 339(464), pp.464–467.

Koshiba, T. et al., 2004. Structural basis of mitochondrial tethering by mitofusin complexes. *Science (New York, N.Y.)*, 305(5685), pp.858–862.

De La Cruz, E.M., 2009. How cofilin severs an actin filament. *Biophys Rev.*, 1(2), pp.51–59.

Labrousse, a M. et al., 1999. C. elegans dynamin-related protein DRP-1 controls severing of the mitochondrial outer membrane. *Molecular cell*, 4(5), pp.815–826.

Lanzetti, L., 2007. Actin in membrane trafficking. *Current opinion in cell biology*, 19(4), pp.453–8. Available at: http://www.ncbi.nlm.nih.gov/pubmed/17616384 [Accessed December 16, 2013].

Lee, Y.J. et al., 2004. Roles of the Mammalian Mitochondrial Fission and Fusion Mediator Fis1, Drp1, and Opa1 and Apoptosis. *Molecular biology of the cell*, 15(1), pp.5001–5011.

Liang, J. et al., 2015. USP30 deubiquitylates mitochondrial Parkin substrates and restricts apoptotic cell death. , 16(5), pp.618–627.

Van de Linde, S. et al., 2011. Direct stochastic optical reconstruction microscopy with standard fluorescent probes. *Nature protocols*, 6(7), pp.991–1009.

Liu, T. et al., 2013. The mitochondrial elongation factors MIEF1 and MIEF2 exert partially distinct functions in mitochondrial dynamics. *Experimental Cell Research*, 319(18), pp.2893–2904. Available at: http://dx.doi.org/10.1016/j.yexcr.2013.07.010.

Losón, O.C. et al., 2013. Fis1, Mff, MiD49, and MiD51 mediate Drp1 recruitment in mitochondrial fission. *Molecular Biology of the Cell*, 24(5), pp.659–667. Available at: http://www.molbiolcell.org/content/24/5/659\nhttp://www.molbiolcell.org/content/24/5/659.full.pdf\nhttp://www.molbiolcell.org/content/24/5/659.long.

Losón, O.C. et al., 2014. The mitochondrial fission receptor MiD51 requires ADP as a cofactor. *Structure*, 22(3), pp.367–377.

Mali, P. et al., 2013. RNA-Guided Human Genome Engineering via Cas9. , (February), pp.823–827.

Martin, A.C., Kaschube, M. & Wieschaus, E.F., 2009. Pulsed contractions of an actin-myosin network drive apical constriction. *Nature*, 457(7228), pp.495–499. Available at: http://dx.doi.org/10.1038/nature07522.

Maurer, U. et al., 2006. Glycogen synthase kinase-3 regulates mitochondrial outer membrane permeabilization and apoptosis by destabilization of MCL-1. *Molecular Cell*, 21(6), pp.749–760.

Méré, J. et al., 2005. Gelsolin binds to polyphosphoinositide-free lipid vesicles and simultaneously to actin microfilaments. *The Biochemical journal*, 386(Pt 1), pp.47–56.

Metzger, M.B., Hristova, V. a. & Weissman, a. M., 2012. HECT and RING finger families of E3 ubiquitin ligases at a glance. *Journal of Cell Science*, 125(3), pp.531–537.

Mooren, O.L., Galletta, B.J. & Cooper, J. a., 2012. Roles for Actin Assembly in Endocytosis. *Annual Review of Biochemistry*, 81(1), pp.661–686.

Mourier, a. et al., 2015. Mitofusin 2 is required to maintain mitochondrial coenzyme Q levels. *The Journal of Cell Biology*, 208(4), pp.429–442. Available at: http://www.jcb.org/cgi/doi/10.1083/jcb.201411100.

Nakamura, N. & Hirose, S., 2008. Regulation of Mitochondrial Morphology by USP30, a Deubiquitinating Enzyme Present in the Mitochondrial Outer Membrane. *Molecular biology of the cell*, 19, pp.1903–1911.

Neutzner, A. et al., 2012. The ubiquitin/proteasome system-dependent control of mitochondrial steps in apoptosis. *Seminars in Cell and Developmental Biology*, 23(5), pp.499–508. Available at: http://dx.doi.org/10.1016/j.semcdb.2012.03.019.

Nijman, S.M.B. et al., 2005. A genomic and functional inventory of deubiquitinating enzymes. *Cell*, 123(5), pp.773–786.

Onoue, K. et al., 2012. Fis1 acts as mitochondrial recruitment factor for TBC1D15 that involved in regulation of mitochondrial morphology. *Journal of Cell Science*, pp.176–185.

Orth, J.D. & McNiven, M. a, 2003. Dynamin at the actin–membrane interface. *Current Opinion in Cell Biology*, 15(1), pp.31–39. Available at: http://linkinghub.elsevier.com/retrieve/pii/S0955067402000108 [Accessed December 16, 2013].

Otera, H. et al., 2010. Mff is an essential factor for mitochondrial recruitment of Drp1 during mitochondrial fission in mammalian cells. *Journal of Cell Biology*, 191(6), pp.1141–1158.

Palmer, C.S. et al., 2013. Adaptor proteins MiD49 and MiD51 can act independently of Mff and Fis1 in Drp1 recruitment and are specific for mitochondrial fission. *Journal of Biological Chemistry*, 288(38), pp.27584–27593.

Palmer, C.S. et al., 2011a. MiD49 and MiD51, new components of the mitochondrial fission machinery. *EMBO reports*, 12(6), pp.565–73. Available at: http://www.pubmedcentral.nih.gov/articlerender.fcgi?artid=3128275&tool=pmcentrez&rendertype=abstract [Accessed December 16, 2013].

Palmer, C.S. et al., 2011b. MiD49 and MiD51, new components of the mitochondrial fission machinery. *EMBO reports*, 12(6), pp.565–573. Available at: http://dx.doi.org/10.1038/embor.2011.54.

Park, C.B. & Larsson, N.-G., 2011. Mitochondrial DNA mutations in disease and aging. *The Journal of cell biology*, 193(5), pp.809–818.

Park, Y.-Y. et al., 2010. Loss of MARCH5 mitochondrial E3 ubiquitin ligase induces cellular senescence through dynamin-related protein 1 and mitofusin 1. *Journal of cell science*, 123(Pt 4), pp.619–626.

Park, Y.-Y. et al., 2014. MARCH5-mediated quality control on acetylated Mfn1 facilitates mitochondrial homeostasis and cell survival. *Cell death & disease*, 5(4), p.e1172. Available at: http://www.ncbi.nlm.nih.gov/pubmed/24722297.

Park, Y.-Y. & Cho, H., 2012. Mitofusin 1 is degraded at G2/M phase through ubiquitylation by MARCH5. *Cell division*, 7(1), p.25. Available at: http://www.pubmedcentral.nih.gov/articlerender.fcgi?artid=3542011&tool=pmcentrez&rendertype=abstract.

Partikian, A. et al., 1998. Rapid diffusion of green fluorescent protein in the mitochondrial matrix. *Journal of Cell Biology*, 140(4), pp.821–829.

Pavlov, D. et al., 2007. Actin Filament severing by cofilin. , 365(5), pp.1350–1358.

Popovic, D., Vucic, D. & Dikic, I., 2014. Ubiquitination in disease pathogenesis and treatment. *Nature Medicine*, 20(11), pp.1242–1253. Available at: http://www.nature.com/doifinder/10.1038/nm.3739 [Accessed November 6, 2014].

Pyakurel, A. et al., 2015. Extracellular Regulated Kinase Phosphorylates Mitofusin 1 to Control Mitochondrial Morphology and Apoptosis. *Molecular Cell*, 58(2),

pp.244–254. Available at: http://linkinghub.elsevier.com/retrieve/pii/S1097276515001355.

Qian, W. et al., 2012. Mitochondrial hyperfusion induced by loss of fission protein Drp1 causes ATM-dependent G2/M arrest and aneuploidy through DNA replication stress. *Journal of Cell Science*, 1.

Rapaport, D. et al., 1998. Fzo1p Is a Mitochondrial Outer Membrane Protein Essential for the Biogenesis of Functional Mitochondria in. *Biochemistry*, 273(32), pp.20150 –20155.

Rehman, J. et al., 2012. Inhibition of mitochondrial fission prevents cell cycle progression in lung cancer. *The FASEB Journal*, 26(5), pp.2175–2186.

Richter, V. et al., 2014. Structural and functional analysis of mid51, a dynamin receptor required for mitochondrial fission. *Journal of Cell Biology*, 204(4), pp.477–486.

Riedl, J. et al., 2008. Lifeact: a versatile marker to visualize F-actin. *Nature methods*, 5(7), pp.605–7. Available at: http://www.pubmedcentral.nih.gov/articlerender.fcgi?artid=2814344&tool=pmcentrez&rendertype=abstract [Accessed July 10, 2014].

Rizzuto, R. et al., 2012. Mitochondria as sensors and regulators of calcium signalling. *Nature Reviews Molecular Cell Biology*, 13(9), pp.566–578. Available at: http://dx.doi.org/10.1038/nrm3412.

Römer, W. et al., 2010. Actin Dynamics Drive Membrane Reorganization and Scission in Clathrin-Independent Endocytosis. *Cell*, 140(4), pp.540–553.

Rotty, J.D., Wu, C. & Bear, J.E., 2013. New insights into the regulation and cellular functions of the ARP2/3 complex. *Nature reviews. Molecular cell biology*, 14(1), pp.7–12. Available at: http://www.nature.com.libproxy1.upstate.edu/nrm/journal/v14/n1/full/nrm3492.html.

Santo-Domingo, J. & Demaurex, N., 2010. Calcium uptake mechanisms of mitochondria. *Biochimica et Biophysica Acta - Bioenergetics*, 1797(6-7), pp.907–912. Available at: http://dx.doi.org/10.1016/j.bbabio.2010.01.005.

Schneeberger, M. et al., 2013. Mitofusin 2 in POMC neurons connects ER stress with leptin resistance and energy imbalance. *Cell*, 155(1), pp.172–187.

Schwickart, M. et al., 2010. Deubiquitinase USP9X stabilizes MCL1 and promotes tumour cell survival. *Nature*, 463(7277), pp.103–107. Available at: http://dx.doi.org/10.1038/nature08646.

Sebastian, D. et al., 2012. Mitofusin 2 (Mfn2) links mitochondrial and endoplasmic reticulum function with insulin signaling and is essential for normal glucose homeostasis. *Proceedings of the National Academy of Sciences*, 109(14), pp.5523–5528.

Sesaki, H. et al., 2014. In vivo functions of Drp1: Lessons learned from yeast genetics and mouse knockouts. *Biochimica et Biophysica Acta - Molecular Basis of Disease*, 1842(8), pp.1179–1185. Available at: http://dx.doi.org/10.1016/j.bbadis.2013.11.024.

Sévère, N., Dieudonné, F.-X. & Marie, P.J., 2013. E3 ubiquitin ligase-mediated regulation of bone formation and tumorigenesis. *Cell death & disease*, 4, p.e463. Available at: http://www.pubmedcentral.nih.gov/articlerender.fcgi?artid=3564004&tool=pmcentrez&rendertype=abstract.

Shen, Q. et al., 2014. Mutations in Fis1 disrupt orderly disposal of defective mitochondria. *Molecular biology of the cell*, 25(1), pp.145–59. Available at: http://www.ncbi.nlm.nih.gov/pubmed/24196833.

Shivas, J.M. & Skop, A.R., 2012. Arp2/3 mediates early endosome dynamics necessary for the maintenance of PAR asymmetry in Caenorhabditis elegans. *Molecular biology of the cell*, 23(10), pp.1917–27. Available at: http://www.pubmedcentral.nih.gov/articlerender.fcgi?artid=3350555&tool=pmcentrez&rendertype=abstract [Accessed December 16, 2013].

Smirnova, E. et al., 2001. Dynamin-related protein Drp1 is required for mitochondrial division in mammalian cells. *Molecular biology of the cell*, 12(8), pp.2245–2256.

Song, W. et al., 2011. Mutant huntingtin binds the mitochondrial fission GTPase dynamin-related protein-1 and increases its enzymatic activity. *Nature medicine*, 17(3), pp.377–382. Available at: http://dx.doi.org/10.1038/nm.2313.

Song, Z. et al., 2007. OPA1 processing controls mitochondrial fusion and is regulated by mRNA splicing, membrane potential, and Yme1L. *Journal of Cell Biology*, 178(5), pp.749–755.

Stavru, F. et al., 2013. Atypical mitochondrial fission upon bacterial infection. *Proceedings of the National Academy of Sciences of the United States of America*, 110(40), pp.16003–8. Available at: http://www.pubmedcentral.nih.gov/articlerender.fcgi?artid=3791707&tool=pmcentrez&rendertype=abstract.

Suen, D., Norris, K.L. & Youle, R.J., 2008. Mitochondrial dynamics and apoptosis. *Genes & Development*, 22(301), pp.1577–1590.

Sugiura, A. et al., 2013. MITOL regulates endoplasmic reticulum-mitochondria contacts via Mitofusin2. *Molecular Cell*, 51(1), pp.20–34. Available at: http://dx.doi.org/10.1016/j.molcel.2013.04.023.

Taguchi, N. et al., 2007. Mitotic phosphorylation of dynamin-related GTPase Drp1 participates in mitochondrial fission. *Journal of Biological Chemistry*, 282(15), pp.11521–11529.

Tembe, V. & Henderson, B.R., 2007. BARD1 translocation to mitochondria correlates with bax oligomerization, loss of mitochondrial membrane potential, and apoptosis. *Journal of Biological Chemistry*, 282(28), pp.20513–20522.

Tondera, D. et al., 2009. SLP-2 is required for stress-induced mitochondrial hyperfusion. *The EMBO journal*, 28(11), pp.1589–1600.

Tsuboi, S. et al., 2009. FBP17 mediates a common molecular step in the formation of podosomes and phagocytic cups in macrophages. *Journal of Biological Chemistry*, 284(13), pp.8548–8556.

Tuppen, H. a L. et al., 2010. Mitochondrial DNA mutations and human disease. *Biochimica et biophysica acta*, 1797(2), pp.113–128. Available at: http://dx.doi.org/10.1016/j.bbabio.2009.09.005.

Twig, G. et al., 2008. Fission and selective fusion govern mitochondrial segregation and elimination by autophagy. *The EMBO journal*, 27(2), pp.433–446.

Uruno, T. et al., 2001. mediated actin polymerization by cortactin. , 3(March), pp.259–266.

De Vos, K.J. et al., 2005. Mitochondrial function and actin regulate dynamin-related protein 1-dependent mitochondrial fission. *Current Biology*, 15(7), pp.678–683.

De Vos, K.J. et al., 2005. Mitochondrial function and actin regulate dynamin-related protein 1-dependent mitochondrial fission. *Current biology : CB*, 15(7), pp.678–83. Available at: http://www.ncbi.nlm.nih.gov/pubmed/15823542 [Accessed December 16, 2013].

Wakabayashi, J. et al., 2009. The dynamin-related GTPase Drp1 is required for embryonic and brain development in mice. *Journal of Cell Biology*, 186(6), pp.805–816.

Wang, W. et al., 2015. Mitofusin-2 triggers mitochondria Ca2+ influx from the endoplasmic reticulum to induce apoptosis in hepatocellular carcinoma cells. *Cancer Letters*, 358(1), pp.47–58. Available at: http://linkinghub.elsevier.com/retrieve/pii/S0304383514007800.

Wasiak, S., Zunino, R. & McBride, H.M., 2007. Bax/Bak promote sumoylation of DRP1 and its stable association with mitochondria during apoptotic cell death. *Journal of Cell Biology*, 177(3), pp.439–450.

Weaver, A.M. et al., 2002. Interaction of Cortactin and N-WASp with Arp2 / 3 Complex. *Current*, 12(02), pp.1270–1278.

Westermann, B., 2010. Mitochondrial fusion and fission in cell life and death. *Nature reviews. Molecular cell biology*, 11(12), pp.872–884. Available at: http://dx.doi.org/10.1038/nrm3013.

Wolter, K.G. et al., 1997. Movement of Bax from the cytosol to mitochondria during apoptosis. *Journal of Cell Biology*, 139(5), pp.1281–1292.

Xu, S. et al., 2011. The AAA-ATPase p97 is essential for outer mitochondrial membrane protein turnover. *Molecular biology of the cell*, 22(3), pp.291–300.

Yamaguchi, R. et al., 2008. Opa1-Mediated Cristae Opening Is Bax/Bak and BH3 Dependent, Required for Apoptosis, and Independent of Bak Oligomerization. *Molecular Cell*, 31(4), pp.557–569.

Yoon, Y. et al., 2003. The Mitochondrial Protein hFis1 Regulates Mitochondrial Fission in Mammalian Cells through an Interaction with the Dynamin-Like Protein DLP1 The Mitochondrial Protein hFis1 Regulates Mitochondrial Fission in Mammalian Cells through an Interaction with the. *Molecular and Cellular Biology*, 23(15), pp.5409–5420.

Yue, W. et al., 2014. A small natural molecule promotes mitochondrial fusion through inhibition of the deubiquitinase USP30. *Cell research*, 24(4), pp.482–96. Available at: http://www.ncbi.nlm.nih.gov/pubmed/24513856.

Zhang, K., Li, H. & Song, Z., 2014. Membrane depolarization activates the mitochondrial protease OMA1 by stimulating self-cleavage. *EMBO Reports*, 15(5), pp.576–585.

Zhang, Y. & Chan, D.C., 2007. Structural basis for recruitment of mitochondrial fission complexes by Fis1. *Proceedings of the National Academy of Sciences of the United States of America*, 104(47), pp.18526–18530.

Zhao, J. et al., 2011. Human MIEF1 recruits Drp1 to mitochondrial outer membranes and promotes mitochondrial fusion rather than fission. *The EMBO journal*, 30(14), pp.2762–2778.

Zhong, Q. et al., 2005. Mule/ARF-BP1, a BH3-only E3 ubiquitin ligase, catalyzes the polyubiquitination of Mcl-1 and regulates apoptosis. *Cell*, 121(7), pp.1085–1095.

Zhu, J. et al., 2005. Regulation of cortactin/dynamin interaction by actin polymerization during the fission of clathrin-coated pits. *Journal of cell science*, 118(Pt 4), pp.807–817.

Zigmond, S.H., 2004. Formin-induced nucleation of actin filaments. *Current Opinion in Cell Biology*, 16(1), pp.99–105.

Züchner, S. et al., 2004. Mutations in the mitochondrial GTPase mitofusin 2 cause Charcot-Marie-Tooth neuropathy type 2A. *Nature genetics*, 36(5), pp.449–451.

Zunino, R. et al., 2007. The SUMO protease SENP5 is required to maintain mitochondrial morphology and function. *Journal of cell science*, 120(Pt 7), pp.1178–1188.